ETH
Eidgenössische Technische Hochschule Zürich
Swiss Federal Institute of Technology Zurich

D MTEC

Quantum Walks and Decision Theory

Exploring the opportunities and challenges

MASTER THESIS
Department of Physics

Emma Lucretia Schepers
Zürich, May 2020

Supervisors:
Prof. Didier Sornette
Giuseppe Ferro MSc

ETH Zürich - D-MTEC
Chair of Entrepreneurial Risk

ETH

Eidgenössische Technische Hochschule Zürich
Swiss Federal Institute of Technology Zurich

Declaration of originality

The signed declaration of originality is a component of every semester paper, Bachelor's thesis, Master's thesis and any other degree paper undertaken during the course of studies, including the respective electronic versions.

Lecturers may also require a declaration of originality for other written papers compiled for their courses.

I hereby confirm that I am the sole author of the written work here enclosed and that I have compiled it in my own words. Parts excepted are corrections of form and content by the supervisor.

Title of work (in block letters):

Quantum Walks and Decision Theory, exploring opportunities and challenges.

Authored by (in block letters):

For papers written by groups the names of all authors are required.

Name(s):	**First name(s):**
Schepers	Emma

With my signature I confirm that

- I have committed none of the forms of plagiarism described in the 'Citation etiquette' information sheet.
- I have documented all methods, data and processes truthfully.
- I have not manipulated any data.
- I have mentioned all persons who were significant facilitators of the work.

I am aware that the work may be screened electronically for plagiarism.

Place, date	**Signature(s)**
Luzern, 07/05/2020	

For papers written by groups the names of all authors are required. Their signatures collectively guarantee the entire content of the written paper.

Acknowledgements

First of all, I would like to thank Prof. Didier Sornette for letting me work on this project and being available for discussion whenever needed. His endless energy is inspiring and the things I learned from his way of approaching a topic will certainly benefit my future career.

Second, many thanks go out to my co-supervisor Giuseppe Ferro who spent a lot of time discussing new ideas with me and was always willing to help whenever I got stuck. I really value our good work dynamics and the way in which we could combine our minds to come to new solutions.

Finally, I am very grateful for the people on the sidelines, my boyfriend Robbert and my parents who – even though they did not understand at all what I was working on – always supported me.

Abstract

The goal of this thesis is to explore the possibilities of using quantum walks in a decision theory framework. The inspiration came from the recently developed Stochastic Representation Decision Theory (SRDT) [1] that described the human choice process by a classical random walk. This framework predicts some empirically observed patterns (inverse S-shape probability weighting and risk-seeking attitude for losses) by letting the value and probability of the outcome influence the choice in a non-trivial and non-separable way. By exploring the use of quantum walks in the context of decision making, we aim to generalize and enrich SRDT with typical quantum properties like entanglement and interference, that have already shown useful in the previously developed Quantum Decision Theory (QDT) [2]. Indeed, this line of research contributes to providing a micro foundation for Quantum Decision Theory, in the same spirit of statistical physics for thermodynamics.

This thesis is a collection of explored directions, summarized in Figure 0.1. After a general introduction to Decision Theory and Quantum Walks, we try to extend the SRDT framework into the quantum domain. Based on the found opportunities and challenges we proceed with investigating different parametrizations of the choice problem. After a short intermezzo on continuous-time quantum walks, we return to the previously used coined quantum walk and shift our attention from the position space distribution to the spin. Here, we combine the insights gained before to present a new quantum walk-based framework that combines the influence of probability and value in a novel way. Finally, we review all ideas and provide some possibilities and challenges for the future.

Figure 0.1. – Summary of directions.

Contents

1 Introduction to Decision Theory **1**
- 1.1 State of the Art . . . 1
- 1.2 Stochastic Representation Decision Theory . . . 2
  - 1.2.1 Subjective probabilities . . . 4
  - 1.2.2 Choice between multiple lotteries . . . 6
  - 1.2.3 Risk seeking behavior for losses . . . 7
  - 1.2.4 Violation of Stochastic Dominance . . . 7
- 1.3 Limitations of SRDT . . . 8

2 Quantum Walks **11**
- 2.1 Introduction . . . 11
  - 2.1.1 Mathematical Structure of DTQW . . . 12
- 2.2 Measurements . . . 14
- 2.3 Analytical Solution for the free walk . . . 15
- 2.4 Quantum walk as Markovian process plus interference . . . 17
- 2.5 Decoherence In Quantum Walks . . . 18

3 Extension of the Classical SRDT Framework **21**
- 3.1 Introducing boundaries in Quantum Walks . . . 21
  - 3.1.1 Combinatorial solution: PQRS method . . . 22
  - 3.1.2 Transmittive boundaries by matrix change . . . 25
- 3.2 Biasing Quantum walks . . . 28
- 3.3 Subjective probabilities . . . 31
- 3.4 Interpretation of the Results . . . 35

4 Going beyond SRDT **39**
- 4.1 Objective probability in the initial state . . . 39
  - 4.1.1 Interpretation of the results . . . 41
- 4.2 Walk on a value chain: Biasing the step operator . . . 43
- 4.3 Boundary Effects . . . 46
- 4.4 Choice between lotteries . . . 48
- 4.5 Entropy of measurement . . . 49

5 Continuous Time Quantum walk **51**
- 5.1 Absorption by repeated measurements . . . 51
- 5.2 Interpretation of the Results . . . 56

6 Evolution of the global spin distribution **59**

6.1 The spin at the center of attention 59
6.2 Global spin Distribution 60
6.3 Using the spin as decision variable 62
6.3.1 Evolution of the expected values 64
6.4 Influence of the parameters 65
6.4.1 Subjective expected value 68
6.4.2 Choice probability 70
6.5 Example: The Decoy Effect 72

7 Discussion **75**

8 Conclusion **77**

Bibliography **79**

A Derivation of the absorption probability with the PQRS method **87**

Introduction to Decision Theory

1

1.1 State of the Art

In economics and cognitive science, the field of Decision Theory aims to predict and describe human choice behavior. In the context of economics, the most widely implemented form is *Expected Utility* theory [3]. This simple framework predicts that a decision-maker will choose the option that leads to the highest expected utility, formed by summing subjective values (utility) of events weighted by their objective probabilities. The utility function is defined in such a way that subjects value the outcomes relative to their current wealth (asset integration [4]). By replacing the outcomes with the expected utility of the wealth gain, a new choice problem is created. Within this new decision problem, the decision-maker is assumed to pick *always* the option with the highest expected utility. The exact form of the utility function determines the subject's attitude towards risk. In practise, many violations of this principle can be observed [5], [6]. One of the explanations is the notion of bounded rationality [7]. Rather than seeking the optimal choice, people will turn to a satisfactory option, trading optimality for efficiency.

There have been several attempts to extend or replace expected utility theory. In [8] Quiggin presents a model called *Rank dependent utility theory*, based on the concept that the weight of an option depends on both the probability and the rank of the outcome among other outcomes. Where the 'rank' is given by the position of the alternative when they are ordered from best to worst option. This is implemented by using a transformation function for the probability in combination with a utility function for the outcome. The resulting function can be seen as being composed of two competing forces. In this way, it is possible that the final preferences can be risk-averse even though the utility function is convex if the probability weighting is sufficiently deterministic [9]. This theory is able to capture the empirical observation that people tend to overweight small and underweight large probabilities. Especially, if the outcome is of extreme value. For example, people tend to overweight the probability that a disaster happens at the nuclear power plant because of the severe impact.

Another approach is based on the separation of gains and losses. Empirical evidence shows that people's risk appetite can be very different when faced with gains vs losses [10]. Based on this idea Kahneman and Tversky [11] presented *Cumulative Prospect Theory* where they use a convex value function for losses (risk-seeking) and a concave function (risk-averse) for gains. In this way, they are able to capture the typical behavior governed by the risk appetite, while still employing a deterministic framework.

This deterministic nature seems to be often violated in empirical evidence. For example, when faced with the same decision twice, subjects are not guaranteed to take the same decision in both instances. To deal with this, *Random Utility Theories* were introduced in for example [12]. To allow for deviations from rationality, a stochastic component is added to the utility function: $V(x) = U(x) + \epsilon_x$, with $U(x)$ the usual utility function and ϵ_x the stochastic

component. The assumption on the distribution of ϵ_x determines the exact theory, some example are [13], [14] and [15]. Although this model allows for deviations from expected utility theory, the core is still deterministic, modeling the observed stochasticity as the result of some error or lack of information about the subject. Adding this 'noise component' in an ad-hoc fashion furthermore leads to the problem of joint hypothesis testing [16].

Instead of explaining the observed violations as errors or attributing them to a lack of information when predicting the choice, one could also assume that the choice process is simply not deterministic in nature. This is the starting point for *Quantum Decision Theory* first introduced in [2]. This theory, based on the mathematical structure of Hilbert spaces, exploits the intrinsic probabilistic nature and entanglement properties of quantum mechanics. The assumption is that decision making is an intrinsically probabilistic process giving an explanation for the changes in choice behavior when facing a decision multiple times. Furthermore, the entanglement properties allow interdependence between alternatives, implying that the different possible outcomes in a decision cannot be seen independently. The theory states that each decision is the outcome of the state of mind of the decision-maker represented by Dirac state $|\psi_s\rangle$ and a prospect state $|\pi_n\rangle$ representing the outcome. The resulting choice probability for a prospect π_n can be split into two terms: $p(\pi_n) = f(\pi_n) + q(\pi_n)$. Here, $f(\pi_n)$ accounts for the 'rational' utility of the considered lottery and it is thus called utility factor. The second one, $q(\pi_n)$, termed attraction factor, instead reflects the interference pattern between prospect and state of mind of the decision-maker, mathematically resulting from the non-additive property of quantum probabilities. Descriptively, it embodies all the deviations from rationality, caused by subconscious deliberation, subjective feelings, and momentary influences. The exact form of the functions $f(\pi_n)$ and $q(\pi_n)$ are derived from the axioms of QDT [17]. A different parametrization of the functions is developed in [13].

In this thesis, we will start from another theory that was a first attempt to provide a microfoundation for QDT, called *Stochastic Representation Decision Theory*, henceforth SRDT. The central assumption is the same as in QDT: the decision process is intrinsically probabilistic. Besides support from experimental evidence, research in the field of neuroscience also shows signs of a stochastic component in the decision-making process. For example, Kurtz et al. [18] link the observed choice stochasticity to the inherent variability of neural activity when computing values. Moreover, this theory allows for the probability and value to influence the decision in a non-separable way.

To introduce stochasticity, SRDT is based on the concept of a random walk. The deliberation process is represented by a Brownian particle (the decision-maker) undergoing a random walk in an abstract space, where different events are encoded through absorbing domains. We introduce the framework by looking at the very simple decision problem of choosing between two (or more) lotteries. In the coming sections, we will formally introduce the model and subsequently show its predictions: i) the inverse S-shaped subjective probability as a function of the objective probability; ii) risk-seeking behavior in the loss domain; iii) observed violations of stochastic dominance [19].

1.2 Stochastic Representation Decision Theory

This section is based on the founding paper [1].

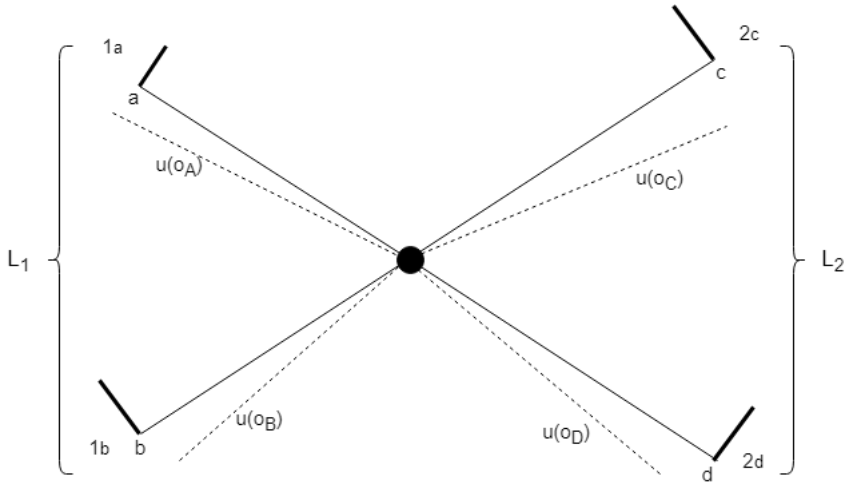

Figure 1.1. – Spatial structure of a random walk between two lotteries (4 lottery outcomes).

The concept of a random walk is used in many scientific fields, as a basis for computer algorithms [20], in economics [21] and physical processes [22]. In one dimension, i.e. on a line, one could imagine a particle taking steps to the left or to the right depending on the outcome of a coin flip. For a fair coin, at each step, the particle moves to the right with probability 0.5 and with the same probability to the left. Thanks to the Central Limit Theorem, the limit distribution of the properly scaled random walk is a Gaussian.

For the SRDT framework, we imagine a walker performing a random walk between two or more absorbing boundaries corresponding to lottery outcomes. Once the particle reaches one of the boundaries, it is absorbed and the walk ends. Doing this many times, we interpret the fractions of walks ending at one wall as the subjective probability of the represented outcome. By using the objective probability and outcome values to bias the trajectory of the walk, we get a non-trivial deliberation process.

For definiteness, imagine the following two lotteries: $L_1 = [o_A, p; o_B, 1-p]$ and $L_2 = [o_C, q; o_D, 1-q]$, where Lottery 1 gives outcome o_A (resp. o_B) with probability p (resp. 1-p). This can be represented as a random walk on four branches. We associate the length of the branches, and thus the distance to the absorbing boundary, with the objective probability of the outcome. That means that the higher the probability that an event occurs, the shorter the distance to the corresponding boundary. On top of that, we can introduce a value dependent force in each branch derived from a potential that biases the walk. The probability of choosing a lottery is composed of the absorption probability in the two branches that belong to that lottery, i.e.

$$P(L_1) = P(1_a) + P(1_b).$$

In this way, the absorption probability at one branch does not only determine the subjective probability of the represented event but also provides a measure of attractiveness for each event. This is a unique feature of the SRDT model.

To introduce the value dependent potential we assume the existence of some utility function endowed with the minimal properties of being concave and non-decreasing in the gain domain to present risk aversion. The potential is linear with the slope proportional to the utility of the outcome $u(o_A)$. The sign is such that the bigger the utility, the stronger the force. Due to the 'starfish' structure of the graph (see Figure 1.1), the problems remains essentially

one dimensional and we can describe the evolution of the probability density on, say, branch 1_a by a Fokker-Planck equation [23], [24].

$$\begin{cases} \frac{\partial p(x,t)}{\partial t} & = u(o_A)\frac{\partial p(x,t)}{\partial x} + \frac{D}{2}\frac{\partial^2 p(x,t)}{\partial x^2} \\ p(a,t) & = 0 \ \forall t (\text{absorbing boundary}) \\ p(0,t) & = f(t) \ (\text{probability mass from the other branches}) \end{cases} \tag{1.1}$$

By simple dimensional analysis, we can foresee that the diffusion coefficient D governs the relative impact of the value and the probability. For very large values of D the decision-maker only cares about the probabilities and neglects the values. For very small values of D the influence of the value dominates the decision and the subjective probability will be redirected towards the highest valued option.

1.2.1 Subjective probabilities

We can now derive an explicit form for the subjective probabilities. We consider one lottery with two outcomes. In this case, the absorption fraction at boundary A represents the subjective probability that the decision-maker assigns to outcome o_A. We begin with a situation without a value dependent potential. The Brownian particle starts at the origin between two branches of length a and b. To derive the absorption probabilities we follow the procedure in [25]. We start by rewriting the Fokker Planck equation for a general starting position x_0:

$$\begin{cases} \frac{\partial p(x,t)}{\partial t} & = -\frac{\partial(-V'(x)p(x,t))}{\partial x} + \frac{D}{2}\frac{\partial^2 p(x,t)}{\partial x^2} \\ p(a,t) & = p(b,t) = 0 \forall t \\ p(x,t=0) & = \delta(x - x_0) \end{cases} \tag{1.2}$$

Given the localized initial condition, we can focus on the conditional probability $P(x,t|x_0,t=0)$ which obeys the same Fokker Planck equation. By introducing the conditional probability current $J(x,t|x_0,0) = -V'(x)p(x,t|x_0,0) - \frac{D}{2}\frac{\partial p(x,t|x_0,0)}{\partial x}$, we can write the Fokker Planck equation as a continuity equation:

$$\frac{\partial p(x,t|x_0,0)}{\partial t} = -\frac{\partial J(x,t|x_0,0)}{\partial x} \tag{1.3}$$

This type of equation one can also find in fluid dynamics. We can now compute the absorption probability after time t as:

$$\begin{aligned} g_a(x_0,t) &= -\int_t^\infty dt' J(a,t'|x_0,0) = \int_t^\infty dt' \Big(V'(a)p(a,t|x_0,0) + \frac{D}{2}\frac{\partial p(x,t|x_0,0)}{\partial x}\Big|_{x=a} \Big) \\ g_b(x_0,t) &= \int_t^\infty dt' J(b,t'|x_0,0) = \int_t^\infty dt' \Big(-V'(b)p(p,t|x_0,0) - \frac{D}{2}\frac{\partial p(x,t|x_0,0)}{\partial x}\Big|_{x=b} \Big) \end{aligned} \tag{1.4}$$

Now $p(a,t|x_0,0)$ satisfies the backward Fokker Planck equation, so we are interested in the absorption probability at $t=0$. Taking the infinite time limit $t \to \infty$ we have:

$$\begin{cases} -V'(x_0)\frac{\partial \pi_a(x_0)}{\partial x_0} + \frac{D}{2}\frac{\partial^2 \pi_a(x_0)}{\partial x_0^2} = 0 \\ \pi_a(a) = 1, \pi_a(b) = 0 \\ \pi_a(x_0) + \pi_b(x_0) = 1 \end{cases} \tag{1.5}$$

where $\pi_a(x_0)$ denotes the probability of being eventually absorbed by the wall at distance a when starting from x_0.

Setting the potential to zero we observe:

$$\begin{aligned}\pi_a(x_0) &= \frac{x_0 - b}{a - b} = \frac{b - x_0}{|a| + b} \\ \pi_b(x_0) &= 1 - \pi_a(x_0) = \frac{|a| + x_0}{|a| + b}\end{aligned} \tag{1.6}$$

Since what matters is the relative distance of the wall to the starting position, we can safely set $x_0 = 0$ such that we get the simple expressions:

$$\pi_a = \frac{b}{a+b} \qquad\qquad \pi_b = \frac{a}{a+b}$$

when no potential is involved. To make this coincide with the objective probabilities of the event we have to set $a = 1 - p$ and $b = p$ up to a scaling factor that we can choose to be 1 without loss of generality. This assignment corresponds to the assumption that people are able to assess the probabilities correctly if no value is involved. This condition allows us to study the consequences of introducing a value dependent potential.

Consider a linear potential of the form:

$$V(x) = \begin{cases} u(o_A)x & \text{if } \; x_0 < 0 \\ u(o_B)x & \text{if } \; x_0 > 0 \end{cases} \tag{1.7}$$

For the Fokker Planck equation that means:

$$\begin{cases} -u(o_A)\frac{d\pi_a^{(L)}(x_0)}{dx_0} + \frac{D}{2}\frac{d^2\pi_a^{(L)}(x_0)}{dx_0^2} = 0 & \text{if } \; x_0 \leq 0 \\ u(o_B)\frac{d\pi_a^{(R)}(x_0)}{dx_0} + \frac{D}{2}\frac{d^2\pi_a^{(R)}(x_0)}{dx_0^2} = 0 & \text{if } \; x_0 > 0 \\ \pi_a^{(L)}(a) = 1, \pi_a^{(R)}(b) = 0 \end{cases} \tag{1.8}$$

Where the superscripts $(L), (R)$ denote $\pi_a(x_0)$ for positive and negative values of x_0 respectively. Choosing again 0 for the starting position the following continuity equations should hold:

$$\begin{aligned}\pi_a^{(L)}(0) &= \pi_a^{(R)}(0) \\ \frac{d\pi_a^{(L)}(x_0)}{dx_0}\Big|_{x_0=0} &= \frac{d\pi_a^{(R)}(x_0)}{dx_0}\Big|_{x_0=0}\end{aligned} \tag{1.9}$$

With these conditions we can solve Equation 1.8 to get:

$$\pi_a(0) = \frac{\frac{u(o_A)}{u(o_B)}(e^{-\frac{2u(o_B)b}{D}} - 1)}{\frac{u(o_A)}{u(o_B)}((e^{\frac{u(o_B)b}{D}} - 1) + (e^{-\frac{2u(o_A)|a|}{D}} - 1))}$$

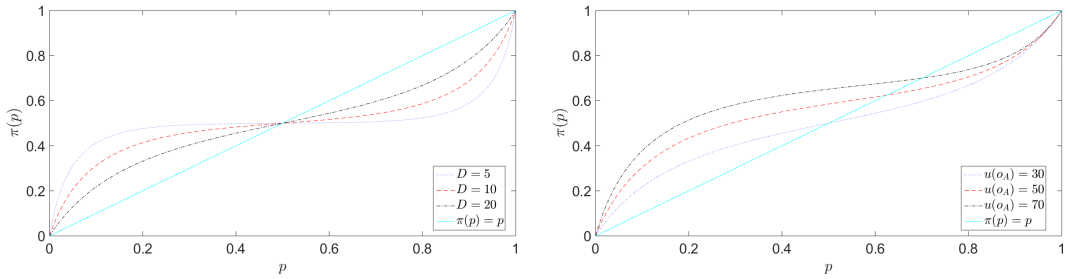

Figure 1.2. – Subjective probability of outcome o_A following Equation 1.10 as a function of the objective probability which is encoded in the initial position. In the left panel, the distribution is plotted for different values of the Diffusion coefficient and fixed $u(o_A) = u(o_B)$, while $u(o_A)$ is varied in the right panel. In the right panel D=20 for all curves.

Using the condition of rationality in the absence of value $|a| = 1 - p$ and $|b| = p$ this gives:

$$\begin{aligned} \pi(p) &:= P(1_a|L_1) = \frac{{}_p(o_A)}{{}_p(o_A) + {}_{1-p}(o_B)} \\ {}_p(o_A) &:= \frac{u(o_A)}{1 - e^{-\frac{2u(o_A)(1-p)}{D}}} \quad , \quad {}_{1-p}(o_B) := \frac{u(o_B)}{1 - e^{-\frac{2u(o_B)p}{D}}} \end{aligned} \tag{1.10}$$

This formula predicts the inverse S-shape of overestimating (underestimating) small (large) probabilities, only by postulating a minimal interaction between probability and value. The exact asymmetry between high and low probabilities is governed by the ratio $u(o_A)/u(o_B)$. The larger the difference between the values, the larger the subjective distortion for small p's compared to high p's. Furthermore, the influence of D and the two typical limits of value only vs probability only is also visible in this equation. In Figure 1.2 we show Equation 1.10 with and without a value bias. The inverse S-shape is clearly visible.

1.2.2 Choice between multiple lotteries

We can extend the ideas from the last section to a choice between multiple lotteries. In this case, the walk takes place on multiple branches in a starlike setting, as in Figure 1.1. For two lotteries, we can represent the choice probabilities as:

$$P(L_1) = \frac{\mathcal{U}(L_1)}{\mathcal{U}(L_1) + \mathcal{U}(L_2)} \tag{1.11}$$

with

$$\begin{aligned} \mathcal{U}(L_1) &= \tilde{\mathcal{U}}_p(o_A) + \tilde{\mathcal{U}}_{1-p}(o_B) = \frac{u(o_A)}{1 - e^{\frac{-2u(o_A)(1-p)}{D}}} + \frac{u(o_B)}{1 - e^{\frac{-2u(o_B)p}{D}}} \\ \mathcal{U}(L_2) &= \tilde{\mathcal{U}}_q(o_C) + \tilde{\mathcal{U}}_{1-q}(o_D) = \frac{u(o_C)}{1 - e^{\frac{-2u(o_C)(1-q)}{D}}} + \frac{u(o_D)}{1 - e^{\frac{-2u(o_D)q}{D}}} \end{aligned} \tag{1.12}$$

Formula 1.11 recovers the ratio scale representation of Luce's choice axiom for binary choices [26]. This implies that the theory possesses the desirable property of stochastic transitivity for pairwise choices. This means that if lottery 1 is equally good as or better than lottery 2, and lottery 2 is equally good or better than lottery 3, then lottery 1 is also equally good or better than lottery 3.

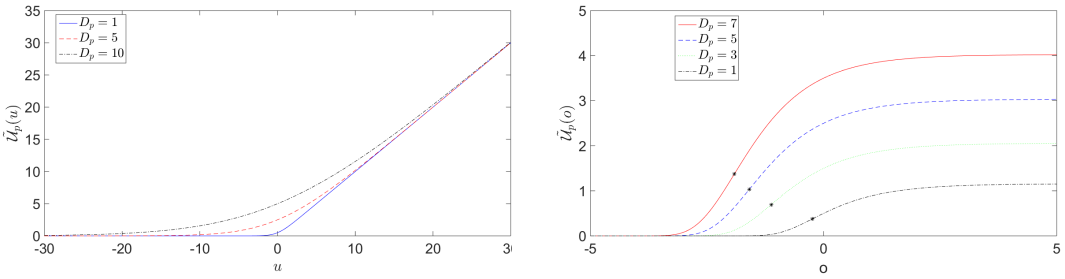

Figure 1.3. – Probability distorted utility function as a function of the original one (left) and value of the outcome (right) for different values of D_p. The black dots on the right indicate the inflection point between a convex and concave function.

This can be generalized to choices between an arbitrary number of lotteries. With N branches the probability to choose lottery L_j is:

$$P_N(L_j) = \frac{\mathcal{U}_j}{\sum_{i=1}^{N} \mathcal{U}_j} \tag{1.13}$$

The effective utilities $\mathcal{U}_j$ are given by expressions similar to equations 1.10. The effective utilities are influenced by the objective probability and the value option in a non-trivial and non-separable way. Their relative importance is governed by the value of D.

1.2.3 Risk seeking behavior for losses

In Equation 1.10 the subjective probability is formed by the objective probabilities and the value of the outcomes. However, we could also define a dual in which the value perception is influenced by the probabilities. The probability distorted utility function as a function of the original utility function and the outcome is shown in Figure 1.3 for different values of $D_p := \frac{D}{2(1-p)}$. Interestingly, the effect of the probability transforms an originally concave utility function into a convex one in (a part of) the loss domain. This means that the theory predicts risk-seeking behavior in the loss domain and the existence of an inflection point in the behavior towards gains vs. losses. This is an empirical observation that is used as the basis for the earlier described Cumulative Prospect Theory, but here arises purely from the interaction between value and probability.

1.2.4 Violation of Stochastic Dominance

Lottery 1 first order stochastically dominates Lottery 2 if $P(L_1 \leq 0) \leq P(L_2 \leq o)$ and $P(L_1 \leq 0) > P(L_2 \leq o)$ for at least one outcome [27]. Most decision theories try to obey this property to reflect the rational behavior 'more is better.' However, violations of stochastic dominance are observed when people are faced with more complex lotteries like:

$$L1 = [€96, 0.9; €14, 0.05; €12, 0.05] \quad L2 = [€96, 0.85, €90, 0.05, €12, 0.1]. \tag{1.14}$$

In this case, Lottery 1 stochastically dominates Lottery 2, but people often choose Lottery 2. In contrast to other theories SRDT can actually account for this with low values of D. In this case, people are mostly guided by the values, paying insufficient attention to the probabilities. In that light, Lottery 2 becomes the more attractive option because there are larger values involved.

1.3 Limitations of SRDT

The above-outlined framework is able to explain some of the empirical observations such as inverse-S shape dependence of the subjective probability on the objective one, violation of stochastic dominance, and risk-seeking behavior in the loss domain. However, there are also issues that remain. First of all, because of the set-up, the framework confirms the usual assumptions on the independence of outcomes. This is in accordance with the choice framework by Luce [26]. It means that each alternative is evaluated on its own and that this evaluation is not influenced by the presence of other outcomes. In the SRDT framework, this clearly arises because the absorption probability in one branch is independent of the absorption probability in other branches. When it comes to choices between multiple lotteries, this assumption is even stronger since the exact geometry of the star-like graph, i.e. which branch is opposite to which, does not matter. Illustratively speaking, the branch does not know to which lottery it belongs. In practice, this independence of alternatives is shown to be violated. A good example is the decoy effect [28] which is easiest explained by an example. Suppose you are looking for a new phone and you see the following two options:

	A	B
Price	€400	€300
Storage	30GB	20GB

Based on you personal valuation, you have some probability of preferring option A over option B. Now suppose there is a third option added to the problem:

	A	B	C
Price	€400	€300	€450
Storage	30GB	20GB	25GB

Option C is dominated by both options A and B so it might not seem like a valuable addition. Furthermore, following the assumption of independence of alternatives, the presence of option C should not affect with which probability you choose option A over B. However, in practice, many people find option A more attractive in the second choice problem than in the first. This is called the decoy effect [28]. Such effects can be incorporated in the earlier described rank dependent theories because, but not in SRDT. In this domain, SRDT is on the same side as expected utility theory because it confirms the independence of alternatives assumption even though many types of violations are known. Next to the decoy effect examples are the attraction, compromise, and similarity effect [29]. Here the extension to quantum might provide a new opportunity for SRDT. Because of its set-up and coherence properties, all alternatives are evaluated at the same time which leads to interdependence and interference effects as will be explained in later chapters.

Something closely related to the violation of the independence of alternatives is the concept of conjunction fallacy [30]. Conjunction is one of the basic rules in probability theory that states that the probability of the conjunction of two events cannot exceed the probability of each event individually. In the famous example, people are asked which of two option they find more probable to be true after a short introduction about a girl named Linda [30]:

"Linda is 31 years old, single, outspoken, and very bright. She majored in philosophy. As a student, she was deeply concerned with issues of discrimination and social justice, and also participated in anti-nuclear demonstrations."

Which is more probable?

1. Linda is a bank teller.
2. Linda is a bank teller and is active in the feminist movement.

Simple mathematics based on the independence of alternatives tells you that option 1 is more probable. In contradiction, most people point out option 2 as most likely to be true. Again, SRDT is not able to deal with such demonstrations of conjunction fallacy. Quantum walks, however, could provide an opening here. One of the special phenomena in quantum walks is that the absorption probability at a wall located on the left is enhanced once a second wall is placed on the right. In the context of the Linda problem, this could be used to explain how the subjective probability of Linda being a bank teller is increased once the second characteristic of Linda is added.

Lastly, SRDT was meant to serve as a microfoundation of Quantum Decision Theory. Using quantum properties like interference and entanglement the theory is able to describe many empirical observations not accounted for by traditional theories [2]. Here, quantum walks could help to establish this relation. As will be explained mathematically later, the evolution of a quantum walk can be split in a (Markovian) transition matrix part plus interference terms [31]. This is very similar to the structure of QDT, where the evolution was given by a classical utility part complemented by a quantum interference term parametrizing the attraction factor. This form was directly derived from fundamental Quantum mechanical principles, namely the Born rule and commutation relations. Within the QDT framework, the exact form of the functions was postulated [17]. The fact that the same functional form arises from a Quantum Walk could help to formulate a microfoundation of the earlier postulated terms, now by only making an assumption of the underlying process.

In the next section, we will introduce the general concept of a Quantum walk and its mathematical structure. After that, we are ready to explore their use in the context of decision making.

Quantum Walks

2

2.1 Introduction

As mentioned before, random walks are extensively used in physics and computer science. They form the basis of many algorithms and process theories. It was this algorithmic power that also led the way to the development of the quantum analog of the random walk, the so-called quantum walk. It is one of the cornerstones of modern quantum information theory and just like the classical counterpart, it is a very powerful algorithmic tool. The concept of a quantum walk is not uniquely defined, there are multiple versions used for different purposes. In the following, we will provide a gentle introduction to the field of quantum walks and break it down to the parts that proved most useful for the development of our framework. An excellent introduction from the perspective of a computer scientist can be found in [20]. Here, we will be mainly concerned with the mathematical and physical properties of quantum walks.

Imagine a random walk on a line, i.e. a particle moving left and right according to a random coin flip. As a direct transition to the quantum world, one could imagine this particle as a wavepacket moving in superposition. Any process in quantum mechanics should be unitary to be physical. Therefore, in this setting, the only possible operation here would be the translation operator moving the particle left or right with equal probability. This results in motion in a single direction, nothing different than the random walk! This fact was recognized by Aharanov et. al [32] and later Meyer [33] who was studying quantum cellular automata. The solution was the introduction of an extra degree of freedom into the system called the *spin*. In analogy with the spin-1/2 particle, the spin can be seen as the direction of the particle and can be labeled by a *left* and *right* state. The quantum walk may now be described as follows: at each step, a unitary transformation is applied to the spin of the particle creating a superposition of left and right states. A conditional shift operator then moves the particle to the neighboring sites according to this superposition. For example, imagine a particle being at location 0 in the state $\sqrt{0.4}\,|right\rangle + \sqrt{0.6}\,|left\rangle$; the evolution operator then shifts "40% of the particle to location +1 and 60% to location -1." Continuing this process of transforming the internal state and shifting the particle accordingly, an interesting pattern arises. As the particle moves in superposition, the different components can interfere with each other giving rise to very rich dynamics which we will discuss in more detail later. One of the key differences between a quantum walk and a moving quantum particle is that the walk takes place in discrete position space (and discrete-time in most cases). This means that the motion is not described by the Schrödinger equation.

The previously discussed class of quantum walks is called discrete-time or 'coined quantum walks' referring to the spin as the *coin state* of the particle in analogy to the classical random walk. However, this is not the only description of a quantum walk used. Closer to traditional quantum mechanics is the concept of continuous-time quantum walks. Unlike the discrete

version, the continuous-time quantum walk takes place entirely in position space. It can be seen as the quantum counterpart of continuous-time classical Markov chains. The concept was first defined in [34]. They described the evolution as being generated by a Hamiltonian as $U(t) = \exp\{-iHt\}$. The form of the Hamiltonian is derived from the adjacency matrix of the underlying graph. For example, on a line, the particle can only move to its nearest neighbors or stay at its current position. This gives a tight-binding-like Hamiltonian:

$$H = \sum_x (2\,|x\rangle\langle x| - |x-1\rangle\langle x| - |x+1\rangle\langle x|), \tag{2.1}$$

where we chose a constant transition rate/ hopping probability of 1. Now we can write the action of the Hamiltonian on a state vector in standard quantum mechanical notation:

$$\langle x|\,H\,|\psi\rangle = 2\,\langle x|\psi\rangle - \langle x-1|\psi\rangle - \langle x+1|\psi\rangle\,.$$

Here we can see the direct analogy with standard quantum mechanics since this equation is the same as the first-order finite difference approximation of ∇^2 in the Schrödinger equation [35]. Now we can write the time-dependent state vector as: $|\psi(t)\rangle = \exp(-iHt)\,|\psi(0)\rangle$.

Although the formulation is very different from the discrete-time quantum walk (no coin space), the evolution follows a very similar pattern. Establishing a relationship between the two types is however not straightforward. Different procedures have been outlined in [36] and [37].

Other classes of quantum walks come for example from the experimental implementation in optical lattices and are then described as a scattering mechanism. We will not consider these other types in this thesis. For completeness, we do want to mention a couple of proposals for the physical implementation of quantum walks. Since quantum walks were designed at first for algorithmic purposes the most straightforward implementation would be on a quantum computer. Since these are not fully developed on larger scales yet, other experimental proposals are investigated ranging from solid-state architectures and nuclear magnetic resonance systems to optical lattices and ion traps [38][39],[40] and [41]. The typical behavior of quantum walks makes it not only interesting for algorithmic purposes but also for the investigation of physical phenomena such as topological phases and protected edge states [42], [43]. This draws even more attention to the field and especially the physical aspects of quantum walks.

In this thesis, we will try to take inspiration from the wide range of uses of quantum walks to develop a framework similar to SRDT with the quantum walk at its core. Our goal is not to design a physical set-up or algorithm that can be run on a quantum computer but to use the mathematical concepts and properties to design a predictive framework. We will see that the special property called coherence of the quantum walk which gives it its interesting behavior, is very sensitive to any introduction of irreversibility making the dynamics rich, but also difficult to deal with.

2.1.1 Mathematical Structure of DTQW

The walk takes place on the combined Hilbert space $\mathcal{H}_t = \mathcal{H}_c \otimes \mathcal{H}_p$, where $\mathcal{H}_p$ is the infinitely large space of position vectors and $\mathcal{H}_c$ the two-dimensional coin space. We use the

canonical basis $|\uparrow\rangle, |\downarrow\rangle$ to denote the left and right coin state respectively. Therefore we can write the state of the walker as $|\psi\rangle = |j\rangle_{coin} \otimes |x\rangle_{position}$.

One evolution step of the walk consists of a rotation of the spin by the coin operator and a conditional position shift by the shift operator. The most general two dimensional coin operator can be written as [44]:

$$\hat{C}_{\xi,\theta,\zeta} = \begin{pmatrix} e^{i\xi}\cos\theta & e^{i\zeta}\sin\theta \\ e^{-i\zeta}\sin\theta & -e^{-i\xi}\cos\theta \end{pmatrix} \tag{2.2}$$

In a later section we will show how the different parameters in the coin operator can be used to bias the quantum walk. The most used coin operator is a symmetric coin leading to the so called Hadamard walk [20]:

$$H = \frac{1}{\sqrt{2}} \begin{pmatrix} 1 & 1 \\ 1 & -1 \end{pmatrix} \tag{2.3}$$

This is an unbiased coin, but whether it will give a symmetric walk strongly depends on the initial state. The coin operator is followed by a shift operator which can be written as:

$$S = |\uparrow\rangle\langle\uparrow| \otimes \sum_x |x-1\rangle\langle x| + |\downarrow\rangle\langle\downarrow| \sum_x |x+1\rangle\langle x|, \tag{2.4}$$

i.e. right spin is moved to the right and left to the left. One time step is then given by $U = S \cdot (C \otimes I)$, where I is the identity matrix in position space. Because the evolution is unitary and deterministic, the state at any later time t can be found by t applications of the evolution operator on the initial state, giving the time dependent state: $|\psi(x,t\rangle = U^t |\psi(x,0)\rangle$. This state $|\psi\rangle$ is essentially a vector consisting of a left and right component: $|\psi\rangle = \begin{pmatrix} \psi^L \\ \psi^R \end{pmatrix}$, which means that the evolution through the application of U is simply a matrix multiplication. To illustrate the differences with the classical random walk described in section 3.2 we evolve the walk starting in initial state $|\psi_{in}\rangle = |\uparrow\rangle \otimes |0\rangle$ three steps by repeatedly applying U with the Hadamard coin operator defined in (2.3):

$$\begin{aligned} |\psi^1\rangle &= \frac{1}{\sqrt{2}}(|\uparrow\rangle \otimes |1\rangle - |\downarrow\rangle \otimes |-1\rangle \\ |\psi^2\rangle &= \frac{1}{2}(|\uparrow\rangle \otimes |2\rangle - (|\uparrow\rangle - |\downarrow\rangle) \otimes |0\rangle + |\downarrow\rangle \otimes |-2\rangle) \\ |\psi^3\rangle &= \frac{1}{2\sqrt{2}}(|\uparrow\rangle \otimes |3\rangle + |\downarrow\rangle \otimes |1\rangle + |\uparrow\rangle \otimes |-1\rangle - 2|\downarrow\rangle \otimes |-1\rangle - |\downarrow\rangle \otimes |-3\rangle) \end{aligned} \tag{2.5}$$

We can see that the quantum walker now occupies 4 different states after the third step, spreading in both directions. Continuing this procedure for T steps, we get the distribution calculated as $\left|\left|\psi^T\right\rangle\right|^2$ shown in Figure 2.1 where it is compared to the distribution of a classical random walk with an unbiased coin. For the quantum walk we chose the initial state $\frac{1}{\sqrt{2}}\begin{pmatrix} 1 \\ i \end{pmatrix}$. Because the right spin component stays imaginary and the left spin part stays real, then the two will not interfere and the walk is symmetric[45], [44]. In section 3.2 we will discuss further how different coins and initial states can be used to tune the spreading and amount of interference of the quantum walk.

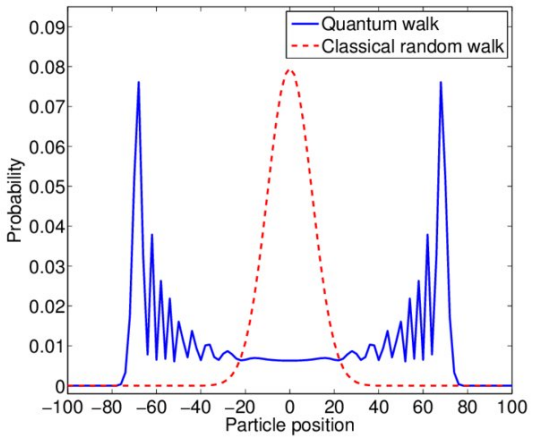

Figure 2.1. – Discrete Time Quantum Walk and Classical Random Walk in position space. The DTQW is formed through evolution with the Hadamard coin departing from the symmetric initial state $\frac{1}{\sqrt{2}}\begin{pmatrix}1\\ i\end{pmatrix}$, the Random Walk uses an unbiased coin [46]

In Figure 2.1 one of the most important properties of quantum walks making them useful for quantum computing can also be seen; they spread quadratically faster than their classical counterparts. That means the variance scales with $\sigma^2 \sim T^2$, potentially giving a quadratic speed up for algorithms based on quantum walks.

The fact that quantum walks evolve as a superposition of left and right moving states gives rise to a wavelike pattern. That also means that the system is subjected to interference, depending on the coin and initial state. As long as the system is not measured, the system will remain coherent and therefore show the typical pattern of the double-peaked distribution and the uneven occupation of even versus odd states.

2.2 Measurements

As in continuous space quantum mechanics, performing measurements has a nontrivial effect on the system. One of the key features of a quantum walk is that, unlike the random walk, it is coherent throughout space. However, this coherence can be destroyed be measuring the walk (either its spin or position). Just like in standard quantum mechanics the walk will collapse to a point upon measurement indicating the position or spin of the particle at that time. More on the effects of the walk will be discussed in Section 2.5.

A general measurement in position space is defined as a standard projection on position space. Formally:

$$P = \sum_x |x\rangle \langle x| . \tag{2.6}$$

Performing the projection over the whole position space gives the amplitude of the wave function at each location, and therefore by taking the absolute value squared, the probability distribution of the particle. Doing such a measurement corresponds to asking the question: 'Where is the particle?' We can also perform a partial measurement which only disturbs the system slightly. For example, we can ask whether the particle is at location n. If the answer is Yes, the wave function collapses to the point n. If the answer is No, the wave function

collapses onto all other points, which means that most of the coherence is maintained. These partial measurements are useful when implementing boundary conditions since enforcing any type of boundary requires some knowledge of whether the particle is at the boundary or not.

2.3 Analytical Solution for the free walk

We introduce the Schrödinger approach [47], [48] to quantum walks, which takes advantage of the translational invariance of the quantum walk. We refer to the walk on a infinite line as 'free' or 'unbounded.' The translational invariance of free walks implies that the walk has a simple representation in Fourier space. To demonstrate the method, we use the general form of the Hadamard walk:

$$H = \begin{pmatrix} \sqrt{\rho} & \sqrt{1-\rho} \\ \sqrt{1-\rho} & -\sqrt{\rho} \end{pmatrix} \tag{2.7}$$

Later we will see that with the appropriate choice for the initial state, this matrix covers all possible quantum walks on the line. Using this matrix in combination with the standard shift operator (2.4) we can write the state vector at time t as:

$$\begin{pmatrix} \psi^L(x,t) \\ \psi^R(x,t) \end{pmatrix} = \begin{pmatrix} \sqrt{\rho}\psi^L(x+1,t-1) + \sqrt{1-\rho}\psi^R(x+1,t-1) \\ \sqrt{1-\rho}\psi^L(x-1,t-1) - \sqrt{\rho}\psi^R(x-1,t-1) \end{pmatrix} \tag{2.8}$$

Since we are working in discrete space, we make use of the discrete Fourier transform:

$$\begin{aligned} \tilde{f}(k) &= \sum_{x=-\infty}^{\infty} f(x)e^{ikx} \\ f(x) &= \frac{1}{2\pi}\int_{-\pi}^{\pi} \tilde{f}(k)e^{-ikx}dk \end{aligned} \tag{2.9}$$

The inverse Fourier transform uses an integral instead of a sum since, in the unbounded walk case, we have a continuum of k values. Therefore the statevector in momentum space is $\tilde{\psi}(k,t) = \sum_x \psi(x,t)e^{ikx}$. We can write the evolution of the right and left component seperately by the introduction of two new matrices [48]:

$$\begin{pmatrix} \psi^L(x,t) \\ \psi^R(x,t) \end{pmatrix} = M_- \begin{pmatrix} \psi^L(x+1,t-1) \\ \psi^R(x+1,t-1) \end{pmatrix} + M_+ \begin{pmatrix} \psi^L(x-1,t-1) \\ \psi^R(x-1,t-1) \end{pmatrix}.$$

With $M_- = \begin{pmatrix} \sqrt{\rho} & \sqrt{1-\rho} \\ 0 & 0 \end{pmatrix}$ and $M_+ = \begin{pmatrix} 0 & 0 \\ \sqrt{1-\rho} & -\sqrt{\rho} \end{pmatrix}$. Using the discrete Fourier transform:

$$\begin{aligned} \tilde{\psi}(k,t) &= M_+ \sum_x \psi(x-1,t-1)e^{ik(x-1)} + M_- \sum_x \psi(x+1,t-1)e^{ik(x+1)} \\ &= (M_+e^{-ik} + M_e^{ik})\psi(\tilde{k},t) \\ &= M_k\tilde{\psi}(k,t), \end{aligned}$$

where we defined $M_k = \begin{pmatrix} e^{-ik}\sqrt{\rho} & e^{-ik}\sqrt{1-\rho} \\ e^{ik}\sqrt{1-\rho} & -e^{ik}\sqrt{\rho} \end{pmatrix}$ which is in general $M_k = \Lambda_k U^T$ with $\Lambda_k = \begin{pmatrix} e^{-ik} & 0 \\ 0 & e^{ik} \end{pmatrix}$. Now we can write the time dependent state as $\tilde{\psi}(k,t) = M_k^t \tilde{\psi}(k,0)$. The reason that we used the Fourier representation is that the time evolution now has a simple form in terms of the eigenvectors and eigenvalues of M_k:

$$M_k^t = (\lambda_k^+)^t \left|\phi_k^+\right\rangle \left\langle\phi_k^+\right| + (\lambda_k^-)^t \left|\phi_k^-\right\rangle \left\langle\phi_k^-\right|. \tag{2.10}$$

We now compute the eigenfunctions of the system. Using $det(M_k - \lambda I) = 0$ we obtain:

$$\begin{aligned} \lambda_k^{\pm} &= \frac{-2i\sqrt{\rho}\sin k \pm \sqrt{4 - 4\rho \sin k^2}}{2} \\ \lambda_k^{\pm} &= \sqrt{\rho}(-i\sin k \pm \sqrt{1/\rho - \sin k^2}) \end{aligned} \tag{2.11}$$

Because M_k is unitary by construction, $\left|\lambda_k^{\pm}\right| = 1$. Therefore we can write the eigenvalues as $\lambda_k^{\pm} = e^{\mp i\omega_k}$ where

$$\begin{aligned} \sin\omega_k^+ &= \sqrt{\rho}\sin k \\ \omega_k^- &= \pi + \omega_k^+. \end{aligned} \tag{2.12}$$

Now we look for eigenvectors of the form: $\begin{pmatrix} \phi^L(x,t) \\ \phi^R(x,t) \end{pmatrix} = \begin{pmatrix} A_k \\ B_k \end{pmatrix} e^{i(kx - \omega_k t)}$

Solving the equation: $e^{-i\omega_k}\begin{pmatrix} A_k \\ B_k \end{pmatrix} = M_k \begin{pmatrix} A_k \\ B_k \end{pmatrix}$ gives [47]:

$$\begin{aligned} A_{k\pm} &= \frac{1}{\sqrt{2N}}\sqrt{1 \pm \frac{\cos k}{\sqrt{1/\rho - \sin k^2}}} \\ B_{k\pm} &= \pm\frac{e^{-ik}}{\sqrt{2N}}\sqrt{1 \mp \frac{\cos k}{\sqrt{1/\rho - \sin k^2}}} \end{aligned} \tag{2.13}$$

Where the eigenfunctions are normalized such that $|A_{k\pm}|^2 + |B_{k\pm}|^2 = 1/N$ such that the probability over N sites sums to 1. Now that we have the eigenvectors and values of the system we can decompose any initial state into the eigenvectors of the evolution operator and use the inverse Fourier transform to write the evolution in position space. For example, for the Hadamard walk with $\rho = 1/2$ and the initial state $\begin{pmatrix} 1 \\ 0 \end{pmatrix}$ the evolution of the left and right component in position space is:

$$\begin{aligned} \psi_L(x,t) &= \int_{-\pi}^{\pi} \frac{dk}{2\pi} \frac{-ie^{ik}}{\sqrt{1+\cos k^2}} e^{-i(\omega_k t - kx)} \\ \psi_R(x,t) &= \int_{-\pi}^{\pi} \frac{dk}{2\pi} \left(1 - \frac{\cos k}{\sqrt{1+\cos k^2}}\right) e^{-i(\omega_k t - kx)}. \end{aligned} \tag{2.14}$$

2.4 Quantum walk as Markovian process plus interference

To gain more insight into the evolution of the discrete-time quantum walk, we can write its evolution as a Markovian transition matrix plus interference terms. Exactly the presence of the interference terms is what makes the walk quantum and gives it its special behavior. This description of a Quantum walk was first introduced by Romanelli et. al. in [31]. Depending on the exact formulation it can be both used to describe the probability distribution in position as well as the distribution of the spin. This second option will come back in Chapter 6, here we focus on the spatial distribution.

Following [31] we write the wave function in space as:

$$|\Psi(t)\rangle = \sum_x \begin{pmatrix} a_x(t) \\ b_x(t) \end{pmatrix} |x\rangle \,. \tag{2.15}$$

We use the general Hadamard matrix:

$$H(\theta) = \begin{pmatrix} \cos\theta & \sin\theta \\ \sin\theta & -\cos\theta \end{pmatrix}. \tag{2.16}$$

We use this parametrization to follow the notation in [31]. Note that this is equivalent to Equation 2.7 when associating $\cos\theta = \sqrt{\rho}$. In this case the usual Hadamard walk is retrieved for $\theta = \pi/4$.

The evolution of the components can be written as:

$$a_x(t+1) = \cos\theta a_{x+1}(t) + \sin\theta b_{x+1}(t) \tag{2.17}$$

$$b_x(t+1) = \sin\theta a_{x-1}(t) - \cos\theta b_{x-1}(t). \tag{2.18}$$

We denote by $P_{x,L}(t) \equiv |a_x(t)|^2$ the probability of being in the left spin state in position x at time t. Using Equation 2.17 we can write the evolution of the right and left distribution as:

$$P_{x,L}(t+1) = P_{x+1,L}(t)\cos\theta^2 + P_{x+1,R}(t)\sin\theta^2 + \beta_{x+1}(t)\sin 2\theta \tag{2.19}$$

$$P_{x,R}(t+1) = P_{x-1,L}(t)\sin\theta^2 + P_{x-1,R}(t)\cos\theta^2 - \beta_{x-1}(t)\sin 2\theta \tag{2.20}$$

where $\beta_x(t) = Re(a_x(t)b_x(t)^*)$, the interference term. Using the fact that the total probability of being in position x is the sum of the two components, the probability can be written in compact form as [31]:

$$P_{xs}(t+1) = \sum_{x=-\infty}^{\infty} \sum_{l=L,R} T_{xy,sl} P_{yl}(t) + \beta_{xs}(t)\sin 2\theta \tag{2.21}$$

where:

$$
\begin{aligned}
T_{xx+1,LL} &= T_{xx-1,RR} = \cos\theta^2 \\
T_{xx+1,LR} &= T_{xx-1,Rl} = \sin\theta^2 \\
T_{xy,ls} &= 0 \\
\beta_{xL} &= \beta_{x+1} \\
\beta_{xR} &= -\beta_{x-1}.
\end{aligned}
$$

$T_{xy,sl}$ has all needed properties of a classical transfer matrix for a Markovian process. That means that in the absence of the interference terms, this simply describes a Markovian process with transition probability given by $T_{xy,sl}$. Furthermore, the Markovian part only depends on the spin and position of the walker in the previous time step.

This structure of a classical part complemented by interference terms is what we also saw in QDT [17].

2.5 Decoherence In Quantum Walks

The coherence of the Quantum walk is a unique property that leads to very different dynamics compared to a classical random walk. However, this also puts a severe restriction on the possible evolution operators. A quantum walk is described by a unitary operator which makes the walk reversible and therefore coherent. On the other hand, a classical random walk, being a simple Markov process, has a dissipative and irreversible dynamics. In an experimental set-up, there are many environmental factors that can influence the walk. In particular, we already described how measurements collapse the wavefunction and therefore break the coherence of the walk. This brings us to another important property: in order to classify as a quantum walk, the walk should reduce to a classical random walk if the amount of decoherence is sufficiently large [49].

In general, any operation that breaks the unitarity of the walk classifies as a decoherence mechanism. Some examples are performing random measurements via projection [32], dephasing [50], [51] or imperfect shifts [39]. The fact that a quantum walk reduces to a classical random walk when decohered can be easily shown by using projective measurements of the position. Imagine a quantum walker in a general state $|\Psi\rangle = \begin{pmatrix} \alpha \\ i\beta \end{pmatrix} \otimes |x\rangle$. After one application of the Hadamard coin and shift operator the walker is in state:

$$
\frac{1}{\sqrt{2}} \begin{pmatrix} \alpha + i\beta \\ 0 \end{pmatrix} \otimes |x-1\rangle + \begin{pmatrix} 0 \\ \alpha - i\beta \end{pmatrix} \otimes |x+1\rangle . \tag{2.22}
$$

If we now measure the position, the walker will be at position $x-1$ with probability $p = \frac{1}{2}(\alpha^2 + \beta^2) = \frac{1}{2}$ because of the normalized initial state. Upon measuring, the wave function collapses to either $x-1$ or $x+1$. When applying the evolution operator to the collapsed state, the walker will again move left or right with probability $\frac{1}{2}$. This is simply a random walk with unbiased coin. When measuring at each time step, the wave function does not move in superposition because it collapses to a point after each measurement. Therefore, no quantum (interference) effects take place. Looking back at the previous section and especially Equation

2.21 we can interpret the process of decoherence as decreasing the factor $\beta_x(t)$. If this factor is 0, the process is simply Markovian.

Both numerical [52] and analytical studies [53] show that the quantum walk is relatively vulnerable to decoherence. The transition to a classical behavior is therefore relatively quick but depends on the specific type of decoherence. All decoherence mechanisms can be roughly divided into two classes, decoherence of the position and decoherence of the coin. Lopez [54] shows with a Wigner function approach that the random walk resulting from decohering the position (for example by measuring the position of the walker) results in a classical walk that is independent of the initial state. Coin decoherence, on the contrary, results in a superposition of two random walks each starting in a different position, depending on the initial coin state.

As a measure of the 'quantumness' people usually turn to the standard deviation. The typical difference between quantum and random walks lies in the fact that the former spread linearly in time, ballistically, while the random walk only spreads as $\sqrt{t}$, diffusively. The transition from ballistic to diffusive behavior marks the quantum-classical transition. In addition to diffusive spreading, the walk can also exhibit Anderson localization for certain types of dynamic or static decoherence as discussed in [55]. The fact that the quantum walk reduces to a classical random walk if we measure its location at each step is a useful tool to compare the two. For instance, this property allows us to compare the bias in the quantum walk with the bias in random walks. For a more elaborate treatment of decoherence in quantum walks, see [49] and references therein.

3 Extension of the Classical SRDT Framework

In Section 1.2 the SRDT framework was introduced where the attractiveness of an alternative is given by the probability for a random walker to be absorbed on the left vs. the right wall. In this chapter, we try to extend this framework by replacing the random walker by a quantum walker. The set-up of SRDT will be followed as closely as possible to be able to compare the classical and the quantum case.

The Chapter is organized as follows. First, we will introduce the quantum equivalent of absorbing walls for the one dimensional walk. We will also discuss two analytical methods to calculate the absorption probability for a quantum walk. Second, we will discuss how to bias a quantum walk in general and tailor the bias factors to the choice problem. In the third section we will compare the quantum walk based framework to the classical SRDT model. We will conclude with some general remarks on this approach.

3.1 Introducing boundaries in Quantum Walks

In SRDT, the key quantity is the probability to be absorbed at one of the boundaries between which the walker moves. Following this set-up, we want to impose these absorbing boundary conditions on a one-dimensional quantum walk system. This is however not straightforward. First of all, the fact that the walker moves in a superposition of states, there is no way to know whether the particle has reached the boundary without performing a measurement. As described in the introduction, measurements affect the system, rendering the walk to be classical if the decoherence is strong. Second, absorbing (part of) the wavefunction during the evolution introduces irreversibility and therefore breaks the unitarity of the system. Third, the introduction of boundaries also breaks the translational invariance of the walk. The earlier described Schrödinger approach to describe the quantum walk evolution will therefore in general not be applicable anymore.

We can draw an analogy with electrons in a solid. These quantum particles that move through a periodic lattice are described by Bloch waves [56]. In the quantum walk we have a very similar situation where quantum particles with an internal degree of freedom (spin) are moving through discrete space [57], [58]. The key feature of the Bloch wave solution is that the translation operator and the full Hamiltonian commute and are therefore diagonalized by the same eigenstates. As soon as the translational invariance is broken, this is no longer true and thus the system cannot be described by the standard Bloch wave solution. This is also true for the quantum walk where the introduction of boundaries breaks the translational invariance and therefore makes the dynamics irreversible and thus non-unitary.

Although a physical boundary might not be natural in the quantum walk system, we can use a protocol carried over from quantum computing to impose the boundaries in a slightly different way. The idea is as follows [59]:

1. Initialize the walker in the state $|\Psi(x,0)\rangle = \sum_x \begin{pmatrix} \alpha \\ \beta \end{pmatrix} \otimes |0\rangle$.

2. Evolve the walk one step with operator U.

3. Perform a partial measurement to check whether the particle is at one of the boundaries: $P = |B_l\rangle\langle B_l| + |B_r\rangle\langle B_r|$. This returns 'Yes' with probability $||\Psi(B_i,t)\rangle|$, with $B_i = B_l, B_r$ at each time step. If the answer for one of the boundaries is Yes, stop the walk. If the answer is No, reinitialize the walker in state $(I-P)|\Psi(x,t)\rangle$ and renormalize the probability by removing the 'absorbed part'.

4. Repeat step 2 until the particle is absorbed by one of the walls.

With this protocol, we use the concept of partial measurement to absorb the particle at each step. Because the measurement is only partial, most of the coherence will be conserved and therefore the walk will not be classical. From now on, we will use this protocol to impose the absorbing boundaries onto the system.

In the literature, several attempts have been done to analytically extract the absorption probability of the system. However, this is very complex and so far only a few limits of the behavior are known [60], [59], [61], [62], [63] and [64]. Here, two of the main contributions will be summarized with the respective references to the literature.

3.1.1 Combinatorial solution: PQRS method

The first approach is based on the counting of paths. The central idea is to count the number of paths that can reach the respective boundary from the initial location at time T, given the evolution operator and initial state. Konno and colleagues are the main contributors in this field, here we give an overview of their method called the PQRS model [59].

For simplicity of notation we paramatrize each unitary quantum walk operator as:

$$U = \begin{bmatrix} a & b \\ c & d \end{bmatrix}$$

Recalling the evolution of the right and left component as in Equation 2.8 we can write the transformation as:

$$|\psi(x,t+1)\rangle = P|\psi(x+1,t)\rangle + Q|\psi(x-1,t)\rangle \tag{3.1}$$

with

$$P = \begin{bmatrix} a & b \\ 0 & 0 \end{bmatrix} \qquad Q = \begin{bmatrix} 0 & 0 \\ c & d \end{bmatrix} \tag{3.2}$$

So $U = P + Q$. We can now introduce two additional matrices:

$$R = \begin{bmatrix} c & d \\ 0 & 0 \end{bmatrix} \qquad S = \begin{bmatrix} 0 & 0 \\ a & b \end{bmatrix} \tag{3.3}$$

such that P, Q, R and S form a complete basis of the vector space of complex 2x2 matrices with inner product $\langle A|B\rangle = Tr(A^*B)$. That means that we can express any complex 2x2 matrix in terms of these four matrices:

$$V = Tr(P^*V)P + Tr(Q^*V)Q + Tr(R*V)R + Tr(S^*V)S$$

Having introduced the basics of the PQRS method, we now turn to the issue of the absorption probability. We introduce the new measure $\Xi_{x_0}^{(N)}(t)$ which is the weighted sum of possible paths for which a particle starting from position x_0 first hits 0 before reaching N at time t. This is defined as a product of left- (P) and right-moving (Q) operators. For example, a particle starting from $x_0 = 1$ with $N = 3$ taking 5 steps can take the following path to reach 0 before reaching 3:

$$\Xi_1^{(3)}(5) = P^2QPQ = ab^2cR \tag{3.4}$$

From $\Xi_{x_0}^{(N)}(t)$ we can directly extract the probability that a particle starting from x_0 in coin state ϕ hits 0 before hitting N by taking the modulus squared:

$$P_k^{(N)}(t;\phi) = \left|\Xi_{x_0}^{(N)}(t)\phi\right|^2 \tag{3.5}$$

Summing over all times yields the total probability.

A system with only one boundary can be seen as taking $N \to \infty$, i.e. absorption means that the particle hits the boundary before escaping to ∞. There we reach the first special property of quantum walks. Recall that an unbiased classical random walk in one-dimension is recurrent, therefore, in the presence of one absorbing boundary, it will be absorbed asymptotically with probability 1. For quantum walks, however, this is not the case. The walker always has a finite probability to escape the boundary (under the constraint that the initial position is not at the boundary), even when it is symmetric. For the particular case of $x_0 = 1$ and $\phi =^T [1, 0]$, assuming Hadamard coin, several authors have proved that the escape probability is $P_1^{(\infty)}(^T[1, 0]) = \frac{2}{\pi}$ [48], [47].

To show how the PQRS decomposition can help to calculate the sum of paths, we will consider the general case of finite N. Using the PQRS basis we can write the sum of paths as:

$$\Xi_{x_0}^{(N)}(t) = p_x^N(t)P + q_x^N(t)Q + r_x^N(t)R + s_x^N(t)S \tag{3.6}$$

The following table will be useful in further computations

	P	Q	R	S
P	aP	bR	aR	bP
Q	cS	dQ	cQ	dS
R	cP	dR	cR	dP
S	aS	bQ	aQ	bS

Let us now compute the coefficients defined in Eq. 3.6. Since $\Xi_{x_0}^{(N)}(t)$ is defined in terms of left and right movements, we can deduce the following difference equation from the general evolution:

$$\Xi_x^{(N)}(t) = \Xi_{x-1}^{(N)}(t-1)P + \Xi_{x+1}^{(N)}(t-1)Q. \tag{3.7}$$

Using the PQRS decomposition, this also gives recurrence relations for the coefficients:

$$\begin{aligned} p_x^N(t) &= ap_{x-1}^N(t-1) + cr_{x-1}^N(t-1) \\ q_x^N(t) &= dq_{x+1}^N(t-1) + bs_{x+1}^N(t-1) \\ r_x^N(t) &= bp_{x+1}^N(t-1) + dr_{x+1}^N(t-1) \\ s_x^N(t) &= cq_{x-1}^N(t-1) + as_{x-1}^N(t-1) \end{aligned}$$

To determine the coefficients we use the boundary conditions from the absorbing boundaries. Because we use a partial measurement protocol, we assume perfect absorption once the particle reaches the boundary. Note that this is really an algorithmic statement since the experimenter stops the process once the particle is found. Physically speaking, any absorbing potential would also lead to some reflection of the wave.

When $x_0 = N$ i.e the particle starts at the other boundary, the probability that it will be absorbed in location 0 is of course 0. That means:

$$P_N^{(N)}(0;\phi) = \left|\Xi_N^{(N)}(0)\phi\right|^2 = 0 \tag{3.8}$$

Using the PQRS decomposition for the null matrix, this gives for the coefficients:

$$p_N^{(N)}(0) = q_N^{(N)}(0) = r_N^{(N)}(0) = s_N^{(N)}(0) = 0 \tag{3.9}$$

In the other extreme case, if $x_0 = 0$ the absorption probability is one, i.e. $\Xi_0^{(N)})(0) = I$ giving:

$$p_N^{(N)}(0) = \bar{a} \qquad q_N^{(N)}(0) = \bar{d} \qquad r_N^{(N)}(0) = \bar{c} \qquad s_N^{(N)}(0) = \bar{b}$$

where we denote the complex conjugation of any number z by $\bar{z}$.

Having constructed the boundary conditions, we can now focus on the $0 < x_0 < N$ case, which also means $t \geq 1$. From the example in Equation 3.4, we can see that we only need two types of paths to describe the evolution, namely P and Q corresponding to right and left movements. Therefore we can simplify the equations by setting $q_x^N(t) = s_x^N(t) = 0$ for $t \geq 1$ in Equation 3.6.

The total absorption probability in 0 with another boundary present at N can be written as (see Lemma 1 in [59])

$$P_{x_0}^{(N)}(\phi) = \sum_{t=1}^{\infty} P_{x_0}^{(N)}(t,\phi) \;\text{ with }\; P_{x_0}^{(N)}(t,\phi) = C_1(t)|\alpha|^2 + C_2(t)|\beta|^2 + 2Re(C_3(t)\alpha\bar{\beta}) \tag{3.10}$$

where we wrote the initial coin state as ${}^T[\alpha,\beta]$ such that $|\alpha|^2+|\beta|^2 = 1$ and the time dependent coefficients are given by

$$\begin{aligned} C_1(t) &= \left|ap_x^N(t) + cr_x^N(t)\right|^2 \\ C_2(t) &= \left|bp_x^N(t) + dr_x^N(t)\right|^2 \\ C_2(t) &= \overline{(ap_x^N(t) + cr_x^N(t))}(bp_x^N(t) + dr_x^N(t)) \end{aligned}$$

To solve the coefficients explicitly, we make use of generating functions. This means that we encode $p_x^N(t)$ and $r_x^N(t)$ as the coefficients of a power series of z:

$$\tilde{p}_x^N(z) = \sum_{t=1}^{\infty} p_x^N(t) z^t \qquad \tilde{r}_x^N(z) = \sum_{t=1}^{\infty} r_x^N(t) z^t \tag{3.11}$$

The details of the derivation are shown in Appendix A. Finally, we can obtain the total absorption probability in the infinite time limit (see Theorem 2 in [59]).

Theorem 3.1.1

$$P_{x_0}^N(\phi) = C_1|\alpha|^2 + C_2|\beta|^2 + 2Re(C_3\bar{\alpha}\beta)$$

with initial state $\phi =^T [\alpha, \beta]$ *and*

$$C_1 = \frac{1}{2\pi}\int_0^{2\pi} \left|a\tilde{p}_x^N(e^{i\theta}) + c\tilde{p}_x^N(e^{i\theta})\right|^2 d\theta$$
$$C_2 = \frac{1}{2\pi}\int_0^{2\pi} \left|b\tilde{p}_x^N(e^{i\theta}) + d\tilde{p}_x^N(e^{i\theta})\right|^2 d\theta$$
$$C_3 = \frac{1}{2\pi}\int_0^{2\pi} \overline{(a\tilde{p}_x^N(e^{i\theta}) + c\tilde{p}_x^N(e^{i\theta}))}(b\tilde{p}_x^N(e^{i\theta}) + d\tilde{p}_x^N(e^{i\theta}))d\theta$$

This gives the absorption probability for a general SU(2) coined walk, from a general starting position and state and for general wall locations. This very general formulation has two downsides: first, it only gives the infinite time limit, although by explicitly inverting the generating functions, Equation 3.10 also gives the finite time case. For every scenario the coefficients have to be obtained from the recurrence relations and given their complicated form, it is often impossible to solve the integrals analytically. Therefore, although the answer is exact, it is too complicated to get a practical intuition of the underlying process.

Other objections to this method could be that the partial measurement protocol as absorbing boundaries is not a real physical process since it requires an active experimenter that stops the walk whenever the particle is found at the boundary. In the next section, we analyze the walk from a more physical example, where we use a matrix change to induce scattering behavior, mimicking a partially transmitting boundary. Specifically, we will analyze this system by adopting the Schrödinger method presented earlier.

3.1.2 Transmittive boundaries by matrix change

Since the quantum particle is spreading like a wave over the position space, the notion of absorption becomes less clear. Strictly speaking, once the wave function hits the boundary, this represents a certain probability that the particle is at the boundary. In the classical case, the absorption probability is formed by looking at a large number of particles. However, in the quantum case, we have only 1 quantum particle that is responsible for the probability distribution. That means that when imposing an absorbing boundary in the classical sense, the probability of being absorbed is essentially the probability of the quantum particle to be at that location at the time of measurement. By implementing a continuous partial measurement protocol, you project onto the bulk states of the system, thereby removing the part of the probability function that indicates the chance of the particle being at the boundary. That means that the probability is not conserved in this case. More figuratively speaking, only part of the particle keeps propagating.

In the last section, we presented the path counting method that calculates the probability of absorption as the number of possible paths leading to the wall. Here, we take a more physical approach, studying the transmission of waves in the presence of some attractive potential. In the quantum walk language, we do this by changing the coin operator to the Pauli z matrix after the boundary. This means that beyond the boundary, there is no more mixing between left and right and once the wave is transmitted, it just wanders off to infinity. This approach is more 'physical' since the total probability over the whole region is conserved. We interpret the part of the wave that is transmitted through the potential as the absorbed part.

Since we now have a transmittive boundary, part of the wave will also be reflected. Exactly this reflection property gives the walk in this set-up similar properties as removing part of the wavefunction does in terms of interference [47]. This is another motivation to use the more physical notion of transmission. Therefore, we imagine a boundary with a variable reflection coefficient. Note that the boundary here is effectively implemented by changing the evolution operator beyond the boundary location.

For the most part we combine the approaches of [47] and [65]. Let us first consider a semi infinite line system with a boundary at n=M. Specifically, we consider the following evolution under the general SU(2) coin:

$$C_{\xi,\theta,\zeta,\phi} = e^{i\phi}\begin{pmatrix} e^{i\xi}\sqrt{\rho} & e^{i\zeta}\sqrt{1-\rho} \\ e^{-i\zeta}\sqrt{1-\rho} & -e^{-i\xi}\sqrt{\rho} \end{pmatrix} \tag{3.12}$$

Once the walker hits the boundary, right movers can be either transmitted through or be reflected, with the ratio depending on the reflection coefficient r. Since only right moving waves can be transmitted through a boundary on the right, there are no left movers outside the domain. This condition gives the following evolution matrix and boundary conditions:

$$\begin{pmatrix} \psi^L(x,t) \\ \psi^R(x,t) \end{pmatrix} = \begin{pmatrix} \sqrt{\rho}e^{i\xi}L(x+1,t-1) + e^{-i\zeta}\sqrt{1-\rho}R(x-1,t-1) \\ e^{-i\zeta}\sqrt{1-\rho}\psi^L(x-1,t-1) - e^{-i\xi}\sqrt{\rho}\psi^R(x-1,t-1) \end{pmatrix} \text{for } x < M-1 \tag{3.13}$$

$$\begin{pmatrix} \psi^L(M,t) \\ \psi^R(M,t) \end{pmatrix} = \begin{pmatrix} L(M+1,t-1) \\ L(M-1,t-1)\sqrt{1-\rho}e^{i\zeta} - R(M-1,t-1)\sqrt{\rho}e^{-i\xi} \end{pmatrix} \tag{3.14}$$

$$\begin{pmatrix} \psi^L(x,t) \\ \psi^R(x,t) \end{pmatrix} = \begin{pmatrix} L(x+1,t-1) \\ kR(x-1,t-1) \end{pmatrix} \text{with } k = \begin{cases} \sqrt{1-r^2} & \text{if } x = M+1 \\ 1 & \text{if } x > M+1 \end{cases} \tag{3.15}$$

And finally the boundary condition:

$$\begin{pmatrix} \psi^L(M-1,t) \\ \psi^R(M-1,t) \end{pmatrix} = \begin{pmatrix} L(M,t-1) + rR(M,t-1) \\ L(M-2,t-1)\sqrt{1-\rho}e^{i\zeta} - R(M-2,t-1)\sqrt{\rho}e^{-i\xi} \end{pmatrix} \tag{3.16}$$

Furthermore, we know that since there are no left-movers beyond the right boundary $L(M,t-1) = 0$. For this to be satisfied at all times $L(M-1,t) = rR(M,t-1)$, different waves

with the same eigenvalue should destructively interfere. We can enforce this by introducing an image particle outside the boundary, such that we write the total wavefunction as:

$$\begin{aligned}\begin{pmatrix}\psi^L(x,t)\\ \psi^R(x,t)\end{pmatrix} = \sum_{k\in(-\pi/2,\pi/2)} e^{-i\omega_{k\pm}t}\Big[\Big(C_{k\pm}\begin{pmatrix}A_{k\pm}\\ B_{k\pm}\end{pmatrix}e^{ikn} + C_{\pi-k\pm}\begin{pmatrix}A_{\pi-k\pm}\\ B_{\pi-k\pm}\end{pmatrix}e^{i(\pi-k)n}\Big)\\ + \Big(D_{k\pm}\begin{pmatrix}A_{k\pm}\\ B_{k\pm}\end{pmatrix}e^{ik(n-2(M-1))} + D_{\pi-k\pm}\begin{pmatrix}A_{\pi-k\pm}\\ B_{\pi-k\pm}\end{pmatrix}e^{i(\pi-k)(n-2(M-1))}\Big)\Big]\end{aligned} \tag{3.17}$$

Imposing the boundary condition gives:

$$D_{k\pm} = \frac{-C_{\pi-k\pm}e^{i\omega_{\pi-k\pm}}A_{\pi-k\pm}e^{i(\pi-k)(M-1)} - rB_{\pi-k\pm}e^{i(\pi-k)M}}{e^{i\omega_{k\pm}}A_{k\pm}e^{-ik(M-1)} - rB_{k\pm}e^{-ik(M-2)}} \tag{3.18}$$

Here $A_{k\pm}$ and $B_{k\pm}$ denote the eigenfunction of the evolution operator. For the one-parameter Hadamard coin these are given by Equation 2.13. Similarly, they can be derived for the more general SU(2) coin as will be done in the next section.

So left from the boundary we can write the wavefunction as:

$$\begin{pmatrix}\psi^L(x,t)\\ \psi^R(x,t)\end{pmatrix} = \sum_{k\in(\pi/2,\pi/2} e^{-i\omega_{k\pm}t}\Big[\mathcal{F}_{k\pm}\begin{pmatrix}A_{k\pm}\\ B_{k\pm}\end{pmatrix}e^{ikn} + \mathcal{G}_{k\pm}\begin{pmatrix}A_{\pi-k\pm}\\ B_{\pi-k\pm}\end{pmatrix}\Big] \tag{3.19}$$

with

$$\begin{aligned}\mathcal{F}_{k\pm} &= C_{k\pm} - e^{-2ik(M-1)}C_{\pi-k\pm}\frac{e^{i\omega_{\pi-k\pm}}A_{\pi-k\pm}e^{i(\pi-k)(M-1)} - rB_{\pi-k\pm}e^{i(\pi-k)M}}{e^{i\omega_{k\pm}}A_{k\pm}e^{-ik(M-1)} - rB_{k\pm}e^{-ik(M-2)}}\\ \mathcal{G}_{k\pm} &= C_{\pi-k\pm} - e^{-2i(\pi-k)(M-1)}C_{k\pm}\frac{e^{i\omega_{k\pm}}A_{\pi-k\pm}e^{ik(M-1)} - rB_{\pi-k\pm}e^{ikM}}{e^{i\omega_{k\pm}}A_{k\pm}e^{-i(\pi-k)(M-1)} - rB_{k\pm}e^{-i(\pi-k)(M-2)}}\end{aligned} \tag{3.20}$$

From this wavefunction we can calculate the probability to escape transmission through the wall by identifying the survival probability as:

$$\Lambda^M = \int_{\frac{-\pi}{2}}^{\frac{\pi}{2}} (|\mathcal{F}_{k\pm}|^2 + |\mathcal{G}_{k\pm}|^2)dk \tag{3.21}$$

Because the total probability is normalized to 1, this also gives us the probability to be absorbed.

We could apply the same approach to the two boundary case, where on the left only left movers can be transmitted. In this setup, we need to account for double reflected waves that go back and forth between the boundary before being transmitted. In other words, in order to satisfy the boundary conditions based on destructive interference on both sides, we have to introduce an infinite amount of image particles, one for each reflected wave. This is not analytically feasible. However, it is still possible to get an idea about the absorption/ transmission at one wall in the presence of the other wall by using the reflection probability and escape probability from the other wall. First, let us write the possible types of waves as a geometric series recalling that the probability of reflection is r^2 and therefore the probability

of absorption is $1 - r^2$. Distinguishing wall 1 and 2 we can write all possible paths that lead to absorption as:

$$\begin{aligned}&(1 - r_1^2)(1 + r_1 r_2 + (r_1 r_2)^2 + (r_1 r_2)^3 + ...\\ &= \frac{(1 - r_1^2)}{1 - r_1 r_2}\end{aligned} \tag{3.22}$$

Using the survival probability from the other wall, we can write the transmission probability at the first wall as [47]:

$$P_1^N = \Lambda^M \frac{(1 - r_1^2)}{1 - r_1 r_2} \tag{3.23}$$

Just like before, this is the absorption probability in the infinite time limit. Because only the asymptotic limit is considered, the influence of different coin parameters and the initial state is not visible. These will mainly have an effect in finite time. Unfortunately, an analytical solution at an arbitrary time under arbitrary conditions is highly non-trivial to obtain, as we also saw in the previous section. To investigate the use of quantum walks in decision making we will therefore mainly use simulations. First of all, we will, however, show how the different parameters influence the dynamics of the quantum walk and therefore the absorption probability.

3.2 Biasing Quantum walks

In the classical SRDT framework the objective probabilities were encoded in the distance to the boundary. In addition, a value dependent potential was added on the two half-lines to either attract or repel the particle to the boundary. Together, these two factors bias the random walker in a certain direction. The novelty of this approach is that the probability and the value affect the walker in a non-separable way, with the diffusion coefficient determining their relative importance. To translate this set-up to the quantum walk and investigate further options, we first show how a quantum walk can be biased in general.

The important difference between a random walk and a quantum walk is that we now have an extra degree of freedom, the spin. In the random walk, the movement of the walker is determined by flipping a (possibly biased) coin. In the quantum walk, the walking direction is given by a rotation of the internal state given by the quantum coin operator. It is important to note that the name 'coin operator' is somewhat misleading in this case. What the coin operator does is basically rotating the basis in which you measure the internal state of the particle [20]. Therefore, it creates a superposition of the two spin states according to which the walker moves to the left and right in one step. This is a deterministic process and for a time- and space independent coin the rotation will be the same throughout the whole process. Therefore, different than for the random walk the dynamics are not the result of picking a move at random from a distribution. The probabilistic nature of the quantum process instead lies in the fact that upon measurement the wavefunction will collapse to a point with the probability for each point given by the underlying distribution.

We first consider a one-dimensional quantum walk in unbounded space. The tools to bias can be categorized into coin operator bias and shift operator bias. In addition the initial state and position of the walker also influence the evolution. However, there is a degeneracy in the bias in the initial spin state and coin state for example. Put differently, even when the

initial state is fixed, we can get te full range of possible quantum walks by adjusting the coin operator and vice versa.

We consider the $SU(2)$ coin, which is the most general two-dimensional rotation matrix:

$$C_{\xi,\rho,\zeta,\phi} = e^{i\phi} \begin{pmatrix} e^{i\xi}\sqrt{\rho} & e^{i\zeta}\sqrt{1-\rho} \\ e^{-i\zeta}\sqrt{1-\rho} & -e^{-i\xi}\sqrt{\rho} \end{pmatrix} \tag{3.24}$$

We can ignore the factor $e^{i\phi}$, as it is just a global phase with no effect on the distribution. The shift operator still looks the same as before (Equation 2.4), i.e. the right-handed coin state is shifted one step to the right and the left-handed one step to the left.

To get a first intuition of how the different parameters bias the walk we can write out one evolution step by applying the operator to the general initial state $|\psi(n,0)\rangle = \begin{pmatrix} \alpha \\ \beta \end{pmatrix} \otimes |0\rangle$[1]

$$|\psi(n,1)\rangle = (e^{i\xi}\sqrt{\rho}\alpha + e^{i\zeta}\sqrt{1-\rho}\beta)\,|-1\rangle + (e^{-i\zeta}\sqrt{1-\rho}\alpha - e^{-i\xi}\sqrt{\rho}\beta)\,|1\rangle \tag{3.25}$$

To make the bias more clear, we now calculate the probability to be found in position -1 after one step

$$\left|\psi^L\right|^2 = |\psi(-1,1)|^2 = \rho|\alpha|^2 + e^{i(\xi-\zeta)}\sqrt{\rho}\sqrt{1-\rho}\alpha\beta^* + \sqrt{1-\rho}\sqrt{\rho}\alpha^*\beta e^{i(\zeta-\xi)} + (1-\rho)|\beta|^2 \tag{3.26}$$

Now we separate the effects of the coin and the initial state by first considering the initial state: $|\psi(n,0\rangle = \frac{1}{\sqrt{2}}\begin{pmatrix} 1 \\ i \end{pmatrix}$ which, without additional bias, leads to a symmetric distribution. Then the probability to move left or right is:

$$\begin{aligned} \left|\psi^L\right|^2 &= \frac{1}{2}(\rho + ie^{i(\xi-\zeta)}\sqrt{\rho}\sqrt{1-\rho} + i\sqrt{1-\rho}\sqrt{\rho}e^{-i(\xi-\zeta)} + 1 - \rho \\ &= \frac{1}{2}(1 - 2\sqrt{\rho}\sqrt{1-\rho}\sin(\xi-\zeta)) \\ \left|\psi^R\right|^2 &= \frac{1}{2}(1 + 2\sqrt{\rho}\sqrt{1-\rho}\sin(\xi-\zeta)) \end{aligned} \tag{3.27}$$

We can immediately see that the walk is symmetric only if $\xi = \zeta$. Since only the difference between the two factors matters, we can achieve the full range of bias by only using one exponential term as long as we adjust the range of that term to $\xi \in (-\pi, \pi)$. Also, note that ρ does not bias the walk, but regulates how strong the bias acts. Indeed, given a fixed value of $\xi - \zeta$, ρ regulates the spreading of the walk. See Figure 3.1 for two examples.

As mentioned before, the bias in the coin and initial state have some degeneracy. To investigate this, we will use the Fourier analysis of the walk as introduced in Section 2.3. We will now do this for the general walk.

[1] For simplicity we chose the initial position to be $x_0 = 0$, the unbounded line is translationally invariant, therefore this choice is without loss of generality. Note that this will be different in a situation with boundaries.

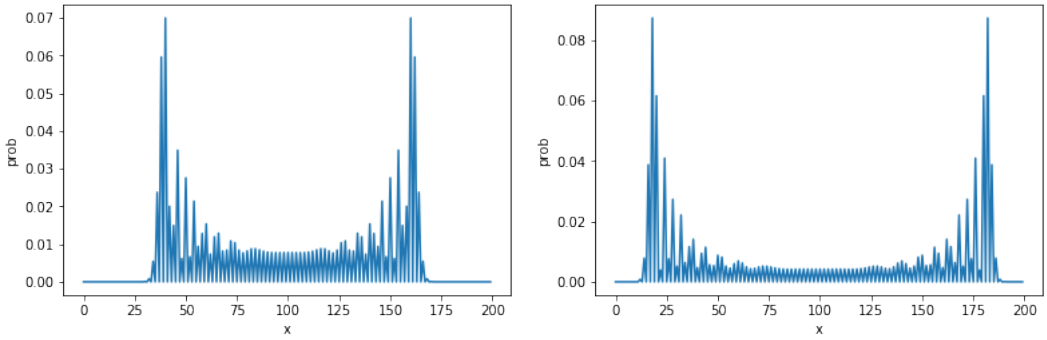

Figure 3.1. – Quantum walk for $\rho = 0.4$ (left) and $\rho = 0.7$ (right) starting from the symmetric initial state and without additional bias in the coin.

To be more specific, we use the fact that $|\alpha|^2 + |\beta|^2 = 1$ for a normalized initial state to parametrize the initial state as $|\psi(n,0)\rangle = \begin{pmatrix} \sqrt{\eta} \\ \sqrt{1-\eta}e^{i\alpha} \end{pmatrix} \otimes |0\rangle$. Using the Fourier transform 2.9, the initial state in momentum space is: $\left|\tilde{\psi}(k,0)\right\rangle = \begin{pmatrix} \sqrt{\eta} \\ \sqrt{1-\eta}e^{i\alpha} \end{pmatrix}$. The coin operator in momentum space is:

$$\tilde{U}_{\xi,\theta,\zeta,\phi}(k) = \begin{pmatrix} e^{i\xi}\sqrt{\rho}e^{-ik} & e^{i\zeta}\sqrt{1-\rho}e^{-ik} \\ e^{-i\zeta}\sqrt{1-\rho}e^{ik} & -e^{-i\xi}\sqrt{\rho}e^{ik} \end{pmatrix} \tag{3.28}$$

The evolution is now given by:

$$\left|\tilde{\psi}(k,t)\right\rangle = \tilde{U}(k)^t \left|\tilde{\psi}(k,0)\right\rangle.$$

As usual, we proceed by diagonalizing $\tilde{U}$. The eigenvalues are given by:

$$\lambda_\pm = -i\sqrt{\rho}\sin(\xi - k) \pm \sqrt{1 - \rho\sin^2(\xi - k)}. \tag{3.29}$$

Since $\tilde{U}(k)$ is still a unitary matrix, we can write eigenvalues as:

$$\lambda_\pm = e^{-i\omega_k^\pm}$$

Where:

$$\begin{aligned} \sin\left(\omega_k^+\right) &= \sqrt{\rho}\sin(\xi - k) \\ \omega_k^- &= \pi - \omega_k^+ \end{aligned} \tag{3.30}$$

The eigenvectors are given by:

$$\begin{aligned} \left|v_k^+\right\rangle &= \frac{1}{\mathcal{N}_k^+}\begin{pmatrix} \sqrt{1-\rho} \\ e^{-i(\omega_k^\pm + \zeta - k)} - e^{i(\xi-\zeta)}\sqrt{\rho} \end{pmatrix} \\ \left|v_k^-\right\rangle &= \frac{1}{\mathcal{N}_k^-}\begin{pmatrix} \sqrt{1-\rho} \\ -e^{i(\omega_k^\pm - \zeta + k)} - e^{i(\xi-\zeta)}\sqrt{\rho} \end{pmatrix} \end{aligned} \tag{3.31}$$

with the normalization factors being:

$$\mathcal{N}_k^\pm = 2 \mp 2\sqrt{\rho}\cos(k \mp \omega_k^+ - \xi)$$

We can now write the evolution of the initial state in terms of the eigenvalues and eigenvectors. Therefore we need to decompose the initial state into eigenvectors of the evolution operator:

$$\left|\tilde{\psi}(k,t)\right\rangle = e^{-i\omega_k^+ t}\left|v_k^+\right\rangle\left\langle v_k^+\middle|\tilde{\psi}(k,0)\right\rangle + e^{-i\omega_k^- t}\left|v_k^-\right\rangle\left\langle v_k^-\middle|\tilde{\psi}(k,0)\right\rangle$$

The inner products are:

$$\left\langle v_k^\pm\middle|\tilde{\psi}(k,0)\right\rangle = \frac{1}{\mathcal{N}^\pm}(\sqrt{1-\rho}\sqrt{\eta} + \sqrt{1-\eta}e^{i(\alpha+\zeta)}(e^{i(\mp\omega_k^+ - k)} - e^{-i\xi}\sqrt{\rho}) \tag{3.32}$$

This equation already gives us insights into the interplay between parameters:

- ρ and η appear in non-trivial ways and therefore have a unique effect on the distribution.
- α only occurs in combination with ζ and ζ does not appear anywhere else. This shows the degeneracy of these bias factors, meaning that we can restrict to using only one of them.

3.3 Subjective probabilities

Based on the previous section we use the following set-up as an extension of the classical SRDT framework. The initial position of the particle between the boundaries is determined by the objective probabilities. For the simulations, we choose to fix the walls at locations 0 and N such that the whole walk takes place on 'positive' positions. Specifically, for a general lottery $L_1 = [o_A, p; o_B, 1-p]$ we associate the left wall with outcome o_A. The initial position will be $x_0 = (1-p) \times N$ where N is the distance between the two absorbing walls. This formula is such that the higher the probability of the event (p), the shorter the distance to the corresponding wall. Since there is no classical counterpart of the coin state, we initialize the system in the state $\psi = \frac{1}{\sqrt{2}}\begin{pmatrix}1\\ i\end{pmatrix}$, which will give a symmetric walk in absence of any bias.

We first look at the situation without any value bias. In this case, SRDT predict an inverse S-shaped relation between the subjective probability given by the relative absorption probability and objective probability of o_A. To extract the absorption probability in the quantum case we use the partial measurement protocol described in Section 3.1. At the end of the simulation (a predefined time T), the subjective probability of outcome A is calculated as the probability of being absorbed by the left boundary divided by the total probability of being absorbed. Note that in all cases, this will be different than the absolute absorption probability because the quantum particle has a non-zero probability to escape all measurements.

We will use the generalized Hadamard coin:

$$H = \begin{pmatrix}\sqrt{\rho} & \sqrt{1-\rho}\\ \sqrt{1-\rho} & -\sqrt{\rho}\end{pmatrix} \tag{3.33}$$

In figure 3.2 we show the subjective probability: $\pi(p) = \frac{P(B_L)}{P(B_L)+P(B_R)}$ as a function of p for different values of ρ. Here $P(B_L)$ $(P(B_R))$ is the probability of being absorbed by the left (right) wall.

As we can see in Figure 3.2, for particular values rho we do retrieve a similar inverse S-shape as in the classical case. Note that we fixed the time, or equivalently the number

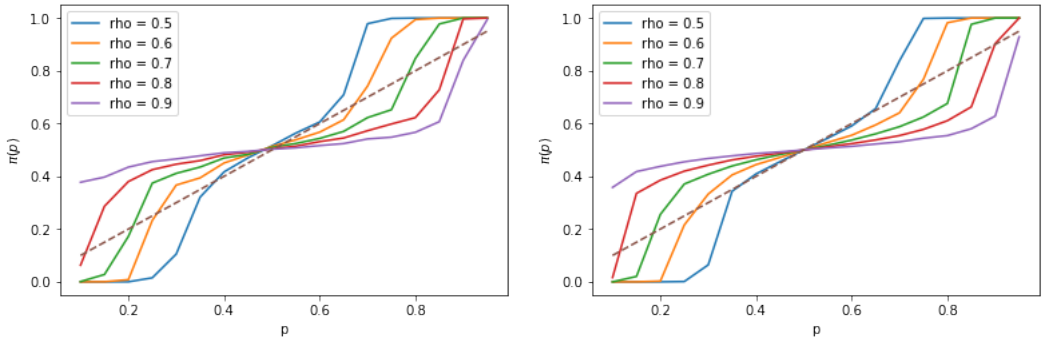

Figure 3.2. – Subjective probability as a function of p for different values of ρ. The number of steps equals the distance between the boundaries, left panel: $T = N = 50$, right panel $T = N = 100$.

of steps, to the distance between the boundaries. Although the ratio between the distance between the boundaries and the number of steps is equal in both figures, we still see a small difference in shape. In further analyses, we will usually fix the number of sites and steps to be equal, not explicitly stating the effect of their absolute magnitude. We have to keep in mind however that the absolute values do have a small effect on the result.

Recall that ρ does not bias the walk, but regulates the variance of the walk through the mixing between the left and right component. For $\rho = 1$ there is no mixing between the two components. That means, the part of the walk that was in the left-handed part of the initial state will walk left and the right-handed part will go right without any interference occurring. In the Bloch wave formulation, two Bloch waves are created in the first step which then both move in their own direction without interfering. This means that the two peaks will just travel away from each other until they have reached the boundary. The absorption probabilities will exactly reflect the initial spin state, which is, in this case, symmetric, so the absorption probability will be 0.5 at both walls.

In the other extreme $\rho = 0$ there is complete mixing between the two components. This means that the walker will stay localized around the starting position and will never reach either wall. This is like two Bloch waves being trapped between mirrors. The distribution will alternate from two equal peaks at the 2 positions just next to the boundary at even steps and one peak at the initial position at odd steps. For all intermediate values, there will be some mixing between the components, determining the spreading rate of the walk. Note that ρ does not alter the relative magnitudes of the peaks. However, because it regulates the variance, it can enhance or decrease the effect of the initial position. For a relatively low value of rho, the variance will be small and therefore the boundary that is hit first will receive a high portion of the wave-function at once, therefore the effect of the starting position is amplified. If we compare this to the double S-shape obtained in the classical version of the theory we can see strong similarities with the curves of $\rho = 0.7$ and $\rho = 0.8$ where we also find this pattern.

We now want to add a value bias similar to the value dependent potential in SRDT. In the quantum walk case, the simplest way to add a left/right bias in a coherent way is through the coin. To be able to compare with the classical framework, we will employ different bias values on the two half-lines. For the quantum walks, this means that we have at least two different evolution operators. The weak position dependence of the operator leads to some decoherence in the system. It is therefore important to keep in mind that introducing the value

bias has a non-trivial effect on the distribution. In the Bloch wave analogy, we can imagine electrons traveling through two different types of solids. Since we use the starting position of the walker to represent the objective probabilities, the walker starts out in one solid and then travels towards the other one. This leads to reflection/ transmission effects at the border between the two solids. The general form of the biased coin is:

$$C = \begin{pmatrix} \sqrt{\rho}e^{i\theta} & \sqrt{1-\rho} \\ \sqrt{1-\rho} & -\sqrt{\rho}e^{-i\theta} \end{pmatrix} \tag{3.34}$$

Note that because the bias is determined by the difference in exponential factors (as discussed in Section 3.2) we only have to add a bias on the diagonal of the matrix to be able to bias both to the right and left. From Equations 3.27 we see that the bias follows a sinus. Therefore, the bias will be maximal for $\theta = \pm\pi/2$. We still have freedom in how to translate the value of an outcome to the bias factor. This is also the case in the classical framework. The only requirement is that the function is non-decreasing in the value. We will, therefore, take a holistic approach and focus on the effects of different values of θ. For a symmetric initial state, the transition probabilities is one step are given by:

$$\begin{aligned} \left|\psi^L\right|^2 &= \frac{1}{2} - \sqrt{\rho}\sqrt{1-\rho}sin(\theta) \\ \left|\psi^R\right|^2 &= \frac{1}{2} + \sqrt{\rho}\sqrt{1-\rho}sin(\theta). \end{aligned} \tag{3.35}$$

Note that the $\sin\theta$ bias is now the equivalent of the value dependent force in the classical case, with an acting strength regulated by ρ.

In analogy to the classical case, there is no value bias at the origin, giving the particle a 50/50 percent chance to go left or right. To summarize, we have three coins in our system, corresponding in spirit to the piece-wise linear potential of the classical theory (Eq. 1.7):

$$\hat{C}_x = \begin{cases} \begin{pmatrix} \sqrt{\rho}e^{i\theta_1} & \sqrt{1-\rho} \\ \sqrt{1-\rho} & -\sqrt{\rho}e^{-i\theta_1} \end{pmatrix} \text{ if } x < x_0 \\ \begin{pmatrix} \sqrt{\rho} & \sqrt{1-\rho} \\ \sqrt{1-\rho} & -\sqrt{\rho} \end{pmatrix} \text{ if } x = x_0 \\ \begin{pmatrix} \sqrt{\rho}e^{i\theta_2} & \sqrt{1-\rho} \\ \sqrt{1-\rho} & -\sqrt{\rho}e^{-i\theta_2} \end{pmatrix} \text{ if } x > x_0 \end{cases} \tag{3.36}$$

As the simplest case, we first investigate the situation where there is a value bias with varying strength on the left part of the line and no bias on the right half. Reducing the number of coins to two. Second, we use three different coins corresponding to two different attractive forces in the classical case.

In Figure 3.3 we plot the subjective probability as a function of p for different values of θ and ρ. Note that the blue line always denotes the baseline $\theta = 0$. We see that for $\rho = 0.9$ non-zero values of θ shift the curves upwards for small p-values. This means that the probability of being absorbed by the left wall is enhanced by the bias to the left, as expected. However, for smaller values of ρ the effects are very small and they mainly act when the particle starts closer to the left wall (large p-values). This is also expected behavior since the bias to the left only acts on the left half of the line. Therefore, if the particle starts out

far from the left wall, it takes a long time (especially for small values of ρ) to enter the bias region. When an opposite direction bias is present on the right side, the probability of being absorbed on the left when starting on the right half-line becomes smaller, also as expected. The differences are larger for small values of ρ. Compared to the case without bias, there is an even sharper transition around $p = 0.5$. The presence of the bias on the right side however only has a very small effect on the influence of the value bias on the left side for larger values of p. This is related to the fact that bias only acts locally. These plots also show that the influence of the starting point is very large. Since in the first step the two Bloch waves are prepared, in which region you start has a very large effect on the final absorption probability, with θ amplifying or damping the absorption probability depending on starting location.

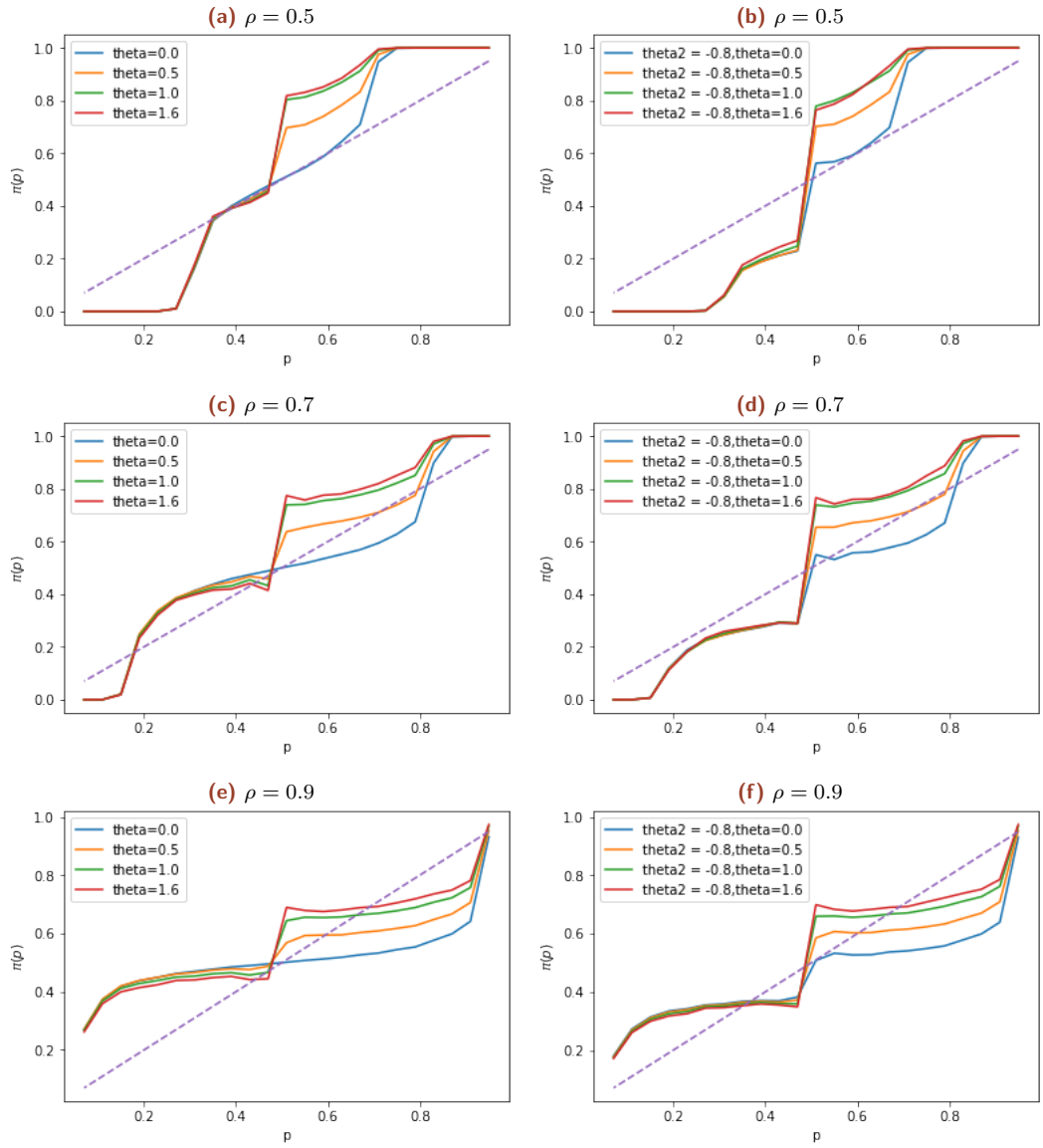

Figure 3.3. – Subjective probability of outcome o_A as a function of the objective probability which is encoded in the initial position for different values of ρ and θ_1 and θ_2. The left column only has a value bias on the left half of the line, the right column has a bias over the whole regions. Here the bias on the right side is fixed, the bias on the left side is varied. In all cases $T = N = 100$.

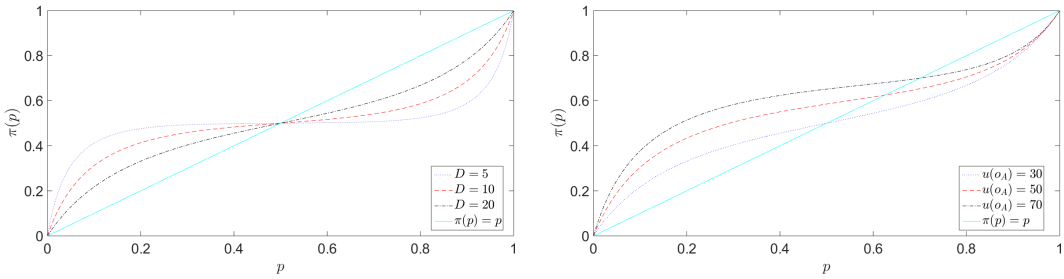

Figure 3.4. – Subjective probability of outcome o_A following Equation 1.10 as a function of the objective probability which is encoded in the initial position. In the left panel, the distribution is plotted for different values of the Diffusion coefficient and fixed $u(o_A) = u(o_B)$, while $u(o_A)$ is varied in the right panel. On the right, D=20 for all curves.

An alternative approach is to let one bias work over the whole region. This keeps the quantum walk coherent and therefore has a more trivial effect. This is however different from the classical framework since one option is now favored over the whole region. That means, that at each evolution step, the probability of moving to the left is enhanced, also if you are already close to the right wall. This right wall has no additional attraction power in this model.

3.4 Interpretation of the Results

The above analysis shows how some of the results found using the classical random walk can be reproduced with the quantum walk. For example, the inverse S-shape dependence on the initial position can be found for particular values of ρ. In addition, with the quantum walk, we have more parameters to play with than in the classical case. First of all, the value of ρ determines a large part of the dynamics. Since ρ is associated with the mixing between the internal states of the quantum walk, we could interpret this as the measure of 'quantumness' in the system. In the extreme case $\rho = 1$ there is no mixing between the right and left moving wave and the subjective probability will represent the initial state. In the other extreme case $\rho = 0$ there is complete mixing between the components and the walk will be concentrated on the initial state or his two neighbors. Therefore, the walker will not be absorbed at all. In all intermediate cases, the components mix, and therefore interference arises. Note that when $\rho < 0.5$ the left component is mainly determined by the right component of its neighbor. This very strong mixing regime seems less useful for our conceptual use. We can interpret this interference as the decision-maker exploring different paths that interfere with each other when they are in the same location. So instead of averaging over a large number of walkers in the classical case, the quantum walk represents all these paths at the same time, allowing them to interfere.

When it comes to adding a value bias, the exponential terms in the coin seem the most straightforward term to bias the walk to the left or right, starting from a symmetric initial state. The bias arises because constructive interference is promoted on the favored side, while extra destructive interference arises on the other hand. We see that the effect is most pronounced for $\rho = 0.5$. Furthermore, when using different coins on different parts of the line leads to a sharp transition around $p = 0.5$ related to the fact that the bias only acts locally.

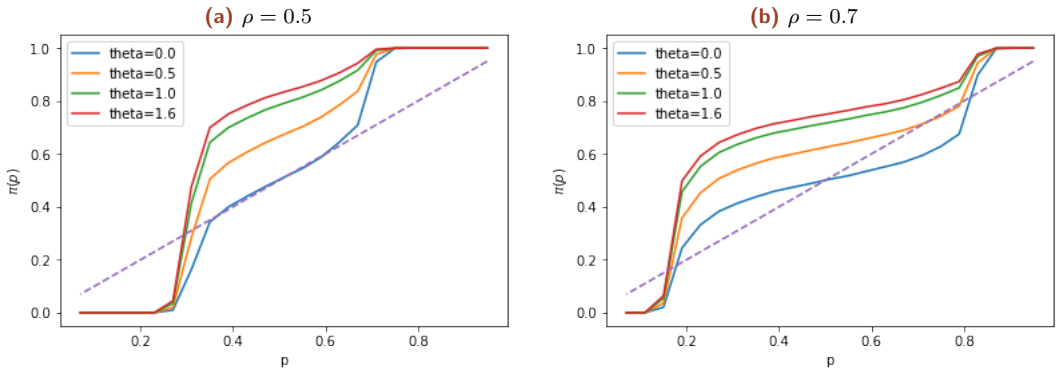

Figure 3.5. – Subjective probability of outcome o_A as a function of the objective probability which is encoded in the initial position for different values of ρ and θ. The same (biased) coin is used over the spatial region. In all cases $T = N = 100$.

In Figure 3.4 we show the value distorted probability derived in the classical SRDT frame (see Section 1.2). In this case, we clearly see an inverse S-shape for all values of D. When varying the value bias in the left half, we see an overall rise in absorption probability on the left side. The intersection with the bisector is shifted to the right.

Comparing the classical and quantum case, we see some large differences in the effect of value bias. Where in the classical case there is an overall shift upwards in the absorption probability, in the quantum walk this is only local. This is due to the fact that changing the coin along the line leads to transmission and reflection effects on top of a change in bias. This also means that the intersection with the bisector is always at $p = 0.5$. Alternatively, if we applied the same coin over the whole region, with a bias towards one side, the effects would be more similar to the classical case. This is shown in Figure 3.5.

Because there is no classical counterpart of the spin, we chose the symmetric state as the initial state in the analysis. However, already from the 'rational' case $\rho = 1$ we can see that the initial state has a large influence on the behavior. In the classical case, the diffusion coëfficient determined the relative importance of value and probability. Although ρ has a large influence on the dynamics, it does not seem to do play the same role in the quantum case. Instead of converging to the diagonal ($\pi(p) \to p$) for large values of D, the distribution converges to the initial state for large values of ρ. We deduce that ultimately the initial spin state has a stronger influence on the dynamics than the initial position. If we again draw the analogy to a Bloch wave, this is expected. In the first step, two Bloch waves are created that both move in opposite directions. As long as the number of time steps is such that both waves can reach the boundary they are moving to, the differences in absorption will be determined by the initial state and the interference and not so much the position. At short times, however, the position bias can have a very large effect if one of the peaks already reached the boundary while the other one has not.

While we can retrieve some of the behavior (inverse-S, shifting of the curves) from the classical case with the quantum framework, the distribution in position space is very different. In the classical case, the total distribution of random walkers will give a Gaussian, here we have a wide variety of distribution once we include bias factors. The initial spin state plays an important role in the dynamics of the quantum walk but has no classical counterpart. Therefore, we used the symmetric initial state for the analysis. In future chapters we will

explore the full potential of the quantum walk by, among other things, varying this initial state.

Going beyond SRDT

4

In the previous chapter, we extended the classical SRDT to the quantum world by making use of a quantum walk. To that end, we used the exponential factors in the coin and the starting position to bias the walk. In this chapter, we will leave the classical SRDT framework behind and explore how quantum walks can be used and interpreted in general in the context of decision making. In the first section we investigate the influence of the initial spin state on the dynamics and use this to encode the objective probabilities of the alternatives. Second we change the interpretation of the abstract space the walker moves in and explore the possibilities of biasing the shift operator. We then shortly look at the effects of 'boundaries' on the evolution. Afterwards, we discuss the choice between lotteries rather than the formation of subjective probabilities. We finish with the introduction of the Entropy of Measurement as a measure for the uncertainty of the choice.

4.1 Objective probability in the initial state

In the previously presented quantum extension of SRDT, the interpretation of ρ was still unclear. Where in the classical case the diffusion coefficient regulates the relative importance of value and initial position bias, this can not be said of ρ. In the extreme case of $\rho = 1$, the probability distribution in position space will be a two-peak distribution with relative magnitude given by the initial spin state. The crucial role of the initial spin state leads us to another parametrization: rather than encoding the objective probabilities of events into branch lengths, we encode them in the initial coin state. For non-zero values of ρ the two probability start to mix leading to a spread out of the probability distribution. This mixing of probabilities is essentially an irrational effect. In this context, ρ is governing the level of 'irrationality' or the 'quantumness' of the decision-maker. One could imagine that the level of irrationality is determined by the character of the decision-maker, but also by the difficulty of the problem. For example, if two outcomes are relatively close in expected value, it is harder to distinguish them. This concept of 'irrationality' in the decision-maker resonates with the notion of bounded rationality [7]. It represents the fact that humans are not always able to assess probabilities truthfully and rationally. On top of that, we could again add a value bias to also influence the probability assessment.

Putting the objective probabilities in the intitial spin state is also appealing from another quantum point of view. We can draw the analogy with the concept of unobserved variables in quantum mechanics. [66]. Due to the conditional form of the shift operator, the spin and the position of the coin are entangled. The movement of the coin in position space is determined by its internal state. If we just look at the position space probability distribution (as we also do when looking at the absorption probability), we trace out the coin. That means that the coin state is essentially unobserved. However, because of the entanglement, it is still possible to obtain information about the coin state through the position space distribution.

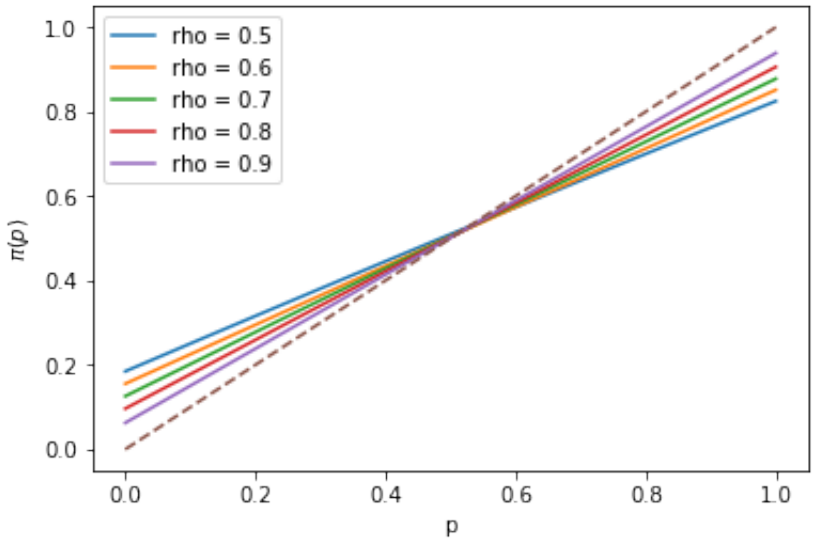

Figure 4.1. – Probability of being absorbed by the left wall as a function of 'p' in the initial coin state $(\sqrt{p}, i\sqrt{1-p})^T$ for different values of ρ.

Descriptively, if we look at a lottery we see something very similar. When playing a lottery, the outcomes are directly visible and can be assessed realistically. The probability, however, will only be visible after a large number of tries. In the frequentist interpretation, the probability is the number of times you get outcome A out of N tries when $N \to \infty$. Counting the frequencies of a limited number of tries only, the observed frequencies can strongly deviate from the objective probabilities. If we encode the objective probabilities in the initial coin state and look at the absorption probabilities we can interpret this as gaining information about the initial coin state. In the extreme case $\rho = 1$ that we can call 'rational' in this case, the absorption probability will be equal to the objective probability. However, when the assessment is imperfect ($\rho < 1$) because of bounded rationality and possibly value effects, the absorption probabilities, and thus the 'observed' spin, will be different from the objective value.

To make this more formal, we start with the general Hadamard coin:

$$H = \begin{pmatrix} \sqrt{\rho} & \sqrt{1-\rho} \\ \sqrt{1-\rho} & -\sqrt{\rho} \end{pmatrix} \tag{4.1}$$

For the initial state we use: $|\psi(x_0, t)\rangle = \begin{pmatrix} \sqrt{p} \\ i\sqrt{1-p} \end{pmatrix}$, where p is the probability to get outcome o_A in the lottery. Note that we still focus on the formation of the subjective probability at this point. The bottom component of $|\psi(x_0, t)\rangle$ is in the imaginary domain so that we retrieve a symmetric distribution for $p = 0.5$. We use the same absorption protocol as before, using partial measurements. In Figure 4.1 we plot the absorption probability at the left boundary as a function of the initial coin state.

We see again the over- and underestimating of small and large probabilities respectively. However, we do not see a nice S-shape like in the initial position bias case. Looking back at the analytical form of Equation 3.32 and the rest of Section 3.2 this is not surprising. We see that the initial coin state always enters as a multiplication factor and thus has a linear effect.

It is important to stress that even if the initial coin state is completely polarized, for example $|\Psi\rangle = \begin{pmatrix} 1 \\ 0 \end{pmatrix}$, there will still be mixing for $\rho \neq 1$. Therefore, it is important to always consider the initial state in combination with ρ for each problem. For example, if one would wish to represent a certain lottery it is not enough to set the initial to $(1, 0)$ for example. To obtain an absorption probability of 1 for the left wall ρ has to be set to 1 as well.

We can add a value dependent bias factor in the same way as we did in the last section, namely by adding an exponential term on the diagonal. We first start with the three different coins from Equation 3.36. The results are shown in Figure 4.2 We see that the value bias adds some non-linearity in the subjective probability. The curves are shifted upwards for small values of p. It is surprising that for larger values of p, the larger probability is not amplified by the value bias but tends to be damped. This is a consequence of the fact that the bias works through interference. The position distribution deviates more from the two-peaked distribution once the bias is added. Because the bias to the left only works in the left region the line is split into two parts. Technically, even three parts because we always implement a bias-free coin at the origin.

We see that the curves are shifted up by this value bias, similar to what we have seen before. This also means that the inflection point lies beyond $p = 0.5$, which means that even if the objective probability for the other outcome is slightly higher, the value bias makes sure that the outcome higher in value still has a larger subjective probability. This is similar to what we saw in the classical case, although the shape of the curves differ. In this case, the bias also adds a non-linearity to the dependence on the initial state. The effect is again more pronounced for smaller values of ρ.

4.1.1 Interpretation of the results

As stated in the introduction to this section, encoding the objective probabilities has some appealing factors conceptually. First of all, the parameter ρ has an attractive interpretation as the 'quantumness' of the problem which could be related to the difficulty of the decision. To formulate a connection between the two, one could, for example, use the difference in expected value. A plausible assumption could be a function that is decreasing in expected value difference. That means that if the two options are close in expected value, the value of ρ is lower and thus the probability assessment will be less 'rational.' However, there are many more ways to quantify the difficulty of the problem and ultimately, the right functional form should be taken from experimental data. We comment more on this later when discussing choices between two or more lotteries where the interpretation of ρ might be more natural.

We saw that adding a value bias leads to non-trivial results, especially when different coins are used along the line. We already used the analogy of electrons traveling from one solid into the other. In this way, the translational invariance is broken and there will be reflection and transmission effects around the edges. Since an analytical solution is very hard to find in this case, it is still unclear how these effects influence the walk exactly. Moreover, since we are now using the initial spin state to encode the probabilities, the walker will always start in the same location, between the two biased coin regions. Decoherence and reflection effects are therefore present from the first evolution step onward. Spatial dependence of the coin may, therefore, be less appealing. Using the same coin over the whole region has the

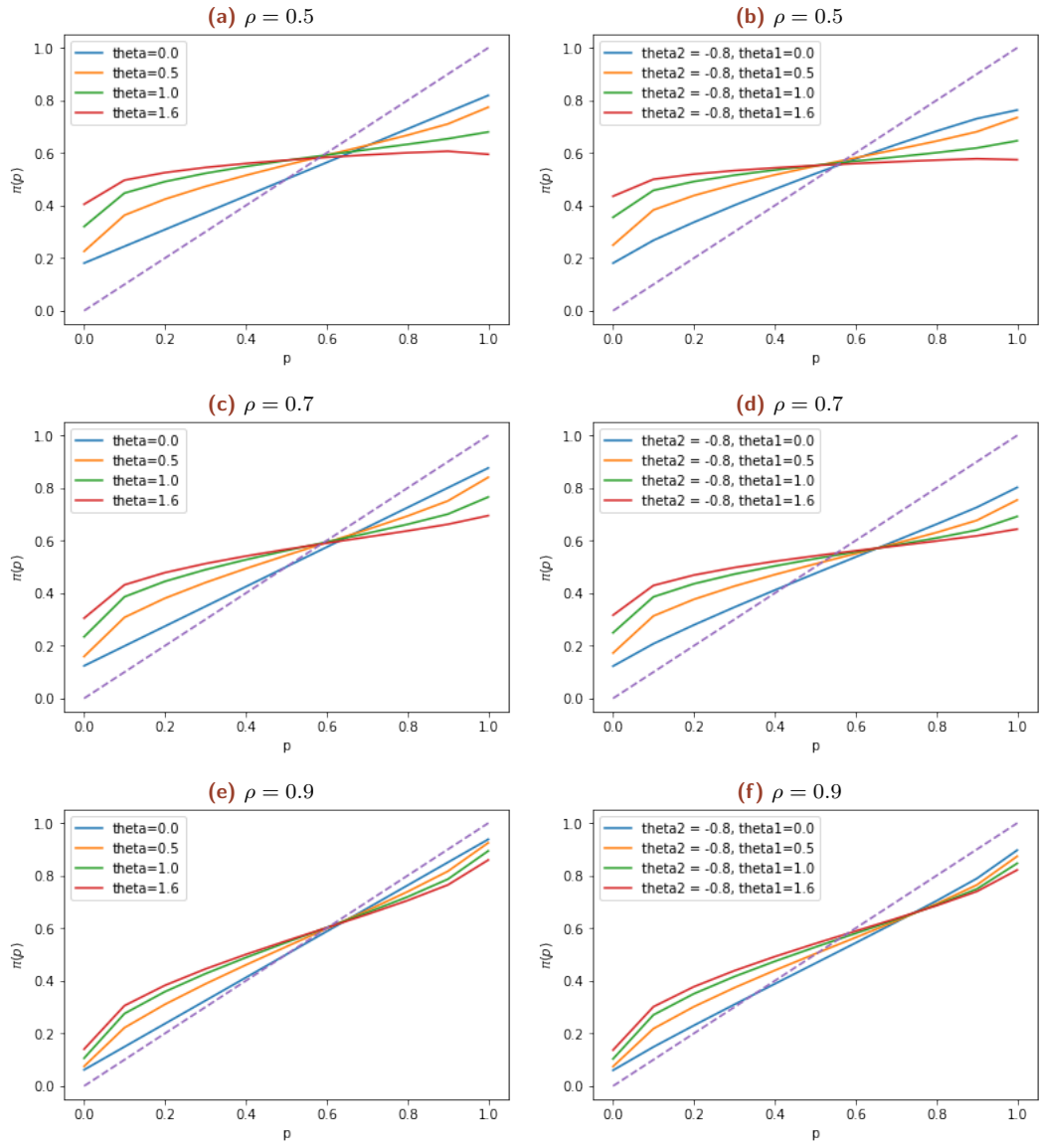

Figure 4.2. – Subjective probability of outcome o_A as a function of the objective probability which is encoded in the initial state for different values of ρ and θ_1 and θ_2. The left column only has a value bias on the left half of the line, the right column has a bias over the whole regions. Here the bias on the right side is fixed, the bias on the left side is varied. In all cases $T = N = 100$.

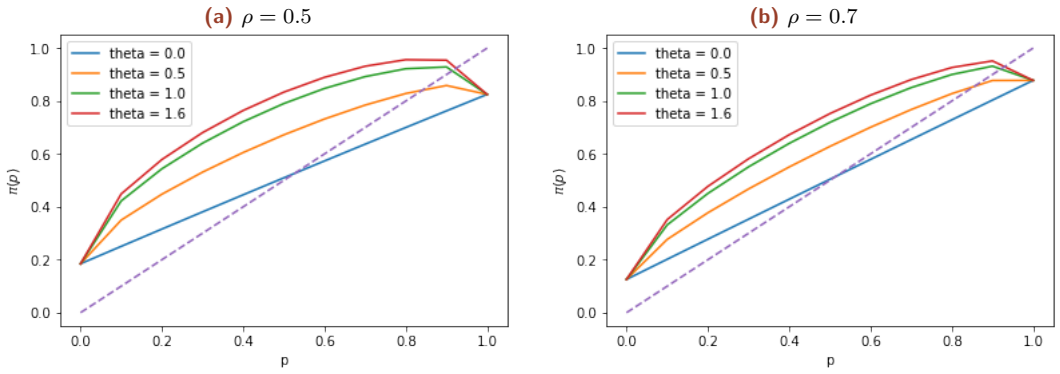

Figure 4.3. – Subjective probability of outcome o_A as a function of the objective probability which is encoded in the initial state for different values of ρ and θ. The coin is the same over the whole region. In all cases $T = N = 100$.

more straightforward consequence of raising the absorption probability for every value of p. This is shown in Figure 4.3.

4.2 Walk on a value chain: Biasing the step operator

Up till this point, we considered a biased coin to change the evolution of the walk. However, we could also alter the step operator by varying the step sizes. This could have different interpretations. First of all, the step size can be related to the probability. If you focus on the absorption probability, events with a larger probability would in this way reach the boundary faster than events with a small probability. In a second, more natural interpretation, one could also associate the step size with a gain in wealth. Obtaining a larger outcome then means taking a bigger step in wealth. This second interpretation asks for a redefinition of the 'space' in which the walk takes place. In the simplest case, we can imagine a lottery with one gain and one loss. We now let the one-dimensional space represent the wealth levels of the individual. With each step, you go up (walking right) or down (walking left) in gains. In this interpretation, there is no absolute need for absorbing boundaries. It is rather the absolute position upon measurement of the walker or the distribution in wealth space that matters.

Without loss of generality, we fix the step length to the left to 1 and vary the sizes of steps to the right. In Figure 4.4 we plot the mean displacement of the walker from its initial position as a function of the step size. We see that the connection is perfectly linear. If we also look at the full probability distribution, we see that the distribution gets shifted to the right and is broader with increasing step size. We also see that this is quite a strong bias since the whole distribution is shifted by the difference in step size. In terms of absorption probability, the right moving part of the walk will reach the boundary way faster than the left moving part, quite a trivial effect.

As it is evident, there is not much room to alter the bias strength. Note that this is mainly a problem when considering absorption for the choice probabilities. For an unbounded walk, the strong bias that the step operator gives could be less of an issue. A different value of ρ will change the variance of the walk and therefore make the distribution wider or narrower. It will

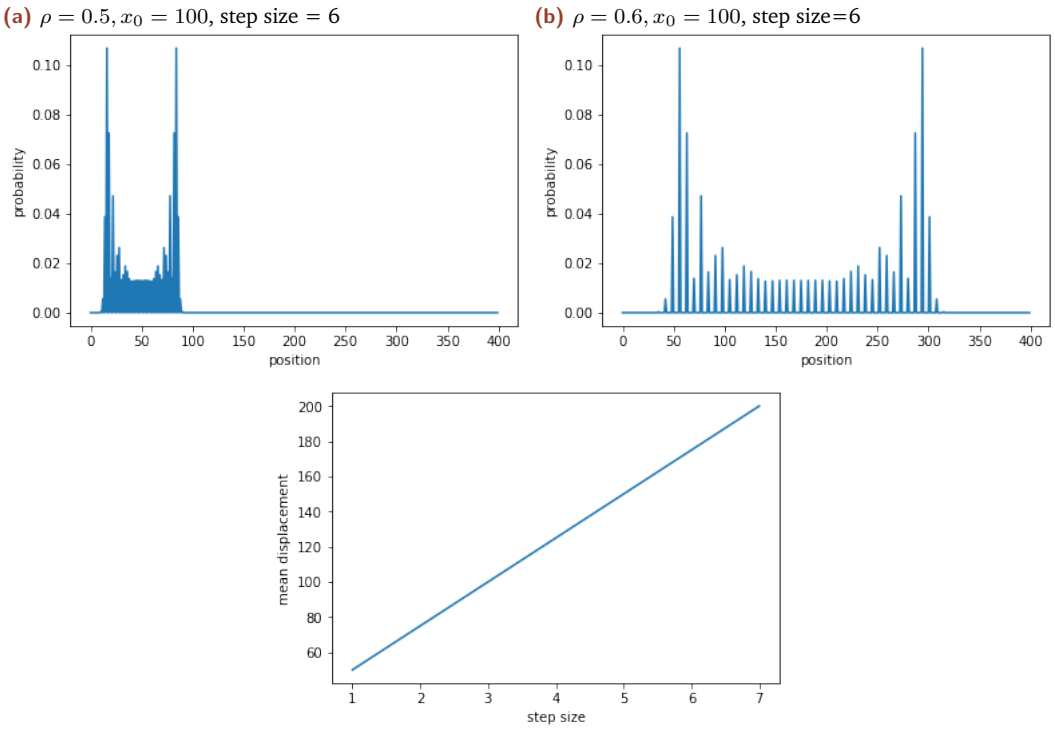

(a) $\rho = 0.5, x_0 = 100$, step size = 6 **(b)** $\rho = 0.6, x_0 = 100$, step size=6

(c) Mean displacement as a function of the stepsize

Figure 4.4. – Displacement dependence on the step size to the right.

however not change the mean displacement of the walk since the variance changes both on the right and on the left.

For a lottery with two gains, we could also imagine that the left and right coin state both move to the right but with different step sizes, corresponding to a greater outcome. Figure 4.5 shows again the means displacement as a function of the step size. Now we see the exact opposite dependence, the larger the step-size the smaller the mean displacement. We also see this if we look at the individual distributions. Due to interference properties, the walker stays closer to the initial position. This is something very counter-intuitive and does not seem appropriate for our framework.

Since two coin states walking in the same direction leads to very non-trivial patterns, this is not a good option for the framework. Building on the fact that we saw a more predictable form of bias in the variant where we had one loss and one gain we could imagine to reformulate the only gain lottery introducing 'relative loss'. For example, we could define moving left as a loss compared to the average value of the outcomes or any other reference value. This, however, does not solve the problem of the step size bias being very strong in nature and not easy to tune.

Another possibility is to leave the 'line structure' and convert it to a regular graph. In this way, each node of the graph can represent a particular wealth level which gives more freedom. In each iteration, the walker can move from one node to two possible new wealth levels, without the restriction that the wealth levels have to differ by a constant amount. An example of a simple value graph with objective transition probabilities is displayed in Figure 4.6. Note that with a quantum walk the transition probabilities from node to node are determined by the coin and current state. There is a large strain of literature on the properties of quantum walk

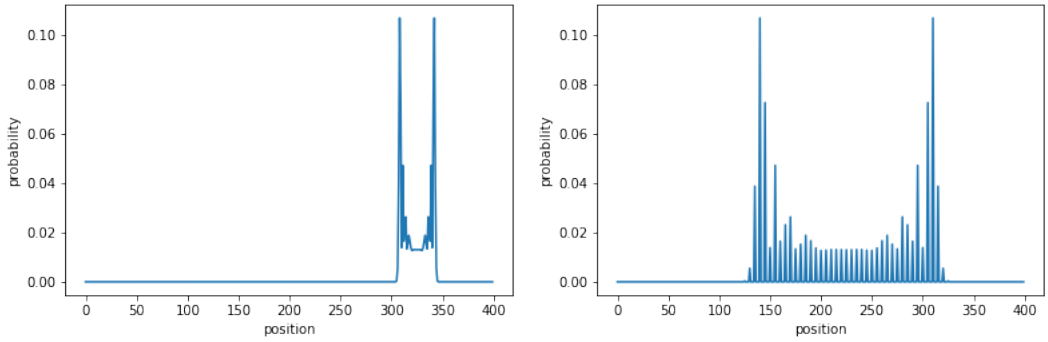

(a) $\rho = 0.5, x_0 = 0$, step size = 2 **(b)** $\rho = 0.5, x_0 = 0$, step size=6

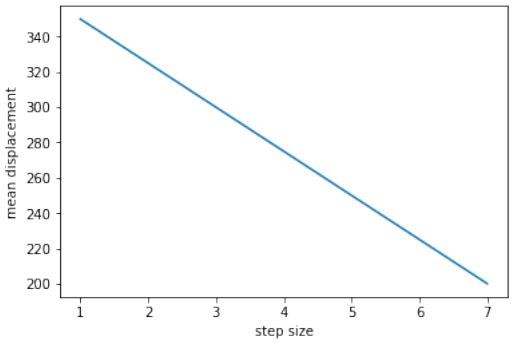

(c) Mean displacement as a function of the stepsize

Figure 4.5. – Displacement dependence when walker to the right only

on graphs see i.e. [32], [38], [67] and [68]. As long as the graph is regular, the properties are very similar to a quantum walk on the line in terms of spreading and interference.

To extract the choice probabilities in terms of absorption one could imagine absorbing nodes in the graph. On the other hand, the distribution over the value graph could be used to extract the total subjective value of a lottery in order to compare it to other lotteries. In this way, it is not the subjective probability of each outcome we focus on, but the total assessment of the lottery that determines the probability of choosing this lottery over another.

Up to this point, we only looked at a symmetric initial state and unbiased coin. Of course, we can tune the strength of the step bias by making the probability of taking the large step very small. In principle, the same linear relations remain although it will only be smaller in absolute size. In conclusion, when focusing on the absorption probability, biasing the walk through variable step size is unfeasible, because it clouds all the other factors at play. However, for an unbounded walk it could be a powerful tool. We will come back to this in Chapter 6.

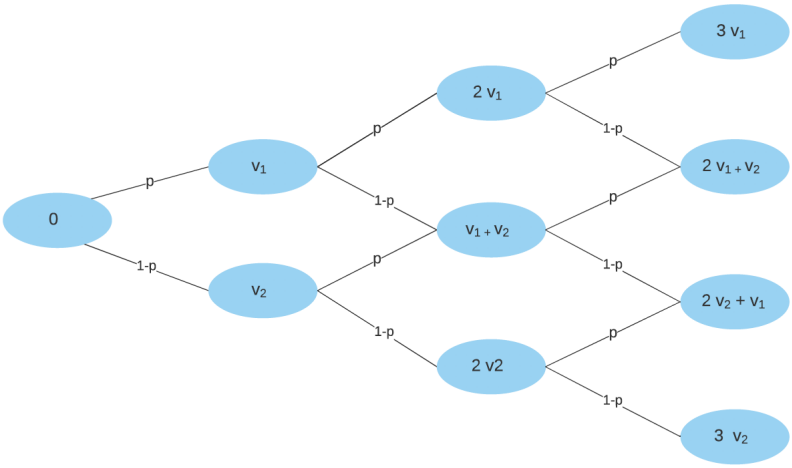

Figure 4.6. – Example of a regular value graph. v_1 and v_2 denote the value of the first and second outcome respectively. p and $1-p$ denote the objective transition probabilities.

4.3 Boundary Effects

As described before, the most straightforward way to introduce irreversibility into the system is by adding absorbing boundaries via partial measurements. Despite its simple computational implementation, analytically this is very challenging. Furthermore, we would like to know the effects of the boundaries on the absolute and conditional absorption probabilities. In this section, we investigate these effects by comparing the distribution to a free quantum walk where we only impose the boundaries in the end. That is, we let the walk evolve for a predefined number of steps and then measure which part of the probability has passed the boundary points. See for an illustration Figure 4.7.

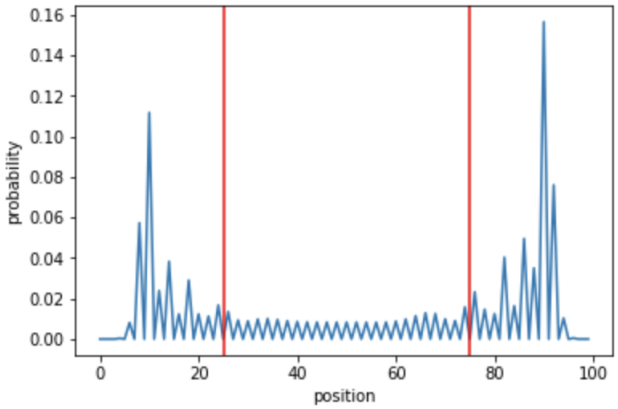

Figure 4.7. – Free walk with virtual boundaries (red lines).

We first investigate the effects of boundaries when the objective probabilities are encoded in the starting position. Figure 4.8 shows the comparison of the 'absorbing' and 'free' walk for both the subjective probability and the absolute absorption on two different time scales. The dotted lines represent the free walk and the solid lines are the walk with absorbing boundaries.

At short times, the curves are quite similar, especially for subjective probability. This changes at longer times. Especially for the absolute absorption probability, the differences are quite large. For the subjective probability, we see that the absorbing walk converges quickly to a 50/50 distribution whereas the free walk remains asymmetric.

We now do the same for the walk where the initial state represents the objective probabilities. Figure 4.9 shows the results. In terms of subjective probabilities, the curves are very similar. The differences are larger for the absolute absorption probability but less pronounced than in the previous example.

All in all, we see similarities between the free and absorbing walks at short times and for the initial state dependence even at longer times. In the absolute absorption probability, the differences are more pronounced. Here the effect of removing part of the wavefunction by partial measurement on the interference patterns is clearly visible. The similarities for the subjective probabilities, however, can help to find at least an approximate solution for the absorption probability by using the solution of the free walk.

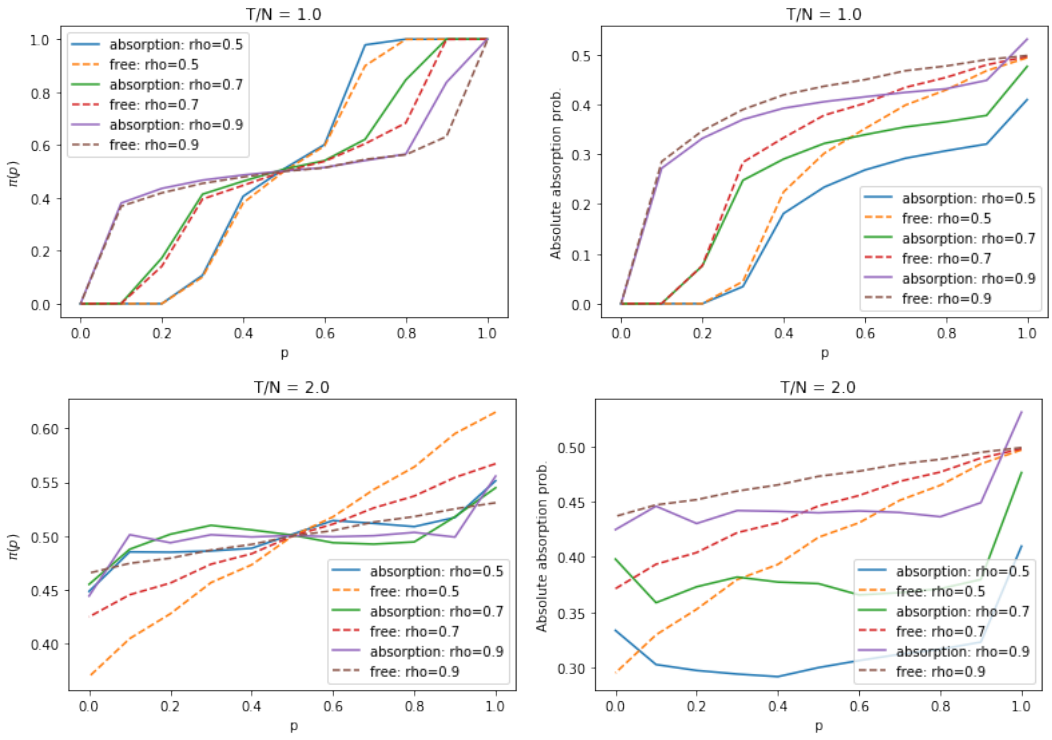

Figure 4.8. – Comparison of the subjective probability (left) and absolute absorption probability (right) of the absorbing and free walk as a function of p at different times. The initial position is given by $x_0 = (1 - p) * N$ with N=100.

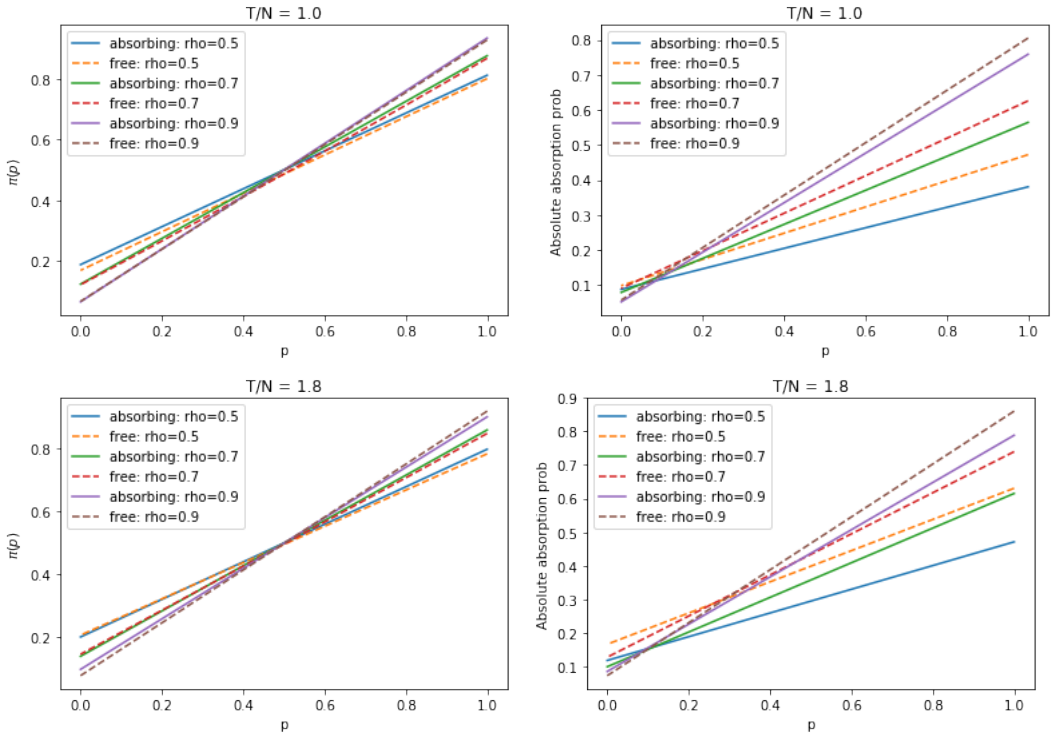

Figure 4.9. – Comparison of the subjective probability (left) and absolute absorption probability (right) of the absorbing and free walk as a function of p at different times. The initial state is given by $(\sqrt{(}p), i\sqrt{1-p})$. N=100, $x_0 = 50$.

4.4 Choice between lotteries

So far, we have concentrated on the formation of subjective probability. We now shortly discuss the probabilities of extracting the choice probabilities for a total lottery.

Instead of a walk between lottery outcomes to quantify the subjective probability and attractiveness of an outcome, we can also imagine a walk between two lotteries. Now we have some different variables that we can use to bias the walks. We could, for example, imagine a walk between two expected values corresponding to the two lotteries. Since ρ determines the mixing between components and therefore the strength of some bias parameters, we could interpret ρ as the 'quantumness' of the decision problem. Intuitively, the harder the decision problem, the higher the 'quantumness', and thus the lower the value of ρ. The most straightforward way to parametrize ρ would be as a function of the difference in the expected utility of both lotteries. The closer the expected utilities, the harder the decision. However, there are some important caveats that are an issue for probabilistic decision theories in general. The most pronounced one is the concept of stochastic dominance [27]. This can be demonstrated by a simple example. Imagine two lotteries: L1 = (60,0.4,20,0.6) and L2 = (60,0.5,20,0.5). Lottery 2 is clearly better than Lottery 1, the outcomes are the same but Lottery 2 has a larger probability of getting the highest outcome. Now if we calculate the expected values of the lotteries we get L1=36 and L2=40, which is not a very large difference. Therefore, if we took ρ as a linear function of the difference, there will still a high probability that the walker gets absorbed by L1, although this is largely irrational behavior. So the challenge is to design a function for ρ that obeys stochastic dominance.

Note that the walk itself will look the same depending on the types of bias used (initial position, initial state, exponential on the diagonal, and variation of ρ) it is just the interpretation that changes here.

One of the downsides of doing a one-dimensional walk between two expected values is that we lose the properties of entangled value and probability dependence, because we only look at the expectation value of the lottery, adding the quantum walk as an ad-hoc layer on top of expected utility theory. On the other hand, the definition of ρ as the quantumness of the process seems more natural in the context of choosing between lotteries than within a single lottery.

In Section 4.2 we discussed the possibilities of using a walk in value space. Instead of imposing some absorbing boundary or region, this could be a tool to calculate the total subjective value of a lottery. In this case, the probability distribution of each value level determines the weight of that value level such that the weighted sum over all nodes gives the total subjective value. By designing a value graph for each lottery and let the walk evolve in this space with an initial state and biased step operator given by the lottery properties we could compare different lotteries based on their subjective value. The relative difference than gives the choice probability. We will proceed with this idea in a slightly different fashion in section 6.

4.5 Entropy of measurement

We already know that ρ regulates the variance of the walk through the amount of mixing between left and right. One interpretation is that ρ therefore quantifies the 'uncertainty' of the decision. In addition to the variance of the walk, we can also use the Entropy of Measurement [44], which also largely depends on ρ, as a measure of uncertainty in the decision. We use the definition of the von Neumann entropy and write the measurement entropy as:

$$H(i) = -\sum_i p_i \ln p_i, \tag{4.2}$$

where p_i is the probability of being at position i (after tracing out the coin). In Figure 4.10 we show the measurement entropy as a function of ρ. The other coin variables have a negligible effect on the measurement entropy. We see an 'arch-like' shape for the measurement entropy as a function of rho, which gets shifted upwards for longer times. This shows that the measurement entropy (and thus the uncertainty of the measurement) is maximal for $\rho = 0.5$. The entropy slowly falls off on both sides of $\rho = 0.5$ and only takes a big drop at extreme values. For very low values of ρ the wavefunction stays close to the initial position and is centered at one (two) sites at odd (even) times. For very large values of ρ the wavefunction again only peaks at two sites, however, these sites are now at location $x_0 \pm T$. For the measurement entropy the exact location of the peaks doesn't matter, hence the symmetric 'arch-like' relation with ρ. Over time, the absolute value of the entropy grows, related to the absence of a stationary distribution for the quantum walk.

If we choose to take ρ as regulating the uncertainty of the decision we can, therefore, restrict the values of ρ to the range $\rho \in (1, 0.5)$ to capture the whole range from certain to maximally uncertain decisions.

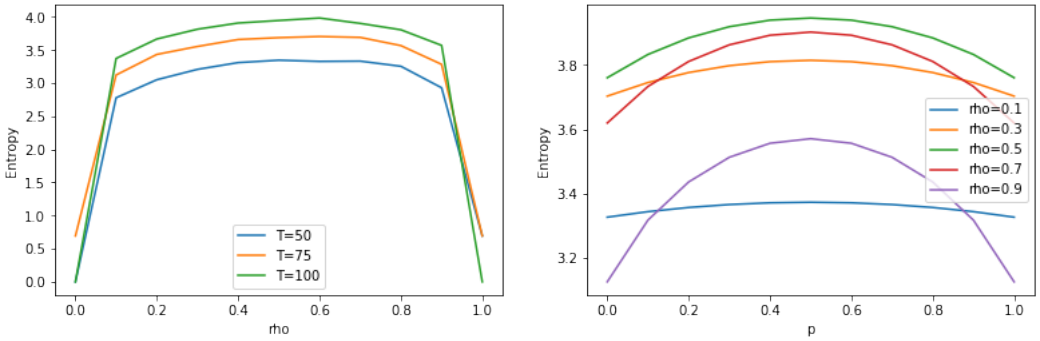

Figure 4.10. – Dependence of the measurement entropy on ρ (left) and the initial state (right).

We now look at the measurement entropy as a function of the initial coin state for different values of ρ, shown in Figure 4.10. We see the same arch-like shape for both dependencies. For the dependence on ρ, the entropy curves are shifted upwards for longer times. This is another indication that the Quantum Walk, in general, does not converge to a static distribution. For the dependence on the initial state, the entropy curves get shifted depending on the value of ρ. As can also be seen in Figure 4.10, the entropy is highest for $\rho = 0.5$. In addition to the absolute magnitude, also the shape of the curves changes with ρ. The measurement entropy is highest for the symmetric initial state belonging to $p = 0.5$, this is quite intuitive. If probabilities are very close together, it is harder to distinguish them.

Continuous Time Quantum walk

5

In previous Chapters, we focused on the use of the discrete-time quantum walk because of its similarities with the classical random walk. However, as stated in the introduction, there is another type of quantum walks with a different underlying mechanism that nevertheless exhibits similar behavior. The continuous-time quantum walk is not simply the continuous-time limit of the coined quantum walk. Instead, its evolution is governed by a Hamiltonian and takes place completely in position space, without the extra coin degree of freedom. In this chapter, we will explore whether this type of quantum walk can be useful for a decision-making framework.

5.1 Absorption by repeated measurements

To introduce irreversibly in the quantum walk we will again use the concept of partial measurements. However, since the evolution is now in continuous time, there is no notion of a 'step' and thus measuring whether the particle is at the boundary at each step needs to be redefined. Therefore, we introduce a measurement frequency, which determines the strength of the effect. Introducing the measurement at two points on the line corresponds to two walls, possibly with a different measurement frequency. We indicate the time between measurements by τ, such that the measurement frequency is given by $1/\tau$. When taking the limit $\tau \to 0$ corresponding to continuous measurement, we recover the quantum Zeno effect [69]. This effect can best be described as 'the system cannot evolve if you are constantly watching it.' It is a property of quantum mechanical systems that states that no evolution takes place if the system is constantly measured. In our case, no evolution means no absorption and thus under continuous measurement, we will measure nothing at all at the boundary sites. As continuous monitoring is thus not possible, we can only account for imperfect absorption. Note that this is very natural in quantum mechanics. Although the walk is now no longer unitary, most of the coherence is still preserved. For appropriate disturbance $\tau << 1/\gamma$ with γ the hopping rate in the Tight-Binding Hamiltonian (see below), we can adopt a perturbative approach to describe the surviving part of the walk. For simplicity, we set the hopping rate to $\gamma = 1$, and thus the approximation will be valid for $\tau << 1$. Since the total probability needs to be conserved, the survival probability of the walker gives us an indirect measure of the absorption probability.

We follow the procedure outlined in [70]. A continuous time quantum walk is described by a tight-binding type Hamiltonian of the form: $H = \sum_{r,s=1}^{N} H_{r,s} |r\rangle \langle s|$, with $H_{r,s}$ a real, symmetric matrix. The non-vanishing elements have strength γ which we set to 1 here for simplicity. The evolution of the quantum walk is then described by the Schrödinger equation whose solution is $|\psi(t)\rangle = U_t |\psi(0)\rangle$ with $U_t = e^{-iHt}$. We distinguish between sites belonging to the system (translational invariant bulk) and the boundary states where the measurements are performed. The projection operator on the boundary set D is defined as $A = \sum_{r \in D} |r\rangle \langle r|$ and the complementary projection onto the system states is $B = 1 - A$. After performing a measurement the system will be in the state $\rho = A |\psi\rangle \langle \psi| A + B |\psi\rangle \langle \psi| B$. However, since

we stop the simulation whenever the particle is detected, we can focus on the evolution of the system states. The state after measurement is described as $|\psi^+\rangle = B|\psi^-\rangle$. We can now describe the evolution operator in terms of measurement intervals τ as $\tilde{U} = BU_\tau$. That means that the survival probability at time $t = n\tau$ is $P_t = \langle\psi_n^+|\psi_n^+\rangle = \langle\psi(0)|\tilde{U}^{\dagger n}\tilde{U}^n|\psi(0)\rangle$. For an initial state in the bulk $\tilde{U} = Be^{-iH\tau}B$, this is now a non-unitary evolution operator acting on the system states. The first application of B projects on the Bulk, such that only these states evolve with the Hamiltonian. Then, the second action of B removes the states that ended up at the boundary after evolution. Note that the evolution is now given in terms of 'measurement instances', i.e. at each step the system gets $t = \tau$ time to evolve. The strength of the non-unitarity is also governed by the measurement interval τ. For small τ we can expand the evolution operator up to second order as:

$$\tilde{U} = B[I - iH\tau\frac{\tau^2}{2}H^2 + ...]B \tag{5.1}$$

We can split the Hamiltonian into three parts: $H = H_s + H_M + V$, one Hamiltonian for the translation invariant bulk (H_s), one for the measurement sites (H_m) and a potential coupling the boundary to the system (V):

$$\begin{aligned} H_s &= \sum_{l,m} H_{l,m}|l\rangle\langle m|; \qquad H_m = \sum_{\alpha,\beta} H_{\alpha,\beta}|\alpha\rangle\langle\beta| \\ V &= \sum l, \alpha V_{l,\alpha}|l\rangle\langle\alpha| + V_{\alpha,l}|\alpha\rangle\langle l|. \end{aligned}$$

Here, we denoted the system state by indices l, m and the boundary sites by α, β. Note that system and boundary states do not overlap. Therefore, all inner products between system and boundary states will vanish and equation 5.1 becomes:

$$\begin{aligned} \tilde{U} &= I - iH_s\tau - \frac{\tau^2}{2}H_s^2 - \frac{\tau^2}{2}\sum_{l,m}\sum_{\alpha} V_{l,\alpha}V_{\alpha,l}\langle l|m\rangle + ... \\ &= e^{-iH_{\text{eff}}\tau} + \mathcal{O}(\tau^3). \end{aligned} \tag{5.2}$$

Where:

$$H_{\text{eff}} = H_s + V_{\text{eff}} \tag{5.3}$$

This is a non-Hermitian Hamiltonian that we will have to diagonalize. As long as the decoherence due to the measurement is relatively small ($\tau < 1/\gamma$), we can treat V_{eff} as a perturbation. In the following, we will assume that we measure on two sites, one at both ends of the line. This will determine the specific form of the effective potential that couples the system sites to the boundary. For the system states, we will assume the general tight binding Hamiltonian:

$$H_s = -\sum_{x=1}^{N-2}(|x+1\rangle\langle x| + |x-1\rangle\langle x|). \tag{5.4}$$

The potential for two measurement sites at $n = 1, N$ is given by:

$$V_{\text{eff}} = -\frac{i\eta}{2}|2\rangle\langle 2| - \frac{i\tau}{2}|N-1\rangle\langle N-1|. \tag{5.5}$$

Here, η and τ are the measurement intervals at the left and right wall respectively. These determine the strength of the potential on both sides.

We can now calculate the evolution of the wavefunction with repeated measurements with perturbation theory. Therefore, we first compute the eigenvalues $\{\epsilon_s\}$ and eigenvectors $\{|\phi_s\rangle\}$ of the system Hamiltonian. Note that there are now $N-2$ states in the system.

$$\epsilon_s = -2\cos\left(\frac{s\pi}{N-1}\right) \tag{5.6}$$

$$\langle x|\phi_s\rangle = \phi_s(x) = \sqrt{\frac{2}{N-1}}\sin\left(\frac{s\pi(x-1)}{N-1}\right) \tag{5.7}$$

We can now determine the perturbation to the eigenvalues due to the potential by calculating the expectation value of V_{eff}:

$$\begin{aligned}\langle V_{eff}\rangle &= \langle\phi_s|V_{eff}|\phi_s\rangle \\ &= -\frac{i\eta}{N-1}\phi_s(2)^2 - \frac{i\tau}{N-1}\phi_s(N-1)^2 \\ &= -\frac{i\eta}{N-1}\sin^2\left(\frac{s\pi(N-2)}{N-1}\right) - \frac{i\tau}{N-1}\sin^2\left(\frac{s\pi}{N-1}\right).\end{aligned} \tag{5.8}$$

The perturbed eigenvalues are written as $\epsilon'_s = \epsilon_s - \frac{i}{2}(\alpha_s + \beta_s)$ with $\alpha_s = -\frac{2\eta}{N-1}\sin^2\left(\frac{s\pi(N-2)}{N-1}\right)$ and $\beta_s = \frac{2\tau}{N-1}\sin^2\left(\frac{s\pi}{N-1}\right)$. The resulting evolution of a system eigenstate is:

$$|\phi_s(t)\rangle = e^{-iH_{\text{eff}}t}|\phi_s(0)\rangle = e^{-\alpha_s t/2}e^{-\beta_s t/2}e^{-i\epsilon_s t}|\phi_s(0)\rangle\,. \tag{5.9}$$

The evolution of a particle initially located in x_0 in terms of system eigenstates reads:

$$|\psi(t)\rangle = e^{-iH_{\text{eff}}t}|x_0\rangle = \sum_{s=1}^{N}\phi_s(x_0)e^{-\alpha_s t/2}e^{-\beta_s t/2}e^{-i\epsilon_s t}|\phi_s(0)\rangle\,. \tag{5.10}$$

Here $\phi_s(x_0)$ denotes the decomposition of the position state into system eigenstates, which is easily found using Equation 5.7. The quantity we are interested in is the survival probability of the walk, which in turn, also gives us the absorption probability since the total distribution is normalized to 1. The survival probability at a certain time is given by:

$$\begin{aligned}P_{x_0}(t) &= \langle\psi(t)|\psi(t)\rangle \\ &= \sum_{s=1}^{N}\frac{2}{N-1}\sin^2\left(\frac{s\pi(x_0-1)}{N-1}\right)e^{-\frac{2\eta t}{N-1}\sin^2\left(\frac{s\pi(N-2)}{N-1}\right)}e^{\frac{2\tau t}{N-1}\sin^2\left(\frac{s\pi}{N-1}\right)}.\end{aligned} \tag{5.11}$$

For comparison, it will also be instructive to look at the one boundary case where measurements are done at a single site. The derivation is very similar except for the fact that we now have $N-1$ sites in the system and the boundary is placed at location 0. The survival probability reads [70].

$$P_{x_0}(t) = \sum_{s=1}^{N}\frac{2}{N}\sin^2\left(\frac{s\pi x_0}{N}\right)e^{-\frac{2\tau t}{N}\sin^2\left(\frac{s\pi}{N}\right)}. \tag{5.12}$$

We first look at the survival probability for this one boundary case (Eq. 5.12). In Figure 5.1 we plot the survival probability over time for different starting positions of the walk. We can see roughly two types of behavior depending on the initial position. For states close to the boundary ($x_0 < 10$) the decay is fast, whereas for states initially in the bulk ($x_0 > 10$) the

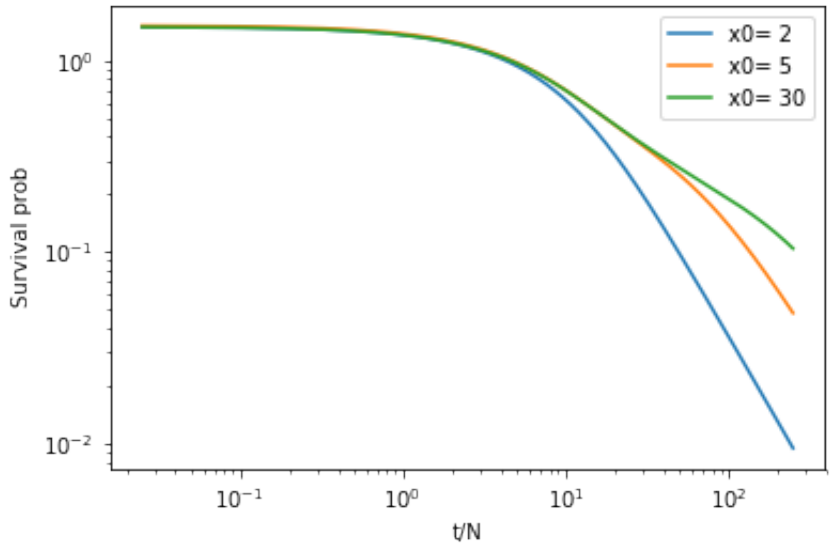

Figure 5.1. – Survival probability over time for different initial position states, in the presence of one measurement site with measurement interval $\tau = 0.1$.

curve is way flatter. There is a relatively quick transition between the two. For a lattice of 60 sites, all starting positions $x_0 > 5$ sites from the boundary will roughly give the same curve. From times $t/N = 100$ up to $t/N = 10^3$, we can see some interesting power-law behavior. More specifically, in [70] they derived the following dependence on the starting position:

$$P_{x_0}(t) = \frac{1}{\sqrt{\frac{8\pi\tau t}{N}}}(1 - e^{-x_0^2 N/2\tau t}). \tag{5.13}$$

In Figure 5.2 we plotted this function as dotted lines. We can see the similarity, although the curves are shifted.

We can now look at the behavior of the survival probability in the presence of two walls (Equation 5.11). In Figure 5.3 the survival probability is shown for an initial state close to one of the boundaries and for an initial state well in the bulk. First, we chose the measurement intervals at both walls to be $\eta = \tau = 0.1$.We see very similar behavior as in the one boundary case. From the equations, it is easy to verify that in this case, the decay constant will be roughly twice as big. In general, we can say that:

$$\begin{aligned} \alpha_s + \beta_s &= -\frac{2\eta}{N-1}\sin^2\left(\frac{s\pi(N-2)}{N-1}\right) + \frac{2\tau}{N-1}\sin^2\left(\frac{s\pi}{N-1}\right) \\ &= \frac{2t}{N-1}\sin^2\left(\frac{s\pi}{N-1}\right)(\eta+\tau) \end{aligned} \tag{5.14}$$

Now for large N, $N - 1 \approx N$ such that if $\eta = \tau$ the decay constant is indeed twice as big as for the one boundary case. This is also visible in the graphs, see Figure 5.3 where we plotted the one boundary case as solid lines and the two boundary case as dotted lines for three different starting positions. Here we see that the relative patterns do not change, the curves just get shifted. This supports our analytical finding that the survival probability should decay twice as fast if all measurement intervals are equal.

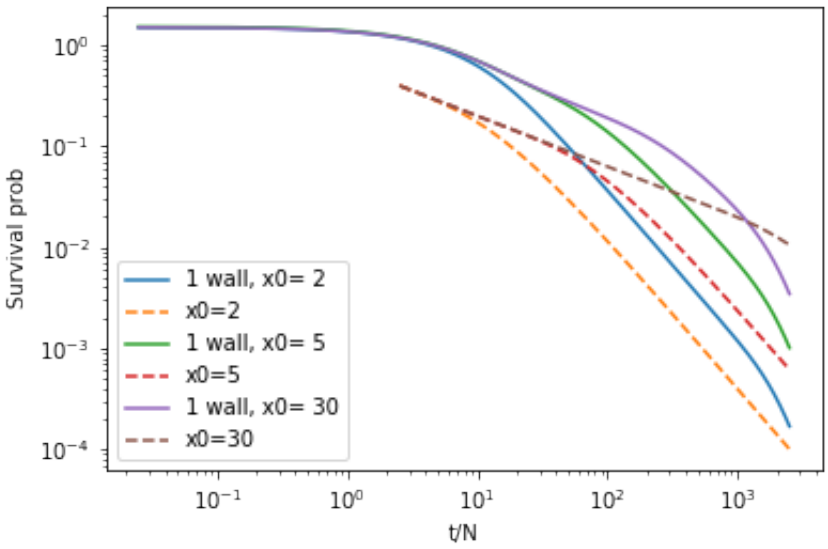

Figure 5.2. – Survival probability in the presence of one measurement site with interval $\tau = 0.1$. The dotted lines represent the power law as in Equation 5.13.

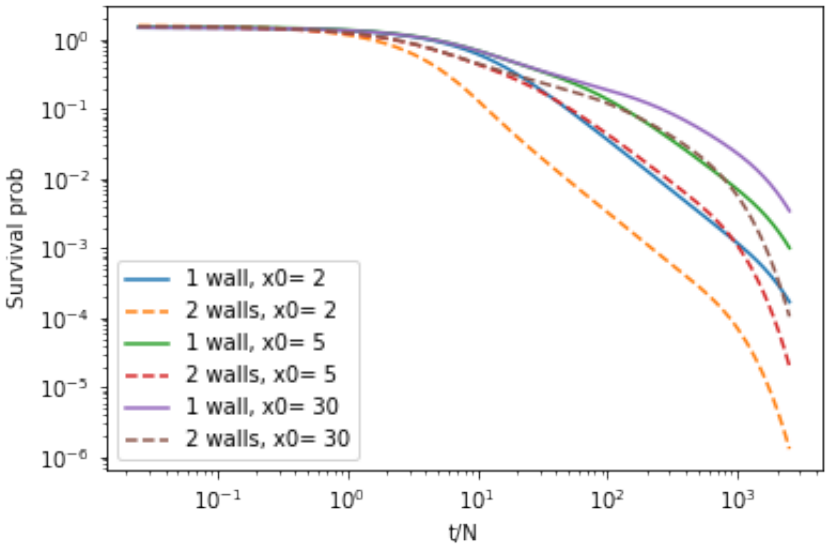

Figure 5.3. – Survival probability over time in the presence of one and two measurement sites in position N=1,100 with measurement interval $\tau = \eta = 0.1$.

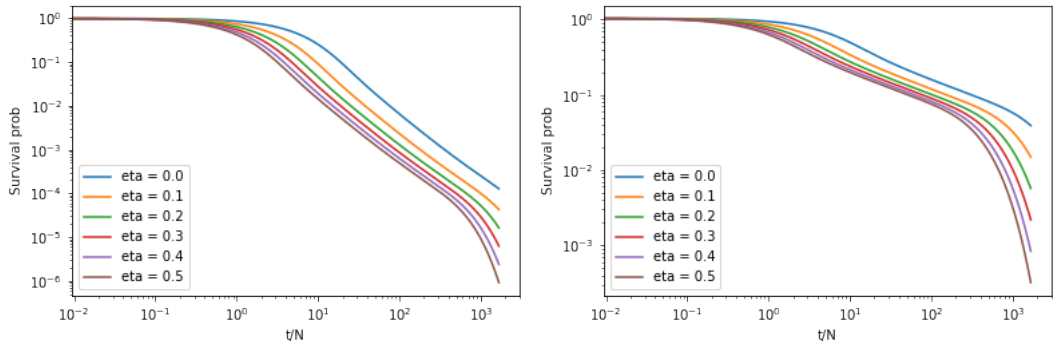

Figure 5.4. – Survival probability over time for different values of η, τ is fixed at 0.1. $N = T = 100$, $x_0 = 2$ (left) and $x_0 = 10$ (left).

We now vary the measurement interval at the second boundary, while keeping the first one fixed at $\tau = 0.1$. See Figure 5.4. The curves get shifted downwards for higher values of η, corresponding to more frequent measurements.

5.2 Interpretation of the Results

Focusing on the absorption probability of the walls, a power-law kind of behavior over time is observed. The exact power depends on whether the initial state is located well within the bulk or close to one of the boundaries. This is summarized by Equation 5.12 for one boundary. In Figure 5.1 we observe two types of behavior, which is readily explained by Equation 5.12. When x_0 is small (close to the boundary) and Nx_0 is small compared to $t\tau$, we can expand the exponential as:

$$e^{-Nx_0/2\tau t} \approx 1 - \frac{Nx_0^2}{2\tau t} + \frac{1}{2}\left(\frac{Nx_0^2}{2\tau t}\right)^2 + \dots \tag{5.15}$$

where $x = \frac{t\tau}{N}$. Focusing on the dependence on t, to first order the survival probability decays as:

$$P(t) = \frac{1}{\sqrt{\frac{8\pi\tau t}{N}}}(1 - e^{Nx_0^2/2\tau t}) \approx 1/t^{3/2}. \tag{5.16}$$

Apart from the region where x_0 is very small, the factor $Nx_0/2\tau t$ is big for a large range of t. Therefore, the survival probability will be dominated by the prefactor $1/\sqrt{\frac{8\pi\tau t}{N}}$ and thus decay over time like $1/t^{1/2}$. The transition between these two regimes is the transition from an intermediate asymptotic behavior for the small values of x_0 to the full asymptotic behavior of the system and takes place over only a couple values of x_0. In the case of two boundaries, the behavior is not very different, the decay is just faster. The relative speed of decay is given by the measurement frequencies. If the same frequencies are used for all walls in the single and double wall system, the decay is exactly twice as fast in the two boundary system.

This power-law type of behavior for the survival probability is something we also find in the classical random walk. In that sense, the continuous-time quantum walk does not provide many new insides. This is mainly because the coherence is not so important for the dynamics, in this case, leading to unsurprising absorption behavior. Furthermore, because of the Hamiltonian structure and absence of the coin, there are only limited ways to bias the walk. On top of that, although the continuous-time quantum walk also reduces to a classical

random walk when introducing a sufficient amount of decoherence, the connection between the two is less clear. All in all, the continuous-time quantum walk does not provide us with enough new opportunities for a decision-making framework. Therefore, we will return to the coined quantum walk for the remainder of this thesis.

6 Evolution of the global spin distribution

6.1 The spin at the center of attention

So far, we have essentially followed the classical SRDT framework, in the sense that the subjective- or choice probabilities are given by the relative absorption probabilities, somehow imposing from outside a choice criterion. However, with the quantum walk, we might as well switch views and focus on the spin of the walker instead. This approach is appealing in multiple ways. First, the quantum spin is a discrete entity, as is the choice between lotteries. Roughly, we encode the information about lotteries in the walker position space; then, we study how the evolution in position space affects the evolution in the spin space, representing now the choice probabilities. The spin here is not treated as a redundant degree of freedom; rather, its distributional properties, intrinsically coupled with the 'external environment', directly reveal the decision-maker preferences.

Note that since no boundaries are involved in this case, the walk is completely coherent and translational invariant, permitting an analytical solution. Lastly, the interpretation of ρ governing the level of 'irrationality' as discussed in Section 4.1 still holds in this case. Thus, without introducing decoherence we have a 'rational' limit in which the choice probabilities will be given by the initial state.

The next question is how to measure the spin. During the evolution, the probability distribution of the walker spreads out over multiple positions. The amplitude at each site is given by the spin components. Depending on where and when you measure, the relative magnitude of these two components can be completely different. In order to understand how the spatial degree of freedom influences the spin, we will start from the evolution of the global spin distribution. In essence, by tracing out the position by summing over all sites, we get the "total" spin probability of the system, i.e. the probability of measuring the spin-independent of the particle position. We will now first give an introduction to the evolution of such global spin distribution for the usual two-dimensional coin state. Then, to build the framework for a choice between two binary lotteries, we will enlarge the spin space to four dimensions, giving us the opportunity to use the individual lottery components to shape the evolution. Finally, we will tie everything together and present a framework of decision making based on the weighted spin distribution of the four-spin state quantum walk in one dimension.

6.2 Global spin Distribution

The description of the global spin evolution is very similar to the one used in 2.4. We follow the notation of [71] and write the general Hadamard coin as:

$$\hat{C} = \begin{pmatrix} \cos\theta & \sin\theta \\ \sin\theta & -\cos\theta \end{pmatrix}. \tag{6.1}$$

Note that we only take a one parameter coin to keep the notation clear. The extension to a more general coin is straightforward. The wavefunction of the walker can be written as:

$$|\psi(x,t)\rangle = \begin{pmatrix} a_x(t) \\ b_x(t) \end{pmatrix}, \tag{6.2}$$

where the subscript x denotes the spatial position and t the time step. With the usual step operator, the evolution of the two components is given by:

$$a_x(t+1) = \cos\theta a_{x+1}(t) + \sin\theta b_{x+1}(t) \tag{6.3}$$

$$b_x(t+1) = \sin\theta a_{x-1}(t) - \cos\theta b_{x-1}(t) \tag{6.4}$$

The probability to be in the left-spin state at position x at time t is given by: $P_u(x,t) = |a_x(t)|^2$. Therefore, the total left and right spin probabilities at time t are given by:

$$P_L(t) = \sum_x |a_x(t)|^2 \quad P_R(t) = \sum_x |b_x(t)|^2. \tag{6.5}$$

These two components form the so called global spin distribution: $\begin{bmatrix} P_L(t) \\ P_R(t) \end{bmatrix}$. Given Equation 6.3, we can write the evolution of the global spin as:

$$\begin{bmatrix} P_L(t+1) \\ P_R(t+1) \end{bmatrix} = \begin{pmatrix} \cos\theta^2 & \sin\theta^2 \\ \sin\theta^2 & \cos\theta^2 \end{pmatrix} \begin{bmatrix} P_L(t) \\ P_R(t) \end{bmatrix} + \mathrm{Re}(Q(t)) \sin 2\theta \begin{bmatrix} 1 \\ -1 \end{bmatrix}, \tag{6.6}$$

where $Q(t) = \sum_x a_x(t) b_x^*(t)$. With this equation, the evolution is split in a Markovian and an interference part regulated by $Q(t)$. If $Q(t) = 0$ for all t, the process is Markovian. However, since $Q(t)$ is time dependent, we cannot generally solve this equation. However, if we assume that $Q(t)$ is constant in time, the Equation 6.6 is readily solved to be [71]:

$$\begin{bmatrix} P_L(t) \\ P_R(t) \end{bmatrix} = \frac{1}{2} \begin{pmatrix} 1+\cos 2\theta^t & 1-\cos 2\theta^t \\ 1-\cos 2\theta^t & 1+\cos 2\theta^t \end{pmatrix} \begin{bmatrix} P_L(0) \\ P_R(0) \end{bmatrix} + Re(Q) \frac{1-\cos 2\theta^t}{\tan\theta} \begin{bmatrix} 1 \\ -1 \end{bmatrix}. \tag{6.7}$$

This shows that in the absence of interference the evolution is described by a master equation.

Because of the conditional nature of the shift operator, the spin and position are entangled. The entanglement can be quantified by the entanglement entropy defined as [72]:

$$S_E = -Tr(\rho_c \log \rho_c) \tag{6.8}$$

where ρ_c is the reduced density matrix $\sum_x |\Psi(x)\rangle \langle\Psi(x)|$ in coin space. Using the shorthand notation:

$$A = \sum_x |a_x|^2 \tag{6.9}$$

$$B = \sum_x a_x b_x^* \tag{6.10}$$

$$C = \sum_x |b_x|^2 \tag{6.11}$$

$$\Delta = AC - |B|^2 \tag{6.12}$$

we can write the eigenvalues of ρ_c as [72]:

$$r_{1,2} = \frac{1}{2}[1 \pm \sqrt{1 - 4\Delta}]. \tag{6.13}$$

Then the entropy of entanglement is given by:

$$S_E = -(r_1 \log_2 r_1 + r_2 \log_2 r_2). \tag{6.14}$$

The fact that the entropy of entanglement is non-zero means that the spin and position can influence each other. However, the entropy of entanglement does not give a causal relation, i.e. it is still unclear how the spin affects the spatial distribution and vice versa. By focusing on the absorption probability while encoding the objective probabilities in the initial spin state we investigated how the spin affects the position degree of freedom. Now, focusing on the distribution of the spin, we investigate the inverse relation. In the following sections, we will first enlarge the spin space to four dimensions to encode a binary choice between binary lotteries. We will redefine the shift and coin operator accordingly and investigate their influence on the spin distribution.

6.3 Using the spin as decision variable

Our first goal is to model the decision between two binary lotteries. This means that we have four lottery components in total that can be evaluated. Because we want to allow the components and lotteries to be evaluated in a dependent way we only use one walker to model the choice process as a whole. To still account for all individual components we enlarge the coin space to four dimensions. The wave vector is now described by:

$$|\psi(x,t)\rangle = \begin{pmatrix} a_x(t) \\ b_x(t) \\ c_x(t) \\ d_x(t) \end{pmatrix}. \tag{6.15}$$

To tailor the state to the choice between lotteries we associate the first two components with the first lottery and the last two with the second lottery. In general, we consider two lotteries of the form: $L_1 = [v_1, p; v_2, 1-p]$ and $L_2 = [v_3, q, ; v_4, 1-q]$. Similar to what we did in Section 4.1 we use the initial spin state to encode the objective probabilities of the lotteries, i.e. our initial spin state is given by:

$$\begin{pmatrix} L_1^{\uparrow}(0) \\ L_1^{\downarrow}(0) \\ L_2^{\uparrow}(0) \\ L_2^{\downarrow}(0) \end{pmatrix} = \frac{1}{\sqrt{2}} \begin{pmatrix} \sqrt{p} \\ i\sqrt{1-p} \\ i\sqrt{q} \\ \sqrt{1-q} \end{pmatrix}. \tag{6.16}$$

The state is normalized such that each lottery holds 1/2 of the total probability prior to evolution. At time 0, the probability of choosing Lottery 1 and getting the highest value is thus $p/2$, $1/2$ from choosing Lottery 1 and p from getting the highest outcome. After the first step, this probability will be given by $\left|L_1^{\uparrow}(1)\right|^2$. Note that we fixed the phase factors such that the two middle components start out in the imaginary domain. This ensures that if all probabilities are equal to 0.5 the probability distribution in position space will be symmetric for every value of ρ and η. However, different choices for the phase factors are also possible. To evolve the walker we need to adapt the coin and shift operator to the four dimensional spin state. We create a four dimensional coin by taking the outer product of two two-dimensional generalized Hadamard coins (see Equation 2.7) $H(\rho) \otimes H(\eta)$:

$$C_4 = \begin{pmatrix} \sqrt{\eta}\sqrt{\rho} & \sqrt{1-\eta}\sqrt{\rho} & \sqrt{\eta}\sqrt{1-\rho} & \sqrt{1-\eta}\sqrt{1-\rho} \\ \sqrt{1-\eta}\sqrt{\rho} & -\sqrt{\eta}\sqrt{\rho} & \sqrt{1-\eta}\sqrt{1-\rho} & -\sqrt{\eta}\sqrt{1-\rho} \\ \sqrt{\eta}\sqrt{1-\rho} & \sqrt{1-\eta}\sqrt{1-\rho} & -\sqrt{\eta}\sqrt{\rho} & -\sqrt{1-\eta}\sqrt{\rho} \\ \sqrt{1-\eta}\sqrt{1-\rho} & -\sqrt{\eta}\sqrt{1-\rho} & -\sqrt{1-\eta}\sqrt{\rho} & \sqrt{\eta}\sqrt{\rho}. \end{pmatrix} \tag{6.17}$$

Because of the structure, ρ and η both have a different role. Consider the limiting case $\rho = 1$. In this case, the coin is a block diagonal matrix. This means that within each lottery the components can mix, however, there is no mixing between the two lotteries. On the other hand, if we take $\eta = 1$ only components from different lotteries mix. In general, we can say that ρ regulates the mixing between lotteries and η the mixing within. However, ρ and η do not act independently and can amplify or decrease each other's effects.

The next step is to define how the walker moves in space. We still want the problem to be one-dimensional in space and therefore we go back to the wealth space we discussed in Section 4.2. For the moment we restrict ourselves to gain lotteries only. The walker starts out in position x_0 representing 0 additional wealth. Both to the left and right the wealth level goes up by a certain amount per step. For simplicity we set this amount to €1 per site, i.e. taking one step to the left or right corresponds to gaining €1 unit. Conceptually, the walk in value space represents a decision-maker imagining playing the lotteries multiple times to see which lottery gives the highest expected value. Because the two lotteries are evaluated at the same time the multiple possible paths that lead to the same wealth level can interfere. Furthermore, by adjusting the coin operator, different components mix during the evolution, representing the inability to assess all options rationally and independently.

Since the walk now takes place in wealth space, we can use the step operator to encode the values of the lotteries. In general we define the shift operator as:

$$\begin{aligned} S_v = \sum_x |x\rangle \langle x - v_1| \otimes \left|L_1^{\uparrow}\right\rangle \left\langle L_1^{\uparrow}\right| + |x\rangle \langle x - v_2| \otimes \left|L_1^{\downarrow}\right\rangle \left\langle L_1^{\downarrow}\right| \\ + |x\rangle \langle x + v_3| \otimes \left|L_2^{\uparrow}\right\rangle \left\langle L_2^{\uparrow}\right| + |x\rangle \langle x + v_4| \otimes \left|L_2^{\downarrow}\right\rangle \left\langle L_2^{\downarrow}\right|. \end{aligned} \tag{6.18}$$

With this shift operator, each component is shifted a number of sites equal to the gain in wealth that the outcome represents. Here, the two components of Lottery 1 are shifted to the left, and the components of Lottery 2 are shifted to the right. As an illustration, think of the two lotteries as being coin flips. For the first lottery, if the coin shows head you gain €v_1, if it shows tail you get €v_2. Now if the walker ends up in the first spin state, this corresponds to choosing to play Lottery 1 and the outcome being heads. In this case, you take v_1 steps to the left, representing an increase in wealth of v_1 units. The shift operator is fixed at each step, however, which portion of the wave-function takes which step is determined by the spin state and thus by the subjective probabilities. Note that in this way the probability and value influences are in principle in different Hilbert spaces, but because of the entanglement between spin and position they both influence the walk in a non-trivial and non-separable way.

The concept of interference is also intuitive in this set-up. Components can interfere if they are at the same site, meaning at the same wealth level. The interference is then between different paths that lead to the same wealth level. As the walk evolves, the probability distribution will spread out over many different wealth levels depending on the parameters of the coin. The goal of this approach is to describe the formation of the subjective expected values of each lottery. To quantify this, we measure the spin distribution after a predefined number of evolution steps. To account for the achieved wealth levels, we take a weighted distribution over the position space. The weighting function can be seen as a utility function with the minimal property that it increases in $|x - x_0|$. This, because the components that are located the furthest away from the starting position represent the highest gain in wealth and should, therefore, get a larger weight. To extract the expected value of each lottery we group the first two and last two spin components together to get the total subjective expected value of Lottery 1 and 2 respectively. Mathematically this means that the subjective expected value of a lottery is given by:

$$\mathbb{E}^s(L_i(x)) = \frac{1}{t} \sum_x f(x)(\left|L_i^{\uparrow}(x,t)\right|^2 + \left|L_i^{\downarrow}(x,t)\right|^2), \tag{6.19}$$

where $f(x)$ is the weighting function (utility function) and $\left|L_i^{\uparrow}(x,t)\right|^2$ represents the probability of being in position x and spin state $L_i^{\uparrow}$ at time t. The prefactor $1/t$ denotes that we are taking the time average. By looking at the time average we account for the fact that the walker spreads in position space over time, therefore achieving a higher bias factor at larger times. Taking the average makes sure that we can retrieve the rational expected values when $\rho = \eta = 1$, we will show this explicitly in Subsection 6.4.

Based on these expected values we can define the choice probability. There are different choices possible, just like there are multiple possible choices for the weighting function. Here, we will consider the simple case of a linear weighting function:

$$f(x) = \begin{cases} (x_0 - x) & \text{for } L_1 \\ (x - x_0) & \text{for } L_2. \end{cases} \tag{6.20}$$

Note that the signs are different for Lottery 1 and 2 because lottery 1 walks to the left and thus $(x - x_0)$ would be negative. We choose not to use the absolute value here to distinguish between the left and right domains. Components that are found in the left half of the line were part of Lottery 1 for at least 1 step longer than for Lottery 2 since only Lottery 1 components are shifted to the left. This means that we can denote the left half as the 'Lottery 1 domain'. Because of mixing between the components, it is still possible to find Lottery 2 components in the Lottery 1 domain. Conceptually, this could represent a decision-maker that chose Lottery 1 multiple times but then switched to Lottery 2 in the last step. By allowing the weighting function to be negative, the components that are found in the 'wrong' domain contribute negatively to the total expected value therefore indirectly raising the choice probability of the other lottery. This assumption amplifies the effects of the coin parameters ρ and η and therefore we use it here to illustrate the model. However, many more options are possible for the utility function.

The choice probability is a function of the subjective expected values. We here use the most straightforward definition of choice probability as the ratio of subjective expected values:

$$P^c(L_1(t)) = \frac{\mathbb{E}^s(L_1(t))}{\mathbb{E}^s(L_1(t)) + \mathbb{E}^s(L_2(t))}. \tag{6.21}$$

To compare the outcomes of the walk with the 'rational' case we also define the rational choice probability, given by the ratio of objective expected values:

$$P^r(L_1) = \frac{pv_1 + (1-p)v_2}{pv_1 + (1-p)v_2 + (1-q)v_3 + qv_4}. \tag{6.22}$$

This represents the rational choice probability of Lottery 1 with the familiar lottery parametrization: $L_1 = [v_1, p; v_2, 1-p]$ and $L_2 = [v_3, q, ; v_4, 1-q]$.

6.3.1 Evolution of the expected values

To understand the properties of the model, we look at the evolution of the subjective expected values. Note that the weighting function is always imposed afterward and therefore thus not actively influence the evolution.

Analogously to Equation 6.6, we can again write the evolution of the global spin distribution as a Markovian part plus interference terms. The evolution is given by the repeated

application of $U_4 = S_v(I_N \otimes C_4)$ where the shift and coin operator are given by Equation 6.18 and 6.17 respectively. Note that instead of one interference term, we now have several, which can be compactly written in matrix form. We denote by $\mathbb{L}^{\uparrow}_{\downarrow\kappa}$ the expected value of the first component of Lottery 1 at time t, the other components are defined in a similar fashion.

$$\begin{pmatrix} \mathbb{E}(L_1^{\uparrow})(t+1) \\ \mathbb{E}(L_1^{\downarrow})(t+1) \\ \mathbb{E}(L_2^{\uparrow})(t+1) \\ \mathbb{E}(L_2^{\downarrow})(t+1) \end{pmatrix} = \begin{pmatrix} \eta\rho & (1-\eta)\rho & \eta(1-\rho) & (1-\eta)(1-\rho) \\ (1-\eta)\rho & -\eta\rho & (1-\eta)(1-\rho) & -\eta(1-\rho) \\ \eta(1-\rho) & (1-\eta)(1-\rho) & -\eta\rho & -(1-\eta)\rho \\ (1-\eta)(1-\rho) & -\eta(1-\rho) & -(1-\eta)\rho & \eta\rho \end{pmatrix} \begin{pmatrix} \mathbb{E}(L_1^{\uparrow})(t) \\ \mathbb{E}(L_1^{\downarrow})(t) \\ \mathbb{E}(L_2^{\uparrow})(t) \\ \mathbb{E}(L_2^{\downarrow})(t) \end{pmatrix}$$
$$+ \begin{pmatrix} \sqrt{\eta(1-\eta)}(1-\rho) & \sqrt{\eta(1-\eta)}\rho & \sqrt{\rho(1-\rho)}(1-\eta) & \sqrt{\rho(1-\rho)}\eta \\ \sqrt{\eta(1-\eta)}(\rho-1) & -\sqrt{\eta(1-\eta)}\rho & \sqrt{\rho(1-\rho)}\eta & \sqrt{\rho(1-\rho)}(1-\eta) \\ \sqrt{\eta(1-\eta)}\rho & (1-\rho)\sqrt{\eta(1-\eta)} & \sqrt{\rho(1-\rho)}(\eta-1) & -\sqrt{\rho(1-\rho)}\eta \\ -\sqrt{\eta(1-\eta)}\rho & (\rho-1)\sqrt{\eta(1-\eta)} & -\sqrt{\rho(1-\rho)}\eta & \sqrt{\rho(1-\rho)}(\eta-1) \end{pmatrix} \begin{pmatrix} A(t) \\ B(t) \\ C(t) \\ D(t) \end{pmatrix}$$
$$+ \sqrt{\eta(1-\eta)}\sqrt{\rho(1-\rho)} \begin{pmatrix} 1 \\ -1 \\ -1 \\ 1 \end{pmatrix} \tag{6.23}$$

where

$$\begin{aligned} A(t) &= \sum_x f(x) Re(L_2^{\uparrow}(x,t) L_2^{\downarrow}(x,t)^*) \quad B(t) = \sum_x f(x) Re(L_1^{\uparrow}(x,t) L_1^{\downarrow}(x,t)^*) \\ C(t) &= \sum_x f(x) Re(L_1^{\downarrow}(x,t) L_2^{\downarrow}(x,t)^*) \quad D(t) = \sum_x f(x) Re(L_1^{\uparrow}(x,t) L_2^{\uparrow}(x,t)*) \\ E(t) &= \sum_x f(x) (Re(L_1^{\uparrow}(x,t) L_2^{\downarrow}(x,t)^*) + Re(L_1^{\downarrow}(x,t) L_2^{\uparrow}(x,t)^*)) \end{aligned} \tag{6.24}$$

The presented set-up described a decision-maker that imagines playing the lotteries multiple times. By keeping track of the wealth gains a subjective expected value of each lottery is formed. The expected values are defined as the time average of the weighted sum over position space. Because of the interference, this time average is no longer equal to the ensemble average which you would get by averaging over a large number of walkers. This means it breaks ergodicity.

In the next section, we look at the influence of the parameters of the walk on the subjective expected values and the choice probabilities.

6.4 Influence of the parameters

Before we dive into the role of the different parameters, we show explicitly how taking the time average makes sure that we retrieve the rational choice probabilities for $\rho = \eta = 1$. In this 'rational' case, the coin operator is simple a four-dimensional identity matrix, thus the spin distribution is given by the initial state in each step. The application of the shift operator then shifts each component according to the value of the outcome. For simplicity, we set $x_0 = 0$ such that the displacement is simply given by the absolute value of the position. Because there is no mixing during the T timesteps, the four occupied states during the evolution are $v_i \times t$.

Using Equation 6.19 the subjective expected value of the first components is simply given by:

$$\mathbb{E}(L_1^{\uparrow})(t) = \frac{1}{t}\sum_x x\left|L_1^{\uparrow}\right|^2 = \frac{1}{t}v_1 \times t \times p = v_1 \times p. \tag{6.25}$$

So we see that by normalizing the expected value by the number of time steps the case $\eta = \rho = 1$ gives exactly the objective expected value.

We now investigate the role of the parameters of the coin, shift operator and initial state in the evolution. To isolate the effects of ρ and η we first look at the evolution of a completely symmetric initial state:

$$\begin{pmatrix} L_1^{\uparrow} \\ L_1^{\downarrow} \\ L_2^{\uparrow} \\ L_2^{\downarrow} \end{pmatrix} = \frac{1}{2}\begin{pmatrix} 1 \\ i \\ i \\ 1 \end{pmatrix}. \tag{6.26}$$

This initial state represents the lotteries $L_1 = [v_1, 0.5; v_2, 0.5]$ and $L_2 = [v_3, 0.5; v_4, 0.5]$. With all probabilities being equal, the distribution in position space will be symmetric, however the choice probability still depends on the values of the outcomes. For the special case $v_1 = v_3$ and $v_2 = v_4$, the choice probability will be 50/50.

Application of the coin on this state yields

$$\begin{pmatrix} \frac{1}{2}\sqrt{1-\eta}\sqrt{1-\rho} + \frac{1}{2}i\sqrt{\eta}\sqrt{1-\rho} + \frac{1}{2}i\sqrt{1-\eta}\sqrt{\rho} + \frac{\sqrt{\eta}\sqrt{\rho}}{2} \\ \frac{1}{2}i\sqrt{1-\eta}\sqrt{1-\rho} - \frac{1}{2}\sqrt{\eta}\sqrt{1-\rho} + \frac{1}{2}\sqrt{1-\eta}\sqrt{\rho} - \frac{1}{2}i\sqrt{\eta}\sqrt{\rho} \\ \frac{1}{2}i\sqrt{1-\eta}\sqrt{1-\rho} + \frac{1}{2}\sqrt{\eta}\sqrt{1-\rho} - \frac{1}{2}\sqrt{1-\eta}\sqrt{\rho} - \frac{1}{2}i\sqrt{\eta}\sqrt{\rho} \\ \frac{1}{2}\sqrt{1-\eta}\sqrt{1-\rho} - \frac{1}{2}i\sqrt{\eta}\sqrt{1-\rho} - \frac{1}{2}i\sqrt{1-\eta}\sqrt{\rho} + \frac{\sqrt{\eta}\sqrt{\rho}}{2} \end{pmatrix}. \tag{6.27}$$

Application of the biased shift operator now shifts each component to a different site. We can then calculate the probability to end up at the corresponding sites by squaring the amplitudes:

$$\begin{aligned} |\Psi(x,1)\rangle = \sqrt{-(\eta-1)\eta}\sqrt{-(\rho-1)\rho} + \frac{1}{4}|x_0 - v_1\rangle + \frac{1}{4} - \sqrt{-(\eta-1)\eta}\sqrt{-(\rho-1)\rho}\,|x_0 - v_2\rangle \\ + \frac{1}{4} - \sqrt{-(\eta-1)\eta}\sqrt{-(\rho-1)\rho}\,|x_0 + v_3\rangle + \frac{1}{4} + \sqrt{-(\eta-1)\eta}\sqrt{-(\rho-1)\rho}\,|x_0 + v_4\rangle\,. \end{aligned} \tag{6.28}$$

To calculate the choice probability we take the weighted sum over position space

$$P^c_{L_1}(1) = \frac{4\sqrt{(1-\eta)\eta}\sqrt{(1-\rho)\rho}(v_1 - v_2) + v_2 + v_1}{v_1 + v_2 + v_3 + v_4 + 4\sqrt{(1-\eta)\eta}\sqrt{(1-\rho)\rho}(v_1 - v_2 - v_3 + v_4)} \tag{6.29}$$

We see that the weighted distribution makes sure that both ρ and η have an effect on the choice probability as well as the absolute and relative values of the outcomes. Of course, this is only after one step so interference does not play a role yet unless either $v_1 = v_2$ or $v_3 = v_4$ and thus multiple components end up at the same site. We also see that if either $\eta = 1$ or $\rho = 1$ the choice probability is simply given by the values. Note that this is because we chose a symmetric initial state for the probabilities, i.e. each outcome has the same objective probability, otherwise, this would not be the case.

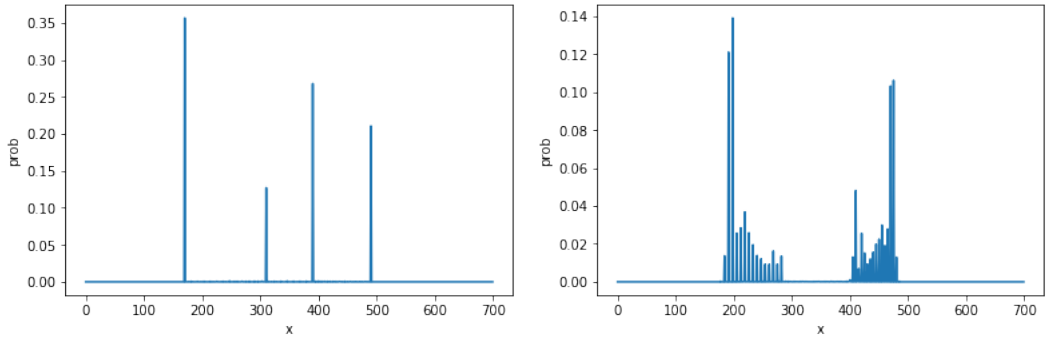

(a) $\rho = 1, \eta = 1$ **(b)** $\rho = 0.1, \eta = 0.5$

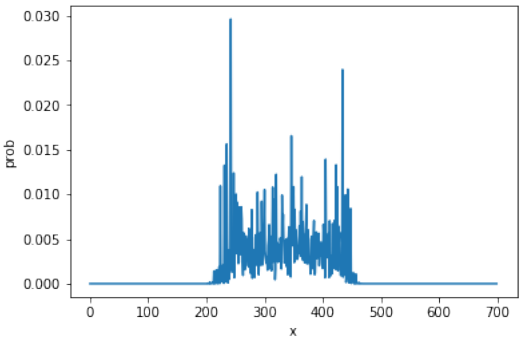

(c) $\rho = 0.7, \eta = 0.5$

Figure 6.1. – Probability distribution in position space for different values of ρ, η. All Figures display lotteries: $L_1 = [9, 0.7; 2, 0.3]$ and $L_2 = [0.4, 2; 0.6, 7]$.

To investigate the interplay between probability, value and coin parameters we numerically investigate the evolution of the general initial state:

$$\begin{pmatrix} L_1^{\uparrow} \\ L_1^{\downarrow} \\ L_2^{\uparrow} \\ L_2^{\downarrow} \end{pmatrix} = \frac{1}{\sqrt{2}} \begin{pmatrix} \sqrt{p} \\ i\sqrt{1-p} \\ i\sqrt{1-q} \\ \sqrt{q} \end{pmatrix}. \tag{6.30}$$

This state represents the lotteries $L_1 = [v_1, p; v_2, 1-p]$ and $L_2 = [v_3, q; v_4, 1-q]$ where $v_1 > v_2$ and $v_3 > v_4$. As a reference we always take the objective expectation values, or equivalently, the case $\rho = \eta = 1$.

To illustrate the distribution that results from the defined walk, we show in Figure 6.1 the distribution in position space for: (Fig. 6.1a) the rational case $\eta = \rho = 1$; (Fig. 6.1b) the case of medium mixing *within* the lottery $\eta = 0.5$ and absence of inter-lottery mixing ($\rho = 1$); (Fig. 6.1c) medium inter lottery mixing $\eta = 0.5$ and $\rho = 0.7$. We see that the fully rational case indeed produces a 4-peaked distribution where the magnitude of the peaks is given by the initial state amplitudes. By allowing for mixing within the lotteries, two separate quantum walk distributions arise in two different parts of the line. By allowing for both mixing within and between lotteries the distribution is no longer split but occupies all states between the two side peaks. In this case, all components of the lotteries can potentially interfere as well.

6.4.1 Subjective expected value

We now take a look at the subjective expected values. First of all we look at lotteries $L_1[10, p; 2, 1-p]$ and $L_2[10, 0.5; 2, 0.5]$. That means, we fix all values and the probabilities in Lottery 2, but vary the probabilities in Lottery 1. Note that the values are the same in both lotteries. Figure 6.2 displays the subjective values of both lotteries for different values of ρ and η.

A first important observation is that varying the probability in Lottery 1 also has an effect on the expected value of Lottery 2, explicitly showing the interdependence of the components. Second, we see that the expected values are underestimated for $\rho \neq 1$. This is because the mixing between components leads to a spread in position space, therefore deviating from the four-peaked distribution of the rational case. Therefore, we now have multiple weighting factors all of them equal to or lower than what we would achieve without mixing. Thus, the amount of probability in the peak located furthest away from the initial position is smaller and thus the portion of the wavefunction receiving maximum weight is also smaller, leading to an overall lower expected value. Since the underestimation occurs for both L_1 and L_2 the relative effects will only be visible in the choice probability.

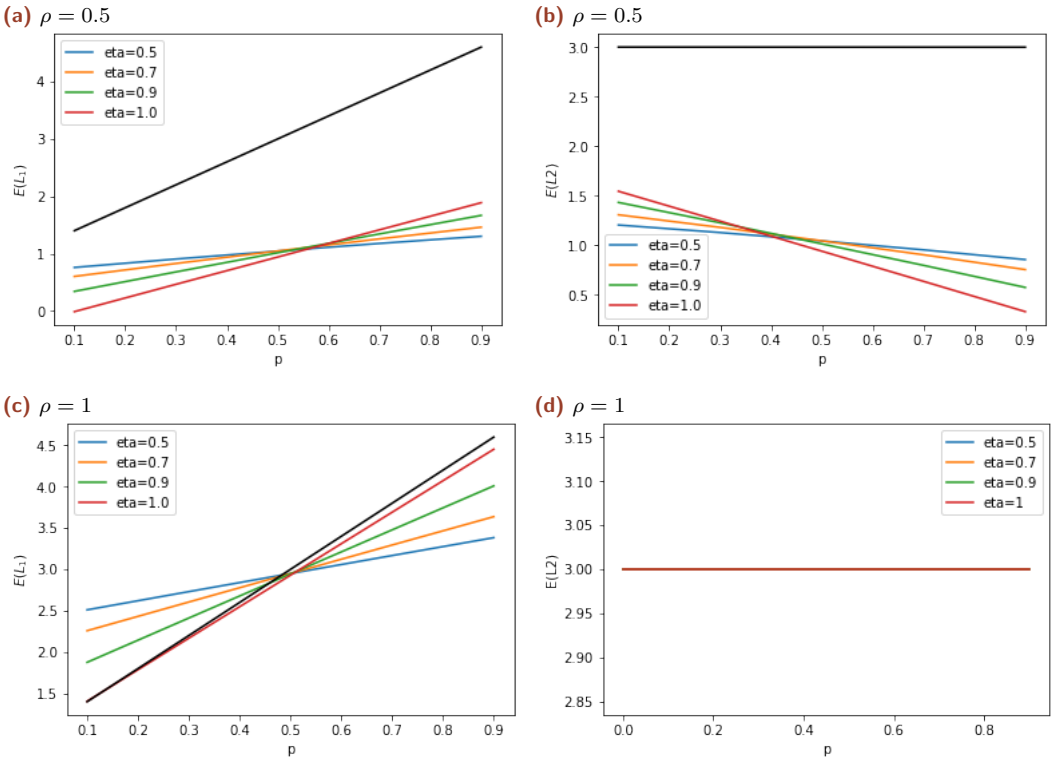

Figure 6.2. – Subjective expectation value of Lottery 1 on the left and Lottery 2 on the right as a function of the probability of the probability p of outcome 1 in Lottery 1 for different values of ρ and η. The displayed lotteries are $L_1[10, p; 2, 1-p]$ and $L_2[2, 0.5; 10, 0.5]$. The black lines represent the rational expectation value of the lottery ($\rho = \eta = 1$).

Third, both ρ and η affect the slope of the curves, with ρ also responsible for an overall shift such that the higher the value of ρ the closer the subjective value comes to the rational value. For $\rho = 1$ the values of η lead to an overestimation (underestimation) of the expected value of Lottery 1 for $p < 0.5$ ($p > 0.5$), while the expected value of Lottery 2 is equal to the

rational value for all values of η in this case. This is intuitive since in the absence of mixing between lotteries they are evaluated independently and thus a change in Lottery 1 does not affect the expected value of Lottery 2.

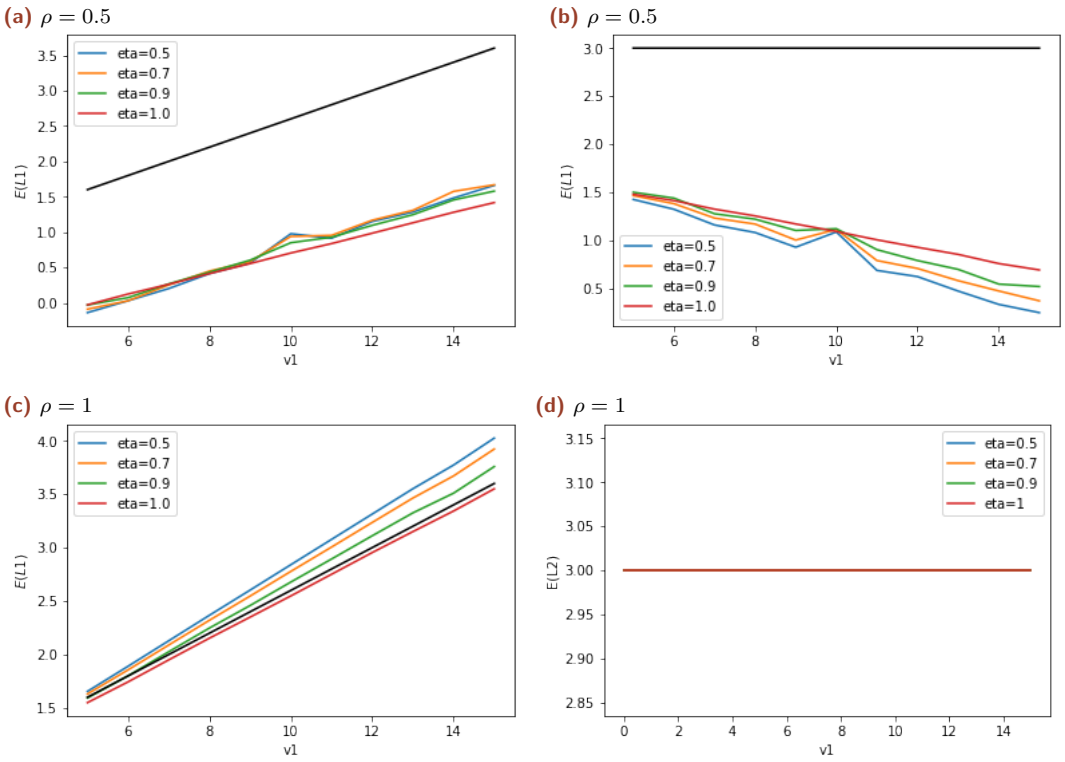

Figure 6.3. – Subjective expectation value of Lottery 1 on the left and Lottery 2 on the right as a function of the value v_1 of the first outcome of Lottery 1 for different values of ρ and η. The displayed lotteries are $L_1[v1, 0.4; 2, 0.6]$ and $L_2[10, 0.5; 2, 0.5]$. The black lines represent the rational expectation value of the lottery ($\rho = \eta = 1$).

We now fix the probabilities, but vary the values in Lottery 1 and again look at the subjective expected value for different values of ρ and η. Figure 6.3 displays lotteries $L_1[v1, 0.4; 2, 0.6]$ and $L_2[10, 0.5; 2, 0.5]$. Again, we see the overall underestimation if $\rho \neq 1$. Furthermore, we see a peak in the distribution for $v_1 = 10$. At this point, the lotteries are equal in value which possibly leads to more interference because the components are more likely to end up at the same site because of the equal step size in both directions. Again, for $\rho = 1$ Lottery 2 is unaffected. For $\rho = 1$ it is clear that a higher value leads to a larger overestimation of the expected value representing a higher attraction for high valued outcomes.

To make the dependence on ρ and η more clear, Figure 6.4 shows directly the dependence of the subjective value of L_1 and L_2 as a function of η while holding ρ fixed and vice versa for two different sets of lotteries. For 2 lotteries with unequal values (right panels) which lottery is over/underestimated changes with the value of η leading to an inflection point. This shows that for lower values of η the expected value of lottery with the higher total value is overestimated. In general, we can also see that the overall shift compared to the rational subjective value is regulated by ρ.

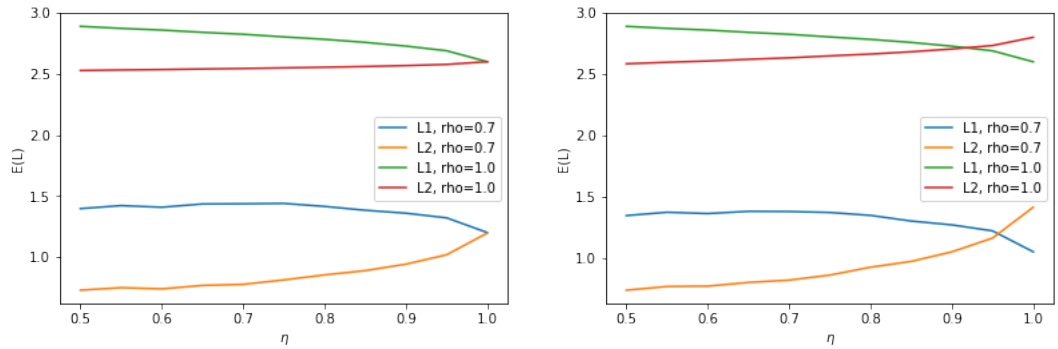

(a) $L_1 : [10, 0.4; 2, 0.6]$ and $L_2 : [4, 0.4; 6, 0.6]$

(b) $L_1 : [10, 0.4; 2, 0.6]$ and $L_2 : [4, 0.2; 6, 0.8]$

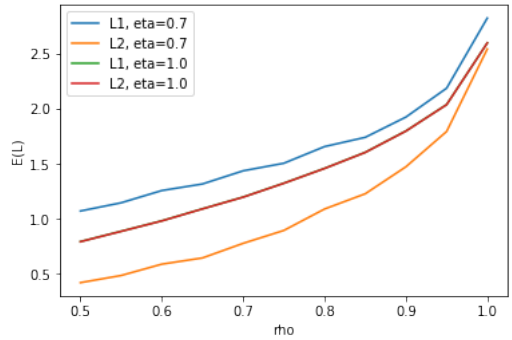

(c) $L_1 : [10, 0.4; 2, 0.6]$ and $L_2 : [4, 0.4; 6, 0.6]$

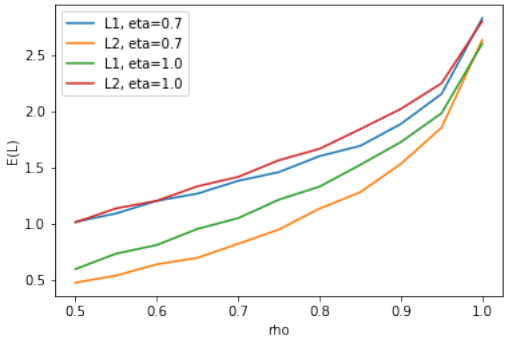

(d) $L_1 : [10, 0.4; 2, 0.6]$ and $L_2 : [4, 0.2; 6, 0.8]$

Figure 6.4. – Dependence of the subjective expectation value of both lotteries on η (top row) and ρ (bottom row). Note that on the left the rational expectation values are equal for both lotteries.

6.4.2 Choice probability

Using the subjective expectation values we now investigate the influence of the parameters on the choice probability. We use the definition of Equation 6.21, i.e. the relative subjective value. Figure 6.5 shows the choice probability for lottery 1 in pair $L_1 = [10, k; 2, 1-k]$ and $L_2 = [2, 0.5; 10, 0.5]$ on the left and $L_1 = [10, k; 2, 1-k]$ and $L_2 = [4, 0.5; 6, 0.5]$ on the right as a function of the rational choice probability as defined by Equation 6.22. Note that because we take the time average the number of steps in general only has a very small influence as long as we allow for sufficient time to spread and interfere. Similar to what we did for the subjective expectation values we fix lottery 2 and vary the probabilities in lottery 1. The influence of value is now visible when comparing the left and right values.

If we first focus on the case $\rho = 1$ in the bottom two panels we see the same over/underestimating behavior as in Section 4.1. Small choice probabilities as overestimated while large probabilities are underestimated. This is also something we saw in SRDT although there the relation followed an inverse S-shape whereas here the relation is linear. Also, note that for the lotteries with equal values the inflection point lies at $p = 0.5$ while on the right side where the values are different the inflection point is shifted. This means that even though the rational probability of Lottery 2 is higher, the higher value of Lottery 1 leads to a subjective choice that favors Lottery 1. The shift of the inflection point is even larger for $\rho \neq 1$. We could interpret this shift as a higher risk appetite when larger values are involved in one lottery. For an inflection point beyond $p = 0.5$, the low probabilities of the outcome are counteracted by

the higher potential gain such that the decision-maker still chooses Lottery 1 although this is rationally not the right option.

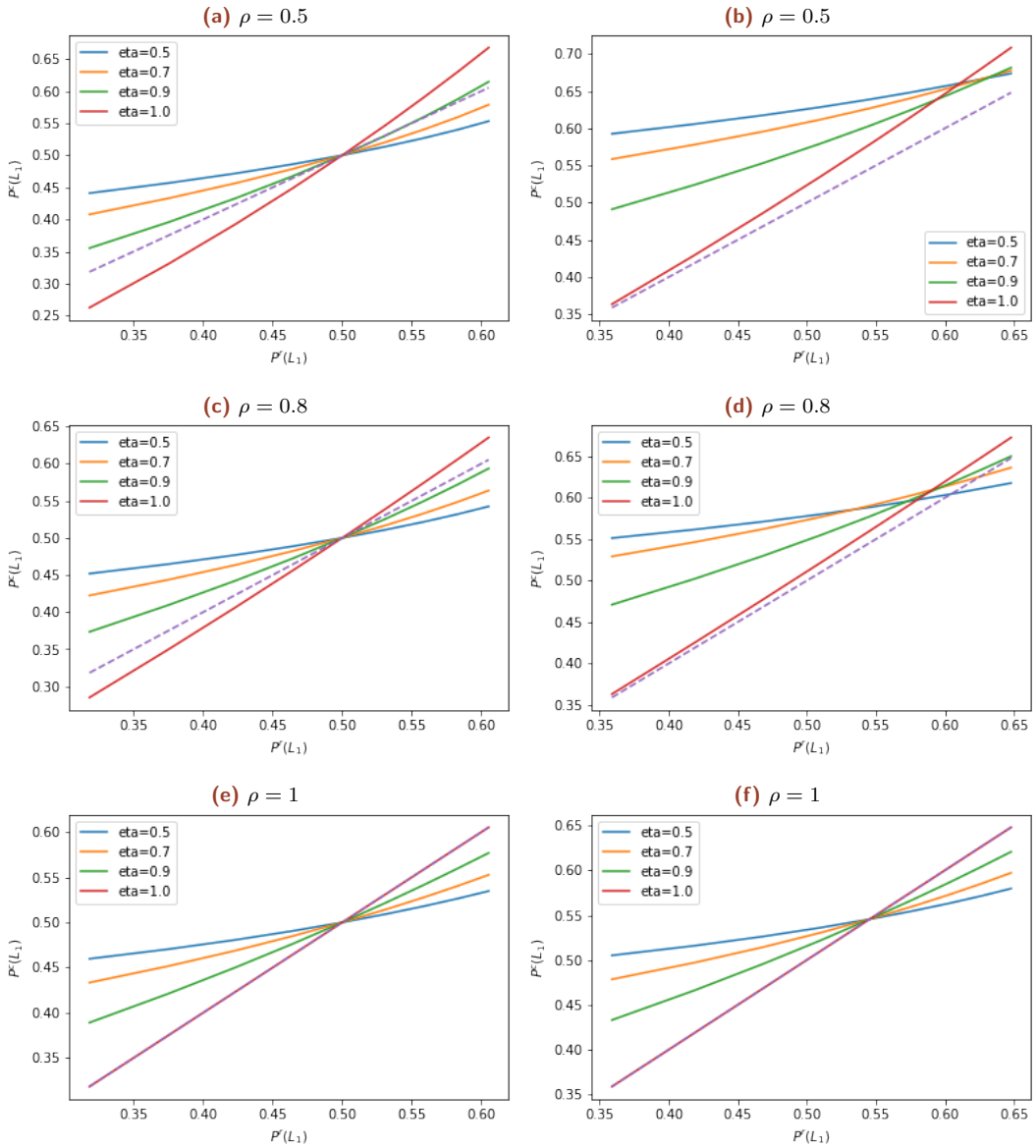

Figure 6.5. – Subjective choice probability ($P^c(L_1)$, Equation 6.21 on the vertical axis as a function of the objective choice probability ($\rho = \eta = 1$) denoted by $P^r(L_1)$. The weighting function is Equation 6.20. The panels on the left display lotteries: $L_1 = [10, k; 2, 1-k]$ and $L_2 = [0.5, 10; 0.5, 2]$. The panels on the right display $L_1 = [10, k; 2, 1-k]$ and $L_2 = [0.5, 6; 0.5, 4]$ where the value of k is varied along the x-axis resulting in an increasing rational choice probability. The dotted line displays the bisector. The number of timesteps is 30.

In general, we can say that η regulates the deviation in slope from the rational value and therefore the amount of under/overestimation. On the other hand, ρ is responsible for the overall shift, especially of the inflection point depending on the value difference. We could, therefore, interpret ρ as the main parameter to regulate the influence of value on the choice probability, where η regulates the importance of objective probability. However, we know that like probability and value η and ρ do not act independently but can amplify or decrease each other's effects.

6.5 Example: The Decoy Effect

One of the limitations of the classical SRDT framework was that it obeyed the independence of alternatives assumption of the Luce choice axiom [26]. We named the decoy effect as one of the empirically observed violations of this assumption [73], [28]. To recap, the decoy effect is the phenomenon that an option becomes more attractive once an extra (stochastically dominated) option is added to the choice problem. See section 1.3 for an explicit example for choices without uncertainty.

Quantum Decision Theory as introduced in Section 1.1 can account for the Decoy Effect because of the mathematical structure of a utility and attraction factor [74]. Imagine again a choice between two phones with two dimension, the quality and the price. We indicate A as the object of higher quality and higher price and B as the one with slightly lower quality, but also a lower price. Now if you add an option C with a slightly better quality than option A, but a price that is double the price of A, this option is in principle not very attractive. However, adding this option attracts the buyers attention to the quality dimension of the decision. Therefore, when comparing options A and B, A will now be favored stronger than before because it clearly wins when it comes to quality. The attraction of attention to the quality of the product can be described by the attraction factor $q(\pi_n)$ in QDT. Therefore, QDT can account for the Decoy or Attraction effect observed in experiments and make quantitative predictions [74].

We will now show how the previously developed spin-based decision framework can also predict the decoy effect when choosing between lotteries.

Imagine a choice between two lotteries: $L_1 = [15, 0.3; 6, 0.7]$ and $L_2 = [5, 0.5; 3, 0.5]$. The expected values are $\mathbb{E}(L_1) = 8$ and $\mathbb{E}(L_2) = 4$. We can now define the 'rational' likelihood to choose L_1 over L_2 as:

$$I^2_{L_1} = \frac{P(L_1 > L_2)}{P(L_2 > L_1)} = 2. \tag{6.31}$$

This means that it is twice as likely to choose L_1 than it is to choose L_2. Now we add a third option to the problem: $L_3 = [3, 0.5; 1, 0.5]$ with expected value $\mathbb{E}(L_3) = 2$. We determine the choice probability of all options of the three lottery choice by pairwise comparison. One can imagine a sequential algorithm [75]. First, you randomly select one of the three possible pairwise choices: $\{L_1, L_2\}, \{L_2, L_3\}, \{L_1, L_3\}$, each pair is picked with probability $1/3$. Then, the chosen alternative from this pair is compared to the third alternative. In this way we can write the probability of choosing L_1 in the presence of three lotteries as:

$$\begin{aligned} P(L_1|L_1, L_2, L_3) = \frac{1}{3}[2 \times P(L_1|L_1, L_2)P(L_1|L_1, L_3) \\ + P(L_2|L_2, L_3)P(L_1|L_1, L_3) + P(L_3|L_2, L_3)P(L_1|L_1, L_3)]. \end{aligned} \tag{6.32}$$

Focusing on the likelihood of picking L_1 over L_2, we can directly write:

$$\frac{P(L_1|L_1, L_2, L_3)}{P(L_2|L_1, L_2, L_3)} = \frac{P(L_1|L_1, L_3)}{P(L_3|L_1, L_3)} \frac{P(L_3|L_2, L_3)}{P(L_2|L_2, L_3)}. \tag{6.33}$$

If the alternatives are evaluated independently, Luce choice model predicts that the relative likelihood of choosing L_1 over L_2 does not change when a third lottery is added [76]. In our example, the rational relative likelihood of L_1 over L_2 when L_3 is present is given by:

$$I^3_{L_1} = \frac{P(L_1|L_1, L_2, L_3)}{P(L_2|L_1, L_2, L_3)} = \frac{P(L_1|L_1, L_3)}{P(L_3|L_1, L_3)} \frac{P(L_3|L_2, L_3)}{P(L_2|L_2, L_3)} = \frac{8}{2}\frac{2}{4} = 2 \tag{6.34}$$

Any violation of this, i.e. an increase of the likelihood when an extra option is added is the decoy effect.

We will now demonstrate that with the framework outlined above that we can predict the decoy effect by allowing for mixing between the components. In Figure 6.6a we plot the likelihood of choosing L_1 over L_2 in the presence of two and three lotteries. Figure 6.6b shows the ratio of the two likelihoods. We can see that the likelihood increases once a third option is added. This is exactly the decoy effect and shows a violation of the independence of alternatives. Based on the ratios of the likelihoods, we can also see that the decoy effect is stronger for lower values of ρ which is expected since ρ regulates the mixing between lotteries. The same can be said of η, which regulates mixing within the lotteries. We know that the effects of η and ρ can amplify each other. The rational case $\rho = \eta = 1$ (although not shown here) again represents the independent evaluation of each component and does indeed confirm Luce's choice axiom.

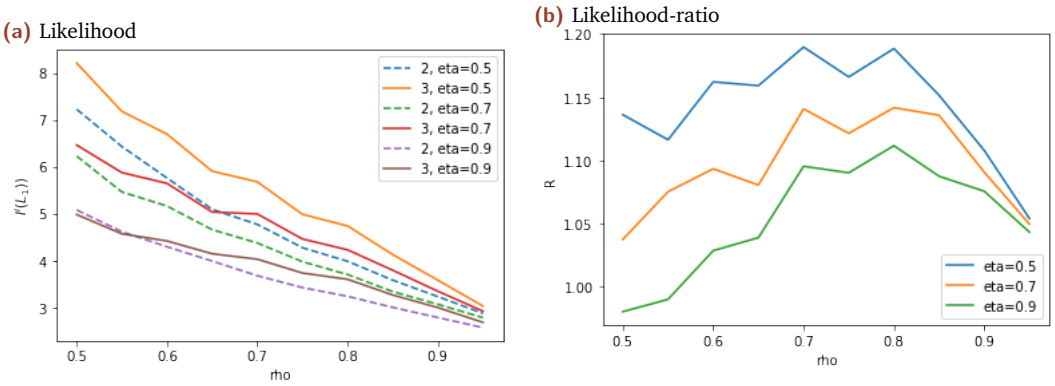

Figure 6.6. – **(a)** The relative likelihood of choosing L_1 over L_2 for two lotteries as in Equation 6.31 (dotted lines) and for three lotteries as in Equation 6.33 (solid lines) as a function of ρ for different values of η. The used lotteries are $L_1 = [15, 0.3; 6, 0.7]$, $L_2 = [5, 0.5; 3, 0.5]$ and $L_3 = [3, 0.5; 1, 0.5]$ such that the 'rational' likelihood is 2. The fact that the solid lines run above the dotted lines is the Decoy Effect. **(b)** We plot the ratio of the two likelihoods i.e. $R = I^3_{L_1}/I^2_{L_1}$ as a function of ρ for different values of η.

7 Discussion

In this thesis, we presented some possible ways in which quantum walks can be used to formulate a Decision Theory. The starting point was the random walk based Stochastic Representation Decision Theory. By substituting the random walk by a quantum walk we extended this theory in the quantum domain. In the absence of a value bias, we were able to retrieve a similar inverse S-shape for the relation between absorption probability and starting position which represents the objective probability as in the classical theory. However, this only works for certain values of ρ. The attractive force resulting from a value dependent potential in the classical case was translated to an exponential term in the coin for the quantum walk. However, since the bias only acts locally three different coins were needed along the line. This position dependence of the coin led to decoherence and reflection effects. Therefore, the results deviated quite a lot from the classical case and were harder to interpret. One important difference is that the intersection with the bisector was shifted in the classical case when a value bias was added, whereas in the quantum case is always stays at $p = 0.5$. Furthermore, ρ is the other main parameter in the quantum walk, however it was shown that its effects cannot simply be related to those of the diffusion coefficient in SRDT. This makes it challenging to compare the two theories on a more absolute level.

Another issue was that the introduction of absorbing boundaries is very non-trivial in the quantum case. We chose an algorithmic protocol based on partial measurements for the implementation. However, this breaks the translational invariance and coherent and reversible nature of the quantum walk. This disturbance makes the formulation of an analytical solution for the absorption probability very challenging. Also, an important feature of the quantum walk, namely its spin degree of freedom, remained unexplored in this theory. This motivated us to go beyond SRDT.

In Chapter 4 we discussed some other parametrizations of the decision problem while investigations different options to bias the quantum walk. This chapter laid the foundation for the spin-based framework presented in Chapter 6. Here, we switched from a walk between absorbing boundaries to a walk in 'wealth space.' The choice between two binary lotteries was modeled with only one walker with a four-dimensional spin vector that represents the probabilities of all alternatives. A special shift operator with value-dependent step-sizes determined the motion based on the probability spin-space. By finally taking a weighted sum over the wealth space for the global spin distribution, the subjective expected values of each lottery were determined. Comparing these expected values gives the choice probabilities. We illustrated the method by showing how the interdependence of alternatives in this framework can predict the Decoy effect.

This spin-based framework can be tuned in multiple ways. First of all, we have the coin parameters ρ and η which regulate the mixing between and within lotteries respectively, although in a non-trivial and non-separable way. Second of all, the weighting function and even the definition of the choice probabilities can take many different forms. We took a linear form as an example, but a more sophisticated function might be needed.

One of the key features of SRDT was that probability and value influence the decision in a non-trivial and non-separable way. Due to the entanglement between and position and spin we were able to achieve that in this set-up as well. However, the dynamics are much more complicated because of the four-dimensional spin space and variable step-operator. Therefore, further research on the dynamics is needed to understand and interpret the influence of all involved parameters. This also asks for an analytical solution that is not yet developed. On the one hand, the many parameters and higher dimension make this challenging. On the other hand, the walk is unitary and translationally invariant admitting a treatment by for example Fourier analysis.

One advantage of this approach is that because of the entanglement between spin and position the value and probability influence the decision in a non-trivial and non-separable way just like in SRDT. However, where in SRDT the diffusion coëfficient determined their relative importance, this cannot be said of ρ and η. Instead, ρ and η are essentially a measure for the 'irrationality' or 'quantumness' of the problem. Therefore, the question is how to relate their values to the decision problem at hand. This should be motivated by a better understanding of the dynamics and, ultimately, experimental data.

The introduction of quantum walks into decision theory was also motivated by the successes of Quantum Decision Theory [2]. We aimed to generalize and enrich SRDT with quantum properties like entanglement and interference to help establish the relation with QDT. Both in the introduction on Quantum walks and for the spin-based framework, we showed that the evolution process can be written as a Markovian process plus interference terms. This structure is very similar to the one in QDT. However, where this functional form was derived from the principles of Quantum mechanics, the exact form of the functions was postulated in QDT. In the framework presented here, we retrieved this form by assuming the underlying process instead. Indeed, this shows that quantum walks are a powerful tool to develop the microfoundation of QDT in the spirit of statistical physics for thermodynamics.

Additionally, we also investigated the possibilities of using Continous-Time Quantum walks for a decision theory framework. For this, we followed the SRDT set-up of a particle between absorbing boundaries. One advantage was that the Hamiltonian structure of this walk permits the use of perturbation theory to analytically calculate the absorption probability. However, because there is no coin space here, the options to bias the walk are limited. Furthermore, the absorption probabilities are very similar as in the classical case and show no surprises. All in all, we concluded that this did not provide enough new opportunities for decision theory.

On the more technical side, most of the results in this thesis are based on simulations. Simple algorithms were used to investigate the qualitative nature of the dynamics. Of course, these simulations are subject to numerical errors and limited computation power. We did not provide an elaborate error analysis of the walk, mainly because the focus was always on shape more than absolute value. All figures were created with Python and are meant to be illustrations of the model more than numerical results. Therefore, we always used stylized lottery examples which occasionally feature extreme values to make the effects more pronounced. The limitations of simulations again highlight the importance of analytical solutions. We provided them where possible, but there is still a lot of work to be done here. Further development of the theory should make it possible for the future to calibrate it against experimental data.

Conclusion

8

The aim of this thesis was to explore the possibilities of using quantum walks to develop a decision theory. More specifically, we aimed to generalize and enrich the classical SRDT with quantum properties and try to connect it to the successful Quantum Decision Theory. As a first step, we translated the set-up of SRDT to a quantum walk. This had some success in terms of qualitative patterns. However, there were also some major differences in terms of the implementation of the value bias and the interpretation of the parameters. For example, we were not able to establish a relation between the diffusion coefficient of SRDT and the coin parameter ρ which makes a comparison in quantitative terms difficult.

Motivated by the rich dynamics of the quantum walk we broadened our horizon and developed a spin-based theory that combines different ways to bias the walk. Although the probability and value terms of the lotteries are initially located in different Hilbert spaces, entanglement and interference allowed them to influence the walk in a non-trivial and non-separable way. This theory is based on some unique quantum features and has no direct classical counterpart. Exactly the coherent and interfering nature violates the independence of alternatives assumption and could, therefore, solve some problems of SRDT. Future research is needed to better understand the dynamics of the four-dimensional walk in value space and to relate all parameters to the decision problem at hand. However, the initial results such as the prediction of the Decoy effect are promising.

Another aim was to provide a micro-foundation for Quantum Decision Theory. By writing the evolution of the quantum walk as a Markovian process plus interference we showed the similarities between the two theories. This shows that quantum walks have the potential of being the key element in the underlying theory of QDT.

Of course, a lot of challenges remain and many new questions were posed in this thesis. Especially the development of an analytical solution and a convincing translation from the decision problem into quantum walk parameters are important avenues for future research. We hope that this thesis can serve as a first step into the bright future of quantum walk-based decision theory.

Bibliography

[1] G. M. Ferro and D. Sornette, "Stochastic representation decision theory: how probabilities and values are entangled dual characteristics in cognitive processes," *ETH Zurich working paper*, 2019.

[2] V. Yukalov and D. Sornette, "Quantum decision theory as quantum theory of measurement," *Physics Letters A*, vol. 372, pp. 6867–6871, 11 2008.

[3] D. Bernoulli, "Exposition of a new theory on the measurement of risk.," *Econometrica*, 1738.

[4] S. Andersen, J. C. Cox, G. W. Harrison, M. I. Lau, E. E. Rutström, and V. Sadiraj, "Asset Integration and Attitudes toward Risk: Theory and Evidence," *The Review of Economics and Statistics*, vol. 100, pp. 816–830, 12 2018.

[5] M. Allais, "Le Comportement de l'Homme Rationnel devant le Risque: Critique des Postulats et axiomes de l'ecole americaine," *Econometrica*, vol. 21, no. 4, pp. 503–546, 1953.

[6] D. Ellsberg, "Risk, Ambiguity, and the Savage Axioms," *Quarterly Journal of Economics*, vol. 75, 1961.

[7] H. Simon, "Theories of Bounded Rationality," *Decision and Organisation*, vol. 1, no. 1, pp. 161–167, 1972.

[8] J. Quiggin, "A Theory of Anticipated Utility," *Journal of Economic Behavior and Organization*, vol. 3, no. 4, 1982.

[9] M. D. Cohen, *Risk-Aversion Concepts in Expected- and Non-Expected-Utility Models*. Dordrecht: Springer Netherlands, 1995.

[10] D. Kahneman and A. Tversky, "Prospect theory: An analysis of decision under risk. ," *Econometrica*, 1979.

[11] A. Tversky and D. Kahneman, "Advances in prospect theory: Cumulative representation of uncertainty," *Journal of Risk and Uncertainty*, vol. 5, pp. 297–323, 10 1992.

[12] D. R. Luce and R. Duncan, *Conditional logit analysis of qualitative choice behavior.* . New York: John Wiley and Sons., 1959.

[13] T. Kovalenko, V. I. Yukalov, D. Sornette, and S. Vincent, "Calibration of Quantum Decision Theory, Aversion to Large Losses and Predictability of Probabilistic Choices," *ETH Zurich working paper*, 2016.

[14] C. I. Bliss, “The Method of Probits,” *Science*, vol. 79, pp. 38–39, 1 1934.

[15] D. Cox, “Simple regression,” *Analysis of Binary Data*, 1970.

[16] J. Popper Shaffer, “Multiple hypothesis testing.,” *Annual review of psy-chology*, vol. 46, no. 1, pp. 561–584, 1995.

[17] V. I. I. Yukalov and D. Sornette, “Mathematical Structure of Quantum Decision Theory,” *Advances in Complex Systems*, vol. 13, pp. 659–698, 10 2010.

[18] V. Kurtz-David, D. Persitz, R. Webb, and D. J. Levy, “The neural computation of inconsistent choice behavior,” *Nature Communications*, vol. 10, 12 2019.

[19] M. H. Birnbaum and U. Schmidt, “An experimental investigation of violations of transitivity in choice under uncertainty,” *Journal of Risk and Uncertainty*, vol. 37, pp. 77–91, 9 2008.

[20] J. Kempe, “Quantum random walks: An introductory overview,” *Contemporary Physics*, vol. 44, no. 4, pp. 307–327, 2003.

[21] E. F. Fama, “Random Walks in Stock Market Prices,” *Financial Analysts Journal*, vol. 51, pp. 75–80, 1 1995.

[22] N. Van Kampen, *Stochastic processes in physics and chemistry. Revised and enlarged ed.* . Amsterdam: Elsevier Science Publishers, 1992.

[23] A. D. Fokker, “Die mittlere Energie rotierender elektrischer Dipole im Strahlungsfeld,” *Annalen der Physik*, vol. 348, no. 5, pp. 810–820, 1914.

[24] M. Planck, *Uber einen Satz der statistischen Dynamik und seine Er-weiterung in der Quantentheorie.* Reimer, 1917.

[25] C. Gardiner, *Stochastic methods*. Berlin: Springer, vol.4 ed., 2009.

[26] R. D. Luce, “The Choice Axiom after Twenty Years*,” *Journal of Mathematical Psychology*, vol. 15, pp. 215–233, 1977.

[27] J. Hadar and W. R. Russell, “Rules for Ordering Uncertain Prospects,” *The American Economic Review*, vol. 59, no. 1, pp. 25–34, 1969.

[28] J. Huber, J. W. Payne, and C. Puto, “Adding Asymmetrically Dominated Alternatives: Violations of Regularity and the Similarity Hypothesis,” *Journal of Consumer Research*, vol. 9, p. 90, 6 1982.

[29] T. Noguchi and N. Stewart, “In the attraction, compromise, and similarity effects, alternatives are repeatedly compared in pairs on single dimensions,” *Cognition*, vol. 132, pp. 44–56, 7 2014.

[30] A. Tversky and D. Kahneman, “Extensional versus intuitive reasoning: The conjunction fallacy in probability judgment.,” *Psychological Review*, vol. 90, no. 4, pp. 293–315, 1983.

[31] A. Romanelli, A. C. Schifino, R. Siri, G. Abal, A. Auyuanet, and R. Donangelo, “Quantum random walk on the line as a Markovian process,” *Physica A: Statistical Mechanics and its Applications*, vol. 338, pp. 395–405, 7 2004.

[32] Y. Aharonov, L. Davidovich, and N. Zagury˜, "Quantum random walks," *Physical Review A*, vol. 48, no. 2, 1993.

[33] D. A. Meyer, "From Quantum Cellular Automata to Quantum Lattice Gases," *Journal of Statistical Physics*, vol. 85, no. 5, 1996.

[34] E. Farhi and S. Gutmann, "Quantum computation and decision trees," *Physical Review A*, vol. 58, no. 2, 1998.

[35] Z. J. Li, J. A. Izaac, and J. B. Wang, "Position-defect-induced reflection, trapping, transmission, and resonance in quantum walks," *Physical Review A - Atomic, Molecular, and Optical Physics*, vol. 87, 1 2013.

[36] A. M. Childs, "On the relationship between continuous- and discrete-time quantum walk," *Communications in Mathematical Physics*, vol. 294, pp. 581–603, 1 2010.

[37] F. M. Andrade and M. G. Da Luz, "Equivalence between discrete quantum walk models in arbitrary topologies," *Physical Review A - Atomic, Molecular, and Optical Physics*, vol. 80, 11 2009.

[38] S. E. Venegas-Andraca, "Quantum walks: a comprehensive review," *Quantum Information Processing*, vol. 11, pp. 1015–1106, 10 2012.

[39] W. Dür, R. Raussendorf, V. M. Kendon, and H. J. Briegel, "Quantum walks in optical lattices," *Physical Review A - Atomic, Molecular, and Optical Physics*, vol. 66, no. 5, p. 8, 2002.

[40] B. C. Travaglione and G. J. Milburn, "Implementing the quantum random walk," *Physical Review A - Atomic, Molecular, and Optical Physics*, vol. 65, no. 3, p. 5, 2002.

[41] H. Schmitz, R. Matjeschk, C. Schneider, J. Glueckert, M. Enderlein, T. Huber, and T. Schaetz, "Quantum Walk of a Trapped Ion in Phase Space," *Physical Review Letters*, vol. 103, p. 090504, 8 2009.

[42] X. Zhan, L. Xiao, Z. Bian, K. Wang, X. Qiu, B. C. Sanders, W. Yi, and P. Xue, "Detecting Topological Invariants in Nonunitary Discrete-Time Quantum Walks," *Physical Review Letters*, vol. 119, 9 2017.

[43] M. S. Rudner and L. S. Levitov, "Topological transition in a non-hermitian quantum walk," *Physical Review Letters*, vol. 102, 2 2009.

[44] C. M. Chandrashekar, R. Srikanth, and R. Laflamme, "Optimizing the discrete time quantum walk using a SU(2) coin," *Physical Review A - Atomic, Molecular, and Optical Physics*, vol. 77, 3 2008.

[45] G. Leung, P. Knott, and J. Bailey, "Controlling discrete quantum walks: coins and initial states," *New Journal of Physics*, vol. 83, no. 5, 2003.

[46] C. M. Chandrashekar, *Discrete-Time Quantum Walk-Dynamics and Applications*. PhD thesis, University of Waterloo, Waterloo, Ontario, 2010.

[47] E. Bach, S. Coppersmith, M. P. Goldschen, R. Joynt, and J. Watrous, "One-dimensional quantum walks with absorbing boundaries," *Journal of Computer and System Sciences*, vol. 69, pp. 562–592, 12 2004.

[48] A. Ambainis, E. Bach, A. Nayak, A. Vishwanath, and J. Watrous, "One-dimensional quantum walks," in *Proceedings of the thirty-third annual ACM symposium on Theory of computing - STOC '01*, pp. 37–49, 2001.

[49] V. Kendon, "Decoherence in quantum walks – a review," *Mathematical Structures in Computer Science*, vol. 17, 12 2007.

[50] T. A. Brun, H. A. Carteret, and A. Ambainis, "Quantum to classical transition for random walks," *Physical Review Letters*, vol. 91, no. 13, 2003.

[51] T. A. Brun, H. A. Carteret, and A. Ambainis, "Quantum random walks with decoherent coins," *Physical Review A - Atomic, Molecular, and Optical Physics*, vol. 67, no. 3, p. 9, 2003.

[52] D. Shapira, O. Biham, A. J. Bracken, and M. Hackett, "One-dimensional quantum walk with unitary noise," *Physical Review A - Atomic, Molecular, and Optical Physics*, vol. 68, no. 6, p. 8, 2003.

[53] N. Konno, "A Path Integral Approach for Disordered Quantum Walks in One Dimension," *arXiv preprint quant-ph/0406233*, 6 2004.

[54] C. C. López and J. P. Paz, "Phase-space approach to the study of decoherence in quantum walks," *Physical Review A - Atomic, Molecular, and Optical Physics*, vol. 68, no. 5, p. 9, 2003.

[55] A. Schreiber, K. N. Cassemiro, V. Potoček, A. Gábris, I. Jex, and C. H. Silberhorn, "Decoherence and disorder in quantum walks: From ballistic spread to localization," *Physical Review Letters*, vol. 106, 5 2011.

[56] U. Rössler, *Solid State Theory*. Berlin, Heidelberg: Springer Berlin Heidelberg, 2009.

[57] D. Witthaut, "Quantum walks and quantum simulations with Bloch-oscillating spinor atoms," *Physical Review A*, vol. 82, p. 033602, 9 2010.

[58] P. Arnault, B. Pepper, and A. Pérez, "Quantum walks in weak electric fields and Bloch oscillations," *arXiv:2001.05346 [quant-ph]*, 1 2020.

[59] N. Konno, T. Namiki, T. Soshi, and A. Sudbury, "Absorption problems for quantum walks in one dimension," *J. Phys. A: Math. Gen*, vol. 36, pp. 241–253, 2003.

[60] E. Bach and L. Borisov, "Absorption Probabilities for the Two-Barrier Quantum Walk," *ArXiv preprint 0901.4349 [quant-ph]*, 1 2009.

[61] E. Bach, S. Coppersmith, M. P. Goldschen, R. Joynt, and J. Watrous, "One-dimensional quantum walks with absorbing boundaries," *Journal of Computer and System Sciences*, vol. 69, pp. 562–592, 12 2004.

[62] N. Konno, T. Łuczak, and E. Segawa, "Limit measures of inhomogeneous discrete-time quantum walks in one dimension," *Quantum Information Processing*, vol. 12, pp. 33–53, 1 2013.

[63] H. Imai, H. Kobayashi, and T. Yamasaki, "Analysis of absorbing times of quantum walks," *Physical Review A - Atomic, Molecular, and Optical Physics*, vol. 68, no. 1, p. 9, 2003.

[64] P. Kuklinski and M. Kon, "Absorption probabilities of quantum walks," *Quantum Information Processing*, vol. 17, p. 263, 10 2018.

[65] F. Wang, P. Zhang, Y. Wang, R. Liu, H. Gao, and F. Li, "Quantum walk with one variable absorbing boundary," *Physics Letters, Section A: General, Atomic and Solid State Physics*, vol. 381, pp. 65–69, 1 2017.

[66] J. Sakurai, "Fundamental Concepts - Incompatible variables," in *Modern quantum mechanics*, pp. 32–35, Addison-Wesley Publishing Company, 1994.

[67] M. Santha, *Quantum Walk Based Search Algorithms*. Berlin, Heidelberg: Springer Berlin Heidelberg, 2008.

[68] E. Feldman and M. Hillery, "Scattering theory and discrete-time quantum walks," *Physics Letters A*, vol. 324, pp. 277–281, 4 2004.

[69] J. Echanobe, A. Del Campo, and J. G. Muga, "Disclosing hidden information in the quantum Zeno effect: Pulsed measurement of the quantum time of arrival," *Physical Review A - Atomic, Molecular, and Optical Physics*, vol. 77, 3 2008.

[70] S. Dhar, S. Dasgupta, A. Dhar, and D. Sen, "Detection of a quantum particle on a lattice under repeated projective measurements," *Physical Review A - Atomic, Molecular, and Optical Physics*, vol. 91, 6 2015.

[71] A. Romanelli, "Distribution of chirality in the quantum walk: Markov process and entanglement," *Physical Review A*, vol. 81, 4 2010.

[72] G. Abal, R. Siri, A. Romanelli, and R. Donangelo, "Quantum walk on the line: entanglement and non-local initial conditions," *arXiv:quant-ph/0507264v5*, 2008.

[73] H. Pechtl, "Value structures in a decoy and compromise effect experiment," *Psychology and Marketing*, vol. 26, pp. 736–759, 8 2009.

[74] V. I. Yukalov and D. Sornette, "Inconclusive Quantum Measurements and Decisions under Uncertainty," *Frontiers in Physics*, vol. 4, 4 2016.

[75] F. H. Chen and J. C. Heckelman, "Winning probabilities in a pairwise lottery system with three alternatives," *Economic Theory*, vol. 26, no. 3, pp. 607–617, 2005.

[76] R. Luce, "Luce's choice axiom," *Scholarpedia*, vol. 3, no. 12, p. 8077, 2008.

Appendix

Derivation of the absorption probability with the PQRS method

A

Having presented the total absorption probability in Equation 3.10, we now want to obtain an explicit form for the coefficient by using generating functions.

$$\tilde{p}_x^N(z) = \sum_{t=1}^{\infty} p_x^N(t) z^t \qquad \tilde{r}_x^N(z) = \sum_{t=1}^{\infty} r_x^N(t) z^t \tag{A.0.1}$$

Using the earlier defined recurrences we can write:

$$\tilde{p}_x^N(z) = azp_{x-1}^N(z) + czr_{x-1}^N(z) \qquad \tilde{r}_x^N(z) = bzp_{x+1}^N(z) + dzr_{k+1}^N(z) \tag{A.0.2}$$

We can solve these equations to get the pure recurrences by multiple substitution:

$$dp_{x=2}^N(z) - \left(\Delta z + \frac{1}{z}\right)p_{x+1}^N(z) + a\tilde{p}_x^N(z) = 0$$
$$dr_{x=2}^N(z) - \left(\Delta z + \frac{1}{z}\right)r_{x+1}^N(z) + a\tilde{r}_x^N(z) = 0$$

with $\Delta = det(U) = ad - cb$. Both equations satisfy the same recurrence, meaning that they have the same roots. These can be found by solving the characteristic equation

$$d\lambda^2 - \left(\Delta z + \frac{1}{x}\right)\lambda + a = 0$$

giving:

$$\lambda_{\pm} = \frac{\Delta z^2 + 1 \pm \sqrt{\Delta^2 z^4 + 1 + 2\Delta z^2 - 4ad}}{2zd}$$

We can use the following relations for a unitary matrix:

$$|a|^2 + |b|^2 = |c|^2 + |d|^2 = 1 \qquad a\bar{c} + b\bar{d} = 0 \qquad c = -\Delta\bar{b} \qquad d = \Delta\bar{a}$$

to rewrite the eigenvalues as:

$$\lambda_{\pm} = \frac{\Delta z^2 + 1 \mp \sqrt{\Delta^2 z^4 + 2\Delta(1 - 2|a|^2)z^2 + 1}}{2\Delta\bar{a}z} \tag{A.0.3}$$

Since $\lambda_+\lambda_-$ = -1 we can now write the coefficients in terms of the eigenvalues as:

$$\tilde{p}_x^N(z) = A_z\lambda_+^{x_0-1} + B_z\lambda_-^{x_0-1} \qquad \tilde{r}_x^N(z) = C_z\lambda_+^{x_0-N+1} + D_z\lambda_-^{x_0-N+1}, \tag{A.0.4}$$

where we used the distance to left and right boundary respectively as exponents. To determine the coefficients A_z, B_z, C_z, D_z we generate some new boundary conditions. Using p_0^N =

$\bar{a}, r_0^N = \bar{c}$ and $r_N^N = p_N^N = 0$ together with the recurrence relations in Eq. A.0.2 we obtain: $p_1^N(z) = z$ and $r_{N-1}^N(z) = 0$. So the coefficients satisfy $A_z + B_z = z; C_z + D_z = 0$. Abbreviating $A_z - z/2 = z/2 - B_z = E_z$:

$$\tilde{p}_x^N(z) = \left(\frac{z}{2} + E_z\right)\lambda_+^{x_0-1}\right) + \left(\frac{z}{2} - E_z\right)\lambda_-^{x_0-1} \tag{A.0.5}$$

$$\tilde{r}_x^N(z) = C_z(\lambda_+^{x_0-N+1} - \lambda_-^{x_0-N+1}) \tag{A.0.6}$$

For the two remaining coefficients we can generate more conditions by using the recurrence relations. For example:

$$r_1^N(z) = (p_2^N(z) - r_2^N(z))z/\sqrt{2}$$

Using a similar relation for r_{N-2}^N we get:

$$\begin{aligned} C_z = \frac{z^2}{\sqrt{2}}(-1)^{N-2}(\lambda_+^{N-3} - \lambda_-^{N-3})\big[(\lambda_+^{N-2} - \lambda_-^{N-2})^2 \\ -\frac{z}{\sqrt{2}}(\lambda_+^{N-2} - \lambda_-^{N-2})(\lambda_+^{N-3} - \lambda_-^{N-3}) - (-1)^{N-3}(\lambda_+ - \lambda_-)^2\big]^{-1} \end{aligned} \tag{A.0.7}$$

$$\begin{aligned} E_z = -\frac{z}{2(\lambda_+^{N-2} - \lambda_-^{N-2})}\Big[2(-1)^{N-3}(\lambda_+ - \lambda_-)(\lambda_+^{N-3} - \lambda_-^{N-3}) \\ \big[(\lambda_+^{N-2} - \lambda_-^{N-2})^2 - \frac{z}{\sqrt{2}}(\lambda_+^{N-2} - \lambda_-^{N-2}) \\ (\lambda_+^{N-3} - \lambda_-^{N-3}) - (-1)^{N-3}(\lambda_+ - \lambda_-)^2\big]^{-1} + (\lambda_+^{N-2} + \lambda_-^{N-2})\Big] \end{aligned} \tag{A.0.8}$$

To obtain the absorption probability following equation 3.10 we need to invert the expression for the generating function to obtain the real coefficients. Instead of dealing with an infinite sum, we can set $z = e^{i\theta}$ and perform an integral over θ to obtain the coefficients C_1, C_2 and C_3. This is similar as inverting the Fourier transform.

$$p_{x_0}^N(e^{i\theta}) = \sum_{t=1}^{\infty} p_x^N(t)(e^{i\theta})^t, \tag{A.0.9}$$

such that

$$p_x^N(t) = \frac{1}{2\pi}\int_0^2 \pi p_{x_0}^N(e^{i\theta})d\theta \tag{A.0.10}$$

Therefore the total absorption probability is (see Theorem 2 in [59]).

Theorem A.0.1

$$P_{x_0}^N(\phi) = C_1|\alpha|^2 + C_2|\beta|^2 + 2Re(C_3\bar{\alpha}\beta)$$

with initial state $\phi =^T [\alpha, \beta]$ *and*

$$C_1 = \frac{1}{2\pi}\int_0^{2\pi} \left|a\tilde{p}_x^N(e^{i\theta}) + c\tilde{p}_x^N(e^{i\theta})\right|^2 d\theta$$

$$C_2 = \frac{1}{2\pi}\int_0^{2\pi} \left|b\tilde{p}_x^N(e^{i\theta}) + d\tilde{p}_x^N(e^{i\theta})\right|^2 d\theta$$

$$C_3 = \frac{1}{2\pi}\int_0^{2\pi} \overline{(a\tilde{p}_x^N(e^{i\theta}) + c\tilde{p}_x^N(e^{i\theta}))}(b\tilde{p}_x^N(e^{i\theta}) + d\tilde{p}_x^N(e^{i\theta}))d\theta$$